DAFNE

A **D**ecision-**A**nalytic **F**ramework to explore the
water-energy-food **NE**xus in complex and transboundary
water resources systems of fast growing developing countries

DECISION ANALYTIC FRAMEWORK

Deliverable D5.2

July 2019

EU H2020 Project Grant No. 690268

Programme Call: Water-5-2014/2015
Project Number: 690268
Project Title: ..... DAFNE

Work-Package: WP5
Deliverable #: D5.2
Deliverable Type: ..... Document
Contractual Date of Delivery: 31 July 2019
Actual Date of Delivery: ..... 31 July 2019
Title of Document: ..... Decision Analytic Framework
Author(s): ..... A. Castelletti, F. Bertoni, M. Zaniolo, J. Zatarain Salazar, M. Giuliani, I. Rosier, R. Hillen, S. Sinclair

Availability: ..... This report is public.

Document revisions		
Author	*Revision content*	*Date*
M. Giuliani	D5.2, v0.0 – Deliverable Development Plan	06/05/2019
F. Bertoni, M. Zaniolo, M. Giuliani	D5.2, v0.1 – deliverable draft	18/07/2019
I. Rosier, R. Hillen	D5.2, v0.2 – KULEUVEN contribution about scenarios of irrigation demands added	24/07/2019
S. Sinclair	D5.2, v0.3 – ETHZ contribution about climate change scenarios and deliverable review	29/07/2019
F. Bertoni, M. Zaniolo, J. Zatarain Salazar, M. Giuliani	D5.2, v0.4 – deliverable full version	30/07/2019
A. Castelletti	D5.2, v1.0 – Final review	31/07/2019
P. Burlando	D5.2 Final version	04/08/2019

Table of Contents

List of Tables

List of Figures

Abbreviations

DAF:	Decision Analytic Framework
NSL:	Negotiation Simulation Lab
SHs:	Stakeholders
WEF:	Water-Energy-Food
MOEAs:	Multi-Objective Evolutionary Algorithms
ZRB:	Zambezi River Basin
OTB:	Omo-Turkana Basin
DP:	Dynamic Programming
SDP:	Stochastic Dynamic Programming
DPS:	Direct Policy Search
EMODPS:	Evolutionary Multi-Objective Direct Policy Search
ANNs:	Artificial Neural Networks
RBFs:	Radial Basis Functions
NPC:	Net Present Cost
RCM:	Regional Climate Model
GCM:	General Circulation Model
DEM:	Digital Elevation Model
NSE:	Nash Sutcliffe Efficiency

1. INTRODUCTION

This document is the deliverable *D5.2 – Decision Analytic Framework,* which is part of Work Package 5 activities undertaken in task *T5.2 Decision Analytic Framework*.

The goal of WP5 is the development of a robust Decision Analytic Framework (DAF) to explore alternative pathways (i.e., temporal sequence of actions) for advancing water management strategies under the baseline (historical) condition and future scenarios, and identify efficient/robust pathways to be negotiated in the Negotiation Simulation Lab (NSL) in WP6. The workflow of WP5 and its interconnections with the other WPs are illustrated in Figure 1: WP2 and WP4 provides WP5 with the full set of evaluation indicators and candidate actions identified through a participatory process involving all the relevant Stakeholders (SHs) supported by the DAFNE Experts. These sets are organized and analyzed in task T5.1 with the purpose of identifying a sub-set of design indicators representative of the main components of the Water-Energy-Food (WEF) Nexus and, dually, a subset of candidate pathways, i.e. temporal sequence of actions, to be evaluated via optimization. These two outputs, which are described in detail in *Deliverable D5.1 (Evaluation of indicators, value functions and pathways)*, are then used in the DAF for the selection via optimization of the efficient pathways.

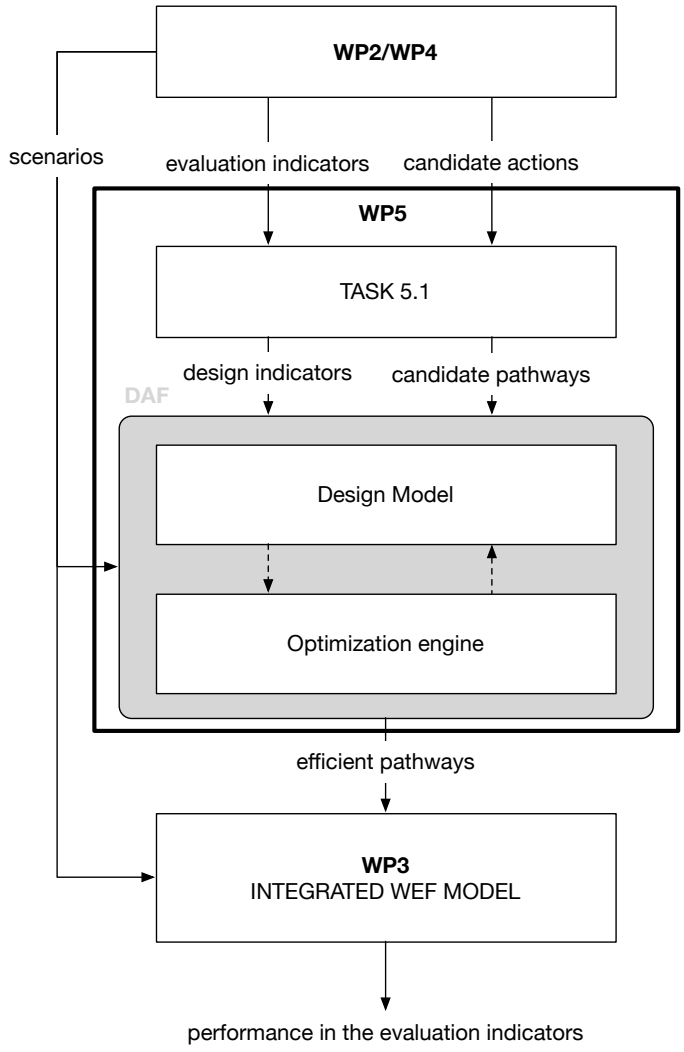

Figure 1 – WP5 workflow.

The DAF architecture (grey box in Figure 1) is composed of a system **design** (or strategic) **model** coupled with an **optimization engine.** The design model is a parsimonious conceptualization of the main natural processes and human decisions at the whole river basin scale, and balances accuracy in process characterization and reduced computational requirements to allow the simulation-based optimization of the efficient pathways. Such optimization is performed by using multi-objective evolutionary algorithms (MOEAs, for a review see Maier et al., 2014), which generate a set of Pareto-optimal solutions representing the tradeoffs across the design indicators selected in Deliverable D5.1 to represent the different WEF components. Technically, a pathway is defined as Pareto-optimal (or nondominated) if no other solution gives a better value for one objective without degrading the performance in at least one other objective. The image in the objective space of the Pareto-optimal solutions is the Pareto front. The advantage of this a-posteriori approach with respect to traditional a Soraja Vucelic priori methods, such as cost-benefit analysis or multi attribute value theory, is that decision makers do not have to state what is preferred in absence of their understanding of what is attainable (Cohon and Marks, 1975). In addition, it allows considering heterogeneous and incommensurable utility functions without going through any monetization process.

Since a pathway is a temporal sequence of actions, including planning and management options, we designed a two-level optimization scheme that first optimizes the system management (e.g. dam operation) for any candidate planning (infrastructural) alternative (e.g. dam construction) and then optimizes the sequencing (i.e., timing) of such infrastructural interventions using a pre-computed management solution. This generic architecture, which is illustrated in the report of *Milestone 34* (*Decision Analytic Framework architecture released*) is then specialized according to the characteristics of the DAFNE case studies derived from the interactions with the local SHs: the infrastructural component of the pathways, particularly in terms of dam expansion, is the most relevant issue in the Zambezi River Basin (ZRB), where instead the investigation of alternative operations appears less important given the current limited extent of multisectoral trade-offs explorable by changing the system management. The exploration of trade-offs generated by alternative system operations is instead the primary focus in the Omo-Turkana Basin (OTB), where the main infrastructural actions are already planned and/or under construction, while different operations might have substantially different impact on the multiple existing sectors. This asymmetry in the implementation of the DAF in the two case studies is not disturbing but rather generates complementary results that allow a complete exploration of the multifaceted complexity of designing pathways that efficiently combines planning and management actions along with their associated timing.

The report is structured as follows: the next chapter describes the two-level optimization scheme of the DAF; Chapters 3 and Chapter 4 introduce the design model of ZRB and discuss the corresponding results; Chapter 5 and Chapter 6 introduce the design model of OTB and discuss the corresponding results; final remarks, along with issues for further research, are presented in the last chapter.

2. TWO-LEVEL OPTIMIZATION ENGINE

2.1 OPTIMIZATION OF SYSTEM MANAGEMENT

The management design problem requires determining optimal sequential decisions at each time step that produce an immediate benefit/cost and affect the next system state, thereby affecting all the subsequent benefits/costs. In particular, the vector of release decisions (e.g. release from a dam, diverted flow at a diversion point) $\boldsymbol{u}_t$ is determined at each time step by an operating policy, i.e. $\boldsymbol{u}_t = p(t, \boldsymbol{x}_t)$. The state of the system (e.g., the reservoir storage) is then altered according to a transition function $\boldsymbol{x}_{t+1} = f_t(\boldsymbol{x}_t, \boldsymbol{u}_t, \boldsymbol{\varepsilon}_{t+1})$ affected by a vector of stochastic external drivers $\boldsymbol{\varepsilon}_{t+1}$ (e.g., reservoir inflows). In the adopted notation, the time subscript of a variable indicates the instant when its value is deterministically known. The storage is observed at time t, whereas the inflow has subscript $t+1$, denoting the realization of the inflow stochastic process in the time interval $[t; t+1)$.

The sequence of states over the time horizon defines a system trajectory, which allows the evaluation of the performance of the operating policy p by means of the different objective functions J^i (with $i = 1,\ldots,M$) capturing the interest of different SHs. Each objective function is hence formulated as a functional of the trajectory τ over the evaluation horizon *[0,h]* and across an ensemble of *K* realizations of the system disturbances $J^i = \Psi_{\varepsilon 1,\ldots,\varepsilon K}\left[\Phi_{t=1,\ldots,h}(\tau)\right]$ for $i = 1,\ldots,M$.

The optimal policy p^* is then obtained by solving the following multi-objective problem:

$$p^* = arg\min_{p} \mathbf{J} = |J^1, \ldots, J^M| \quad (1)$$

Traditionally, this problem has been solved via dynamic programming (DP) and its stochastic extension (SDP) (Yeh, 1985), where the search for optimal policies employs value functions defined over a discrete (or discretized) state-decision space, which are obtained by looking ahead to future events and computing a backed-up value. The modelling assumptions required by SDP for its application are i) finite domains of state, decision, and disturbance variables, and ii) time-separability of objective functions and constraints (A. Castelletti, 2008). These relatively mild assumptions imply, in theory, a wide applicability of SDP to many problems, but in practice its adoption is challenged by three curses (dimensionality, modelling, and multiple objectives) that considerably limit its use in real life complex problems (Giuliani, et al., 2016). The computational cost of SDP grows exponentially with the state vector dimensionality, a feature referred to as the curse of dimensionality (Bellman, 1957). Acceptable computational times are associated with a dimension of the state vector of 2 or 3, while for larger state vectors SDP results inapplicable (Loucks & Van Beek, 2017). In addition, particularly in large systems, the disturbances are likely to be temporally correlated, and accounting for temporal correlation requires the use of a dynamic stochastic model, which contributes additional state variables and exacerbates the curse of dimensionality (Soncini-Sessa, et al., 2007). The curse of modelling refers to the SDP requirement that any information included into the SDP framework must be explicitly modelled to predict the one-step-ahead model transition and ultimately the value function (Tsitsiklis & Van Roy, 1996). The implication of the curse of modelling is that no exogenous information can be added to the model, unless it is turned into a state variable of a dynamic model (adding therefore to the curse of dimensionality) or a stochastic time-independent disturbance. Finally, the curse of multiple objectives (Powell, 2007) is related to those problems where the presence of multiple conflicting objectives requires to generate a set of non-dominated alternatives, i.e., a Pareto front. Most of the DP-family methods are structurally single-objective. Their application to multi-objective problems require the use of a scalarization function to reduce the dimensionality of the objective space to a single-objective problem (Chankong & Haimes, 1983; Revelle & McGarity, 1997). The single-objective optimization is then repeated for every Pareto-optimal point generated by using different scalarization values (Soncini-Sessa, et al., 2007). This process can be computationally very intensive in many-objective optimization problems. Moreover, the Pareto front approximation loses in accuracy given the nonlinear relationships between the scalarization values and the corresponding objectives values.

The three curses of SDP limit its application in complex systems, therefore over the years a number of alternative methods have emerged, seeking to overcome one or more of these curses. Among these approaches, (i) **approximation in value space**, which searches an approximation of the value function (Bertsekas, 2005); (ii) **approximation in policy space**, which first defines the operating policy within a restricted class of parameterized functions and, then, explores the policy parameter space to optimize the system performance (Deisenroth et al. 2011). This latter, also named Direct Policy Search (DPS) (Rosenstein & Barto, 2001), have been recently extended to solve multi-objective problems by using Multi-Objective Evolutionary Algorithms (MOEAs), resulting in a viable option to address all three curses of SDP (Giuliani, et al., 2016).

Evolutionary multi-objective direct policy search (EMODPS) replaces the traditional SDP approach based on the computation of the value function, with a simulation-based optimization that directly operates in the policy space. EMODPS first parameterize the operating policy p_θ within a given

family of functions and, then, explores the parameter space Θ seeking the best parameterization of the operating policy with respect to the expected long-term cost defined by the objectives of the problem, i.e.:

$$p_\theta^* = arg \min_{p_\theta} J_{p\theta} \qquad s.t. \quad \theta \in \Theta; \quad s_{t+1} = f_t(s_t, u_t, q_{t+1}) \tag{2}$$

Finding p_θ^* corresponds to finding the best parameters θ^* for the class of policy p_θ, measured by the objectives J_{p_θ}. A schematization of the EMODPS algorithm is reported in Figure 2. Because of the simulation-based nature of EMODPS, the variables domain does not need to be discretized, overcoming at once the curse of dimensionality and the biases introduced by the discretization of continuous variables (Baxter & Bartlett, 2001). Moreover, DPS allows the direct use of non-modelled exogenous information as additional policy inputs, thus avoiding the curse of modelling (Giuliani, et al., 2016; Denaro, et al., 2017). Finally, the use of MOEAs resolves to curse of multi-objective as EMODPS algorithms allow to produce an approximation of the Pareto front in a single run for up to 10 objectives (Giuliani, et al., 2014).

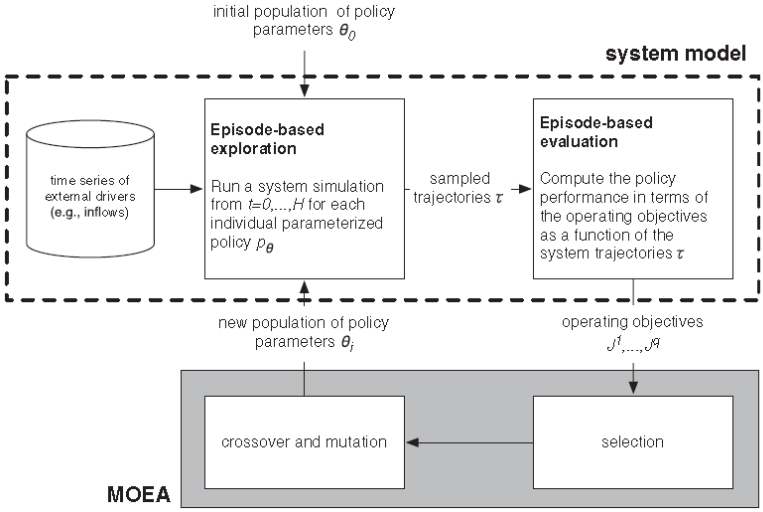

Figure 2 – Schematization of the Evolutionary Multi-Objective Direct Policy Search (EMODPS) approach. Dashed lines represent the model of the system and the grey box represents the MOEA optimization routine (Giuliani, et al., 2016).

Policy structure

EMODPS resolves a problem of parameters optimization for a given policy structure. It can therefore find, at most, the best possible solution for the chosen class of functions. The choice of a function with limited flexibility can thus restrict the search to a subspace of policies that, likely, does not contain the optimal one. It is hence advisable to select a very flexible class of functions, depending on a larger number of parameters, to ensure the possibility of approximating the unknown optimal solution of the problem to any desired degree of accuracy. Usually, the selected functions are universal approximating networks (for a review see Tikk, et al., 2003 and references therein). Two widely used nonlinear universal approximators are artificial neural networks (ANNs) and radial basis functions (RBFs). Although ANNs are more popular in the field of water management then RBFs, a comparative analysis carried out in the Red River basin (Giuliani, et al., 2016) shows the general superiority RBF on ANN for the problem of parameterization of the operating policy. RBF policies thus represent an effective, case study-independent option for solving EMODPS problems and are therefore chosen as the universal approximation network for the DAF optimization.

The RBF policy can be defined as follows:

$$u_t = \sum_{i=1}^{N} w_i \varphi_i(I_t) + a \quad (3)$$

where N is number of RBFs $\varphi(\cdot)$ and w_i are the weight of the *i*-th RBF. A single RBF is defined as

$$\varphi_i(I_t) = \exp\left[-\sum_{j=1}^{M} \frac{[(I_t)_j - c_{j,i}]^2}{b_{j,i}^2}\right] \quad (4)$$

where M is the number of policy inputs $\mathrm{I_t}$ and $\mathrm{c_i}$, $\mathrm{b_i}$ are the M-dimensional center and radius vectors of the i-th RBF, respectively. The centers of the RBF must lie within the bounded input space and the radii must strictly be positives i.e., using normalized variables, $c_i \in [-1, 1]$ and $b_i \in (0, 1]$. The parameter vector θ is therefore defined as $\theta = [a\ , c_{i,j}, b_{i,j}, w_i]$ with $i = 1, \ldots, N,\ j = 1, \ldots, M,$ and it belongs to $\mathrm{Rn\theta}$, where $n_\theta = N(2M + nu) + 1$.

Optimization algorithm – Borg MOEA

Given the non-linear nature of the optimization problem, the two main options for the optimization step of the algorithm (the grey box in Figure 2) are gradient-based methods and global optimization algorithms. Simple parameterizations with few parameters are usually coupled with gradient-based methods, while global optimization algorithms such as MOEAs are preferred when the number of parameters to optimize is high. MOEAs are iterative search algorithms that evolve a Pareto-approximate set of solutions by mimicking the randomized mating, selection, and mutation operations that occur in nature to drive the search for efficient solutions (Coello, et al., 2007). MOEAs have been shown to adapt well to multi-objective problems characterized by multi-modality, nonlinearity, stochasticity, and discreteness (see Maier et al. (2014) and references therein). In addition, MOEAs were proven to better handle performance uncertainties than gradient-based methods (Busa-Fekete, et al., 2014). MOEAs thus represent a promising alternative to gradient-based optimization methods in solving complex EMODPS problems.

Among the different state-of-the-art algorithms, the DAF optimization relies on the self-adaptive Borg Multi-Objective Evolutionary Algorithm, which has been shown to be highly robust in solving multi-objective optimal control problems, where it met or exceeded the performance of other state-of-the-art MOEAs (Zatarain Salazar, et al., 2016). Borg MOEA differs from traditional evolutionary algorithms because the application of these operators is not bound to a fixed probability of occurrence. Their employment is adaptively adjusted during the course of the optimization considering their ability to generate efficient solutions (Hadka & Reed, 2013). Along with the auto-adaptive search, Borg MOEA features other two strategies to contrast the main shortcomings of evolutionary algorithms: overfitting and poor exploration of the whole space when the search is trapped in a local minimum. The first strategy, the so-called ε-box dominance archive, divides the optimization space into hyper-boxes with side-length equal to ε. Pareto efficient solutions are searched into each box ensuring convergence. ε-box dominance also supports the second strategy: time continuation. Time continuation ensures a global search of the space by injecting mutated solutions in each ε-box. Stagnation in a local minimum is prevented with internal algorithmic operators that detect search stagnation, and randomly restart to escape local optima. Borg MOEA has been shown to outperform 9 benchmark evolutionary algorithms in terms of number of solutions returned, ability to handle many-objective problems, ease-of-use, and overall consistency across a suite of challenging multi-objective problems (Reed, et al., 2013).

2.2 OPTIMIZATION OF ACTION SEQUENCING

The aim of the optimization of action sequencing is to identify optimal adaptation pathways, namely optimal time-sequences of planning (i.e., hydropower infrastructures and irrigated areas expansion) and management (i.e., associated operating policies) actions with respect to multiple objectives.

In the DAF, this problem is solved in two steps: we firstly design a set of optimal operating policies using EMODPS for all the possible combination of infrastructures that can be realized in the system. Secondly, we solve an optimal sequencing problem to determine the best timing for the considered infrastructural interventions. This second optimization is again solved by using the Borg MOEA algorithm in order to maintain the exploration of the trade-offs between the *M* objectives formulated for Problem (1) along with an additional objective representing the cost of building a new infrastructure. This additional objective can be formulated as follows:

$$J^{cost} = \sum_r \sum_t \left[\frac{1}{(1+\gamma)^{t_r}} \cdot \alpha \cdot size_t^r - d_H \cdot \frac{\Delta life_{t_r}}{Lifespan} \cdot \alpha \cdot size_t^r \right] \quad (5)$$

where $\gamma = real\ discount\ rate = \frac{Nominal\ Interest - Inflation}{1 + Inflation}$

The nominal interest and the inflation rates are set equal to 0.05 and 0.026 respectively, based on the last's year average for the eight countries belonging to the ZRB (World Bank, 2019), t_r is the year at which the reservoir r is built, α is a factor proportional to the reservoir size, $size_t^r$ is the size of the reservoir r to build at time t, $d_H = \frac{1}{(1+\gamma)^h}$ is the discount factor calculated at the end of the evaluation horizon *H*, $\Delta life_{t_r} = Lifespan - (h - t_r)$ is the remaining life of the new reservoir r at the end of the evaluation horizon *H*, where $Lifespan$ is the new reservoir lifetime assumed to be 100 years. The objective function J^{cost} corresponds to the classic formulation of the Net Present Cost (NPC) metric, where the costs of all the new infrastructures occurring throughout the evaluation horizon *h* are summed on a yearly basis and discounted according to a yearly discount factor. In this case, the operational costs are not considered, since they are negligible with respect to the capital investment cost of building new infrastructures.

J^{cost} will therefore allow the DAF optimization engine to determine the optimal timing of infrastructural development by trading off the marginal costs and benefits associated to investments in capacity expansion. It is worth clarifying that the action sequencing optimization will be based on future projections, where we use a future scenario $\overline{w}$ that evolves in time and impacts the marginal costs and benefits of infrastructural expansions, and consequently, their optimal timing. For example, if a fast increase in energy demand is projected, more dams will be constructed in the near future, given the substantial marginal benefit of increased energy production. On the contrary, with a slow growth scenario, significant construction investments would not be substantiated by the negligible marginal benefit of added energy capacity.

It is important to highlight that once the new infrastructural intervention is chosen, it is also necessary to reselect the operating policy from the pool of optimal operating policies associated to that new solution. When doing so, it is possible to either maintain unaltered the previously adopted tradeoff, or to modify it. However, since the optimal action sequencing has been implemented only for the ZRB where SHs did not request to explore alternative operating policies, the update of the operating policy according to the infrastructural intervention did not change the trade-off and the overall analysis is based on the best operations for the hydropower sector which is a good representation of the current operators' preferences.

Finally, the overall problem requires an additional feasibility constrained when switching to a different portfolio (e.g., construction of a new dam): while it is allowed to switch to a new portfolio that introduces the construction of new infrastructures, the contrary (removal of existing infrastructures) is unfeasible, as it is considered unlikely to happen in developing countries. Consequently, moving forward in time, it is only possible to add new elements to the system topology, moving to more complex portfolios.

3. DESIGN (STRATEGIC) MODEL FOR THE ZAMBEZI RIVER BASIN

In this section, we describe all the elements of the design (or strategic) model developed for the ZRB, which builds upon the illustrative, hypothetical water system presented in *Milestone MS34* (*Decision Analytic Framework Architecture Released*).

3.1 WATER SYSTEM MODEL

The main elements of the model are presented considering the topologic scheme of the existing Zambezi system at 2020 displayed in Figure 3.

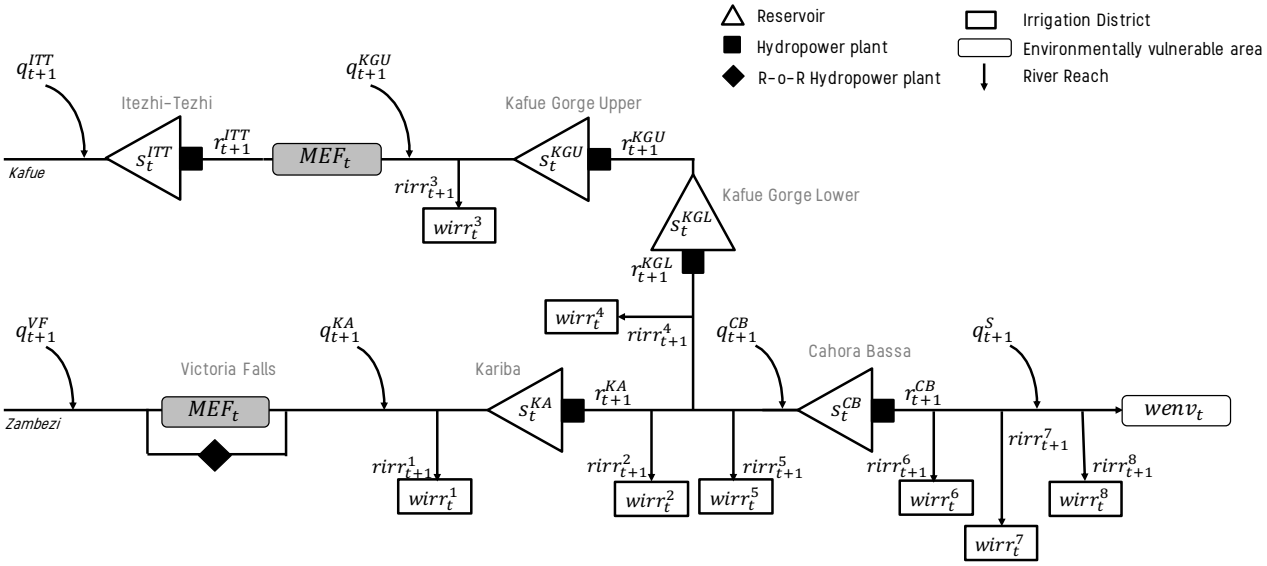

Figure 3 – Topologic scheme of the existing Zambezi system implemented in the strategic model.

As it can be observed, there are several system components that can be grouped into five main categories: five water reservoirs and the associated hydropower plants (including the Kafue Gorge Lower reservoir that is currently under construction), one run-of-the-river hydropower plant (i.e., Victoria Falls), eight irrigation districts, and three environmentally vulnerable river stretches. A monthly modelling time-step is employed to capture the five reservoirs' dynamics through the following water mass balance equations:

$$s_{t+1}^{KA} = s_t^{KA} + (q_{t+1}^{VF} + q_{t+1}^{KA} - rirr_{t+1}^{1}) - e_t^{KA} S_t^{KA} - r_{t+1}^{KA} \quad (6)$$

$$s_{t+1}^{ITT} = s_t^{ITT} + q_{t+1}^{ITT} - e_t^{ITT} S_t^{ITT} - r_{t+1}^{ITT} \quad (7)$$

$$s_{t+1}^{KGU} = s_t^{KGU} + (q_{t+1}^{KGU} + r_{t-1}^{ITT} - rirr_{t+1}^{3}) - e_t^{KGU} S_t^{KGU} - r_{t+1}^{KGU} \quad (8)$$

$$s_{t+1}^{KGL} = s_t^{KGL} + r_{t+1}^{KGU} - e_t^{KGL} S_t^{KGL} - r_{t+1}^{KGL} \quad (9)$$

$$s_{t+1}^{CB} = s_t^{CB} + (q_{t+1}^{CB} + r_{t+1}^{KGL} + r_{t+1}^{KA} - rirr_{t+1}^{2} - rirr_{t+1}^{4} - rirr_{t+1}^{5}) - e_t^{CB} S_t^{CB} - r_{t+1}^{CB} \quad (10)$$

where s_t^r (r = KA, ITT, KGU, KGL, CB) is the storage of the r-th reservoir at the beginning of month t, q_{t+1}^r is the inflow to the reservoir, r_{t+1}^r is the volume of water released, $e_t^r S_t^r$ is the water evaporated in the time interval $[t; t+1)$, and $rirr_{t+1}^{id}$ (id = 1,…,8) represents the water abstracted by the id-th irrigation district according to eq. 6 below. In particular, e_t^r is the mean monthly evaporation rate, while S_t^r is the reservoir surface uniquely defined by a non-linear relation given s_t^r. In order to account for the significant evaporation losses in the Kafue Flats, the evaporation at Kafue Gorge Upper has been calibrated accordingly (Gandolfi, et al., 1997). The actual release of the r-th reservoir is defined as $r_{t+1}^r = f(s_t^r, u_t^r, q_{t+1}^r, e_t^r)$ where $f(\cdot)$ describes the nonlinear, stochastic relation between the release decision determined by the operating policy, i.e. $u_t^r = p(\cdot)$, and the actual release r_{t+1}^r (Piccardi & Soncini-Sessa, 1991). The actual release at the end of the time interval is generally equal to the release decision unless physical constraints prohibit it (e.g., if the prescribed release lies outside the

minimum and maximum allowable releases, if there is insufficient water to meet the prescribed release, or if the prescribed release would result in the reservoir storage capacity being exceeded, and thus spillages occur).

According to the monthly time-step adopted in the model, the river reaches are modelled as plug-flow canals with negligible travel time, in which the velocity and direction of flow are constant everywhere, without any lamination effect. An exception is made for the river reach between Itezhi-Tezhi and Kafue Gorge Upper reservoirs, which requires two months travel time due to the presence of the Kafue Flats.

As for the eight irrigation districts (id = 1,...,8), they can abstract water from the river through a regulated water diversion channel. The volume of water $rirr_{t+1}^{id}$ they can abstract is calculated according to a non-linear hedging rule (Celeste & Billib, 2009). For example, the id = 1 diversion channel upstream of Kariba reservoir is regulated as follows:

$$rirr_{t+1}^{1} = \begin{cases} \min\left(q_{t+1}^{VF} + q_{t+1}^{KA}, wirr_t^1 \cdot \left[\frac{q_{t+1}^{VF} + q_{t+1}^{KA}}{h^1}\right]^{m^1}\right) & if\ q_{t+1}^{VF} + q_{t+1}^{KA} \le h^1 \\ \min\left(q_{t+1}^{VF} + q_{t+1}^{KA}, wirr_t^1\right) & else \end{cases} \quad (11)$$

where $q_{t+1}^{VF} + q_{t+1}^{KA}$ is the volume of water available in the river, $wirr_t^1$ is the monthly water demand, whereas h^1 and m^1 are the parameters regulating the diversion channel. The diversion rules allow hedging the water abstractions to account for downstream users.

As for the three environmentally vulnerable river stretches, the two areas located in the Victoria Falls and along the Kafue Flats (grey rectangles) are protected by Minimum Environmental Flow constraints: the former requires that 250 m^3/s are left in the river every month and cannot be thus diverted to be turbinated by the Victoria Falls run-of-the-river hydropower plant; the latter implies that the Itezhi-Tezhi reservoir is forced to release 40 m^3/s every month, except for March when 315 m^3/s are needed to maintain the natural flooding pattern in the Kafue Flats. In the end, the water volume that is left in the Zambezi River downstream the id = 6, 7, 8 diversion channels, together with the water coming from the confluence with the Shire river, should guarantee adequate environmental conditions to preserve the ecosystem in the river delta. Since no environmental protection of the delta is already in place, we model this environmental interest as an objective function to be used in the pathway design (see the next section).

3.2 OBJECTIVES AND DECISION VARIABLES

Several stakeholders are affected by the operations of the five reservoirs and of the eight irrigation diversions in the ZRB. In the DAFNE project, these conflicting interests are captured by a long set of evaluation indicators which will be evaluated via simulation of the integrated WEF developed in Task 3.2. A subset of these indicators, namely the design indicators selected in Deliverable D5.1 for representing the main components of the WEF nexus, is used here to represent the vector of operating objectives $\boldsymbol{J} = |J^1, \dots, J^K|$ for the DAF optimization. Each single objective function is formulated as follows:

- **Environmental flow deficit** (water):

$$J^W = \frac{1}{h}\left[\sum_{t=0}^{h-1}(\max\left(Qe_t - \bar{r}_{t+1}, 0\right))^2\right] \quad (12)$$

where $Qe_t = 7000\ m^3/s$ is the specified monthly environmental flow in the river delta to be satisfied in February and March only, and $\bar{r}_{t+1} = r_{t+1}^{CB} + q_{t+1}^{S} - rirr_{t+1}^{6} - rirr_{t+1}^{7} - rirr_{t+1}^{8}$ is the amount of water entering the ecosystem in the Zambezi River delta. In particular, r_{t+1}^{CB} is the amount of water released from Cahora Bassa reservoir, q_{t+1}^{S} is the water entering the system after the confluence with the Shire river, whereas $rirr_{t+1}^{6}$, $rirr_{t+1}^{7}$ and $rirr_{t+1}^{8}$ are the water volumes diverted to the id = 6, 7 and 8 irrigation districts respectively. As it can be observed, the squared environmental deficit is averaged across all the months of the evaluation horizon h. In addition, its quadratic formulation aims at penalizing severe deficits within a single time step, while allowing for more frequent, small shortages (Hashimoto, et al., 1982).

- **Hydropower production deficit** (energy):

$$J^E = \frac{1}{Nyears}\left[\sum_{t=0}^{h-1}\sum_{r=1}^{rmax}|Wp_t^r - P_{t+1}^r|\right] \quad (13)$$

where Wp_t^r and $P_{t+1}^r = \eta^r g\gamma \bar{h}_t^r q_{t+1}^{turb,r}$ are the target level of hydropower production (i.e., electricity demand allocated by the Osemosys energy model as described in Deliverable D5.1) and the actual hydropower production of the r-th power plant respectively, and $Nyears$ is the number of years within the evaluation horizon. As for the actual hydropower production P_{t+1}^r at the r-th power plant, $\eta^r\ [-]$ is the turbines efficiency, $g = 9.81\ [m/s^2]$ is the gravitational acceleration, $\gamma = 1000\ [kg/m^3]$ is the water density, $\bar{h}_t^r[m]$ is the net hydraulic head, and $q_{t+1}^{turb,r}\ [m^3/s]$ is the turbinated flow. The annual hydropower production deficit is computed at the ZRB scale by summing the energy deficits occurring at all the existing ($rmax = 5$) operating power plants in each month and averaged across all the years of the evaluation horizon.

- **Normalized irrigation deficit** (food):

$$J^F = \frac{1}{h}\left[\sum_{t=0}^{h-1}\sum_{id=1}^{idmax}\left(\frac{\max\left(wirr_t^{id} - rirr_{t+1}^{id}, 0\right)}{wirr_t^{id}}\right)^2\right] \quad (14)$$

where $wirr_t^{id}$ and $rirr_{t+1}^{id}$ are the irrigation water demand and abstraction of the id-th irrigation district, respectively. As it can be observed, the normalized irrigation deficit is computed at the ZRB scale by summing the normalized deficit occurring at all the existing $idmax = 8$ irrigation districts in each month and averaged across all the months of the evaluation horizon. The normalized formulation allows to weigh all the irrigation districts deficits equally regardless of the magnitude of their demands, thus distributing the overall irrigation deficit almost uniformly among the districts. Therefore, districts characterized by very different demands in terms of their magnitude can be grouped within the same indicator. As in the formulation of the environmental flow deficit, the quadratic formulation aims at penalizing severe deficits within a single time step, while allowing for more frequent, small shortages (Hashimoto, et al., 1982).

The optimal reservoir operation problem requires a vector of sequential release decisions $\boldsymbol{u}_t$ to be taken at discrete time instants based on the current state of the system $(t, \boldsymbol{s}_t)$ (e.g., time, five reservoir storages). Specifically, the vector of release decisions $\boldsymbol{u}_t$ is determined at each time step by a closed-loop operating policy $\boldsymbol{u}_t = p(t, \boldsymbol{s}_t)$, which is optimized with respect to multiple objectives, together with the two time-invariant parameters h^{id} and m^{id} regulating the eight irrigation diversion channels. This multi-objective problem must be solved for each specific combination of infrastructural interventions (i.e., new water reservoir and irrigation expansion), yielding a set of Pareto-optimal operating policies according to the trade-off among conflicting objectives formulated above. Then, the action sequencing optimization requires specifying the best timing τ of infrastructural interventions, along with the update of the operating policy for managing the new system.

Based on the integrated water resources management strategy master plan developed for the ZRB by ZAMCOM (ZAMCOM, 2016), in the design of the pathways we assumed the point of view of a centralized decision maker (e.g., ZAMCOM itself) in charge of managing all water reservoir and irrigation diversions on a basin-wide scale. All the multiple stakeholders with conflicting interests are therefore assumed to act towards the maximization of the global benefit and thus independently from national interests.

3.3 NOMINAL SCENARIO

The optimization of the system management is performed for each portfolio over a historical scenario $\bar{\omega}$, represented by observed hydrologic (i.e., streamflow) and socio-economic factors (e.g., hydropower production targets and irrigation demands), i.e. $\bar{\omega} = \left\{q_1^h; Qe_0^{h-1}; Wp_0^{h-1}; wirr_0^{h-1}\right\}$, presented in *Deliverable 2.1 Baseline Scenario*. On the other hand, the optimization of action sequencing is performed over a reference future scenario $\hat{\omega}$, which includes potential changes in such hydrologic and socio-economic conditions. These changes in the external drivers will trigger new infrastructural

interventions, such as hydropower or irrigated agriculture expansions, for meeting growing energy and food demands across the 2020-2060 time horizon.

Streamflow projections

Streamflow projections for the reference future scenario $\hat{\omega}$ have been assembled by using the precipitation and temperature projections generated by using AWE-GEN-2d (Peleg et al. 2019), a state-of-the-art stochastic weather generator model able to reproduce the historical climate statistics in each of the basins. The model is calibrated on observed data, then used to simulate plausible future climates at high resolution by applying factors of change to the main climate variables as described in Deliverable D2.2. To calculate the factors of change, we analysed an ensemble of 22 Regional Climate Model (RCM) and General Circulation Model (GCM) pairs and compared the changes in meteorological variables (e.g. precipitation, temperature) between a historical control period (1976-2005) and the simulations of the future climate.

To simulate the hydrological processes in the study area, the ZRB has been divided into different sub-catchments acting as primary hydrological units, being the entire Zambezi basin geographically and climatologically heterogeneous. After identifying their boundaries through a 1 km x 1 km Digital Elevation Model (DEM), the drainage direction and area for each sub-catchment has been identified by fixing a specific outlet point for each sub-catchment at the same location where historical streamflow data were recorded. The resulting eight sub-catchment areas are displayed in

Figure 4 and correspond to Victoria Falls (light green), Itezhi-Tezhi (light blue), Kafue Flats (dark blue), Kariba (dark green), Cahora Bassa (yellow), Luanwga (orange), Shire (red), and the Delta (pink) hydrological units.

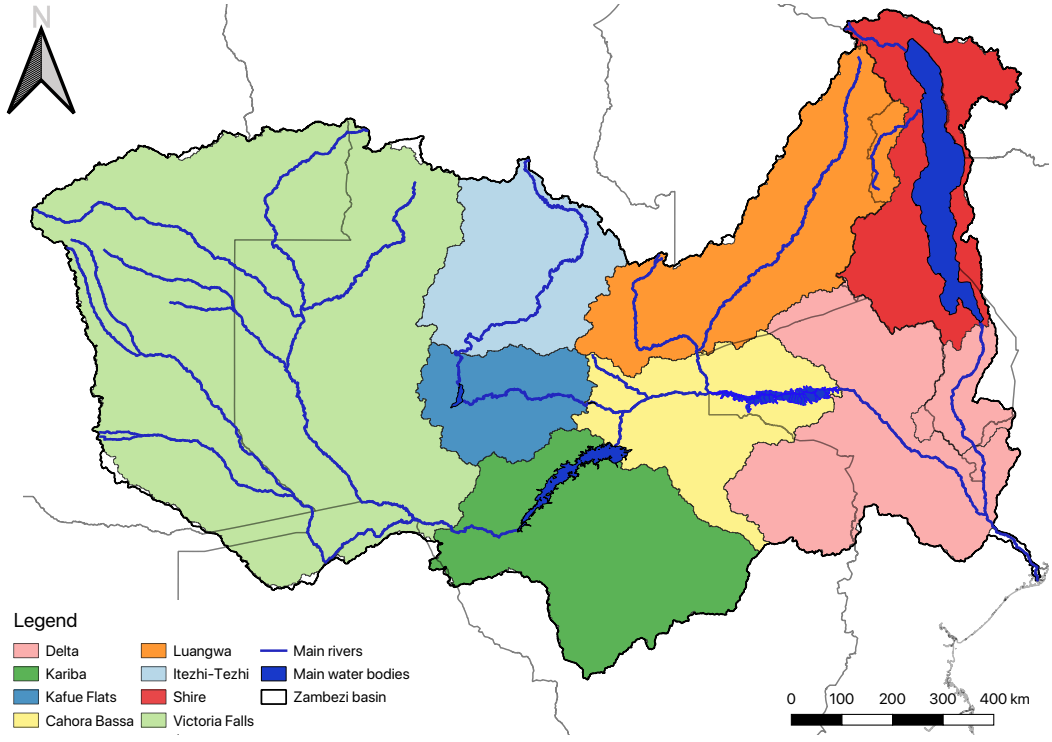

Figure 4 – Zambezi river basin divided into eight sub-catchments acting as primary hydrological units.

For each of these eight sub-catchments, future streamflow projections have been produced following three different methodological approaches, namely the well-known conceptual hydrologic *Hydrologiska Byras Vattenbalansavdelning* (HBV) model (Lindström, et al., 1997), an Artificial Neural Network (ANN), and a coefficient of proportionality. HBV models have been implemented for the Victoria

Falls, Itezhi-Tezhi and Luangwa sub-catchments. The HBV model was originally developed for operational flood forecasting in Sweden, and relies on four storage units, one for snow (which we neglected) and the other three for different soil layers. It requires two inputs, namely precipitation and temperature over the sub-catchment, and it provides the discharge from the sub-catchment as output. Each of the three HBV models implemented has been calibrated and validated over a 25-years dataset of historical records (1981-2005), splitted into a calibration (2/3 of the historical records length) and a validation (1/3 of the historical records length) dataset. The fitness of the model to the observations during both calibration and validation has been quantified according to two metrics, both to be maximized: the Nash Sutcliffe Efficiency (NSE) and the Pearson coefficient. The former can range from -∞ to 1, where NSE=1 indicates a perfect match between the modelled and observed discharge, whereas the latter measures the linear correlation between the modelled and observed discharge and can vary between -1 (negative linear correlation) and 1 (positive linear correlation). Table 1 reports the values of both the NSE and Pearson coefficient metrics calculated for all three sub-catchments during both the calibration and validation phase. For further details about the HBV model and its calibration/validation, please refer to Benigni and Raimondo (2018).

Table 1 – Values of the NSE and Pearson coefficient metrics for the Victoria Falls, Itezhi-Tezhi, and Luangwa sub-catchments during both calibration and validation phase.

Sub-catchment	Calibration		Validation	
	NSE	Pearson Coeff	NSE	Pearson Coeff
Itezhi-Tezhi	0.87	0.94	0.83	0.93
Victoria Falls	0.72	0.85	0.60	0.86
Luangwa	0.73	0.86	0.84	0.93

Modelling the hydrological processes in the Shire sub-catchment resulted more challenging due to the presence of Lake Malawi, whose complex dynamics and large inter-temporal variation and regulation in the levels and releases (defining the Shire river discharge into the main stem of the Zambezi river) cause the HBV model to be inefficient in capturing the relation between climatic variables (i.e., precipitation and temperature) over the entire Shire sub-catchment and the Shire river discharge itself. It was therefore necessary to first model the net inflows to Lake Malawi by means of ANN, which allows reproducing negative net inflows (occurring when evapotranspiration losses exceed the contribution of inflow and precipitation) that cannot be modelled via HBV, and then describe the Lake Malawi storage dynamics. The simulated outflows from Lake Malawi represents the Shire River discharge flowing into the main stem of the Zambezi river. For further details about the ANN model and its calibration, see Benigni and Raimondo (2018).

As far as the Kariba and Kafue Flats sub-catchments are concerned, a strong relation holds with Victoria Falls and Itezhi-Tezhi streamflow respectively. For instance, under historical conditions the Kafue Flats lateral contribution has been estimated to be 30% of the Itezhi-Tezhi inflow (Gandolfi, et al., 1997; Tilmant, et al., 2010), whereas the Kariba lateral contribution has been calculated to be 10% of the Victoria Falls discharge (Balon & Coche, 2012). The same percentage factors have been applied to both the Victoria Falls and Itezhi-Tezhi projected streamflow estimated via HBV model to obtain the future lateral contribution of both the Kafue Flats and Kariba sub-catchments.

In the end, the Cahora Bassa and Delta contributions have been assumed to depend upon the upstream discharges only. They are therefore directly calculated within the water system model when simulating the water reservoir mass balance equations and irrigation water diversions under the reference future scenario $\hat{\omega}$.

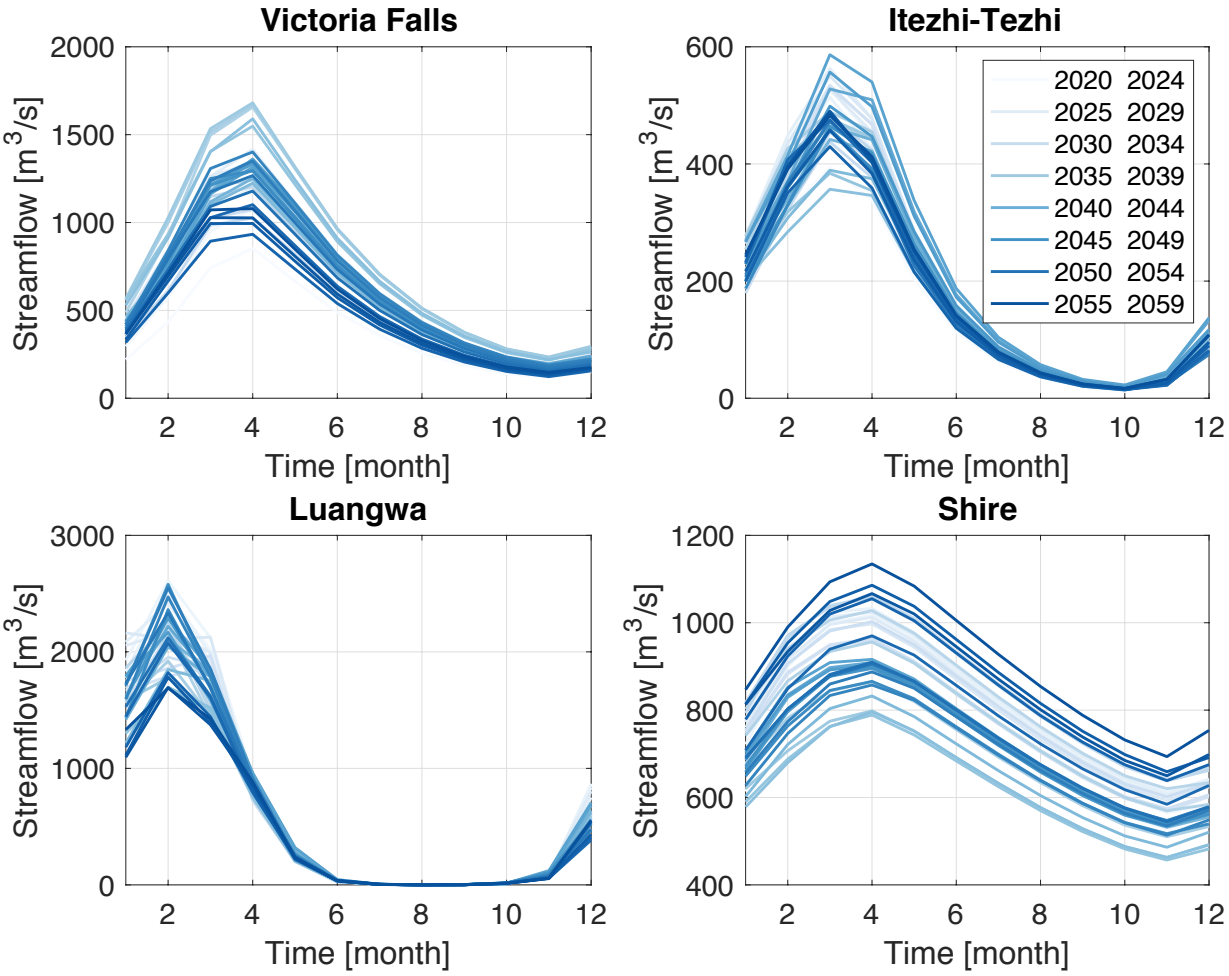

Figure 5 – Monthly streamflow for the Victoria Falls, Itezhi-Tezhi, Luangwa, and Shire sub-catchments in the over the 2020-2060 time horizon. Each colour identifies a group of five years, with lighter colours at the beginning of the evaluation horizon and darker colours towards the end.

Figure 5 shows the projected streamflow in four different sub-catchments, namely Victoria Falls, Itezhi-Tezhi, Luangwa and Shire, over the 2020-2060 time horizon. A trend exists for the first three sub-catchments, showing a potential streamflow reduction as we approach 2060 (lighter colours). It is also striking to notice that the share of inflows coming from the Luangwa sub-catchment is almost null during the dry period ranging from July to October, regardless of the year considered. As for the Shire sub-catchment, no clear trend exists, since the Shire discharge is highly influenced by the presence of a large, partly regulated lake.

Hydropower production targets projections

Following the methodological approach described in Deliverable D5.1, the projections of future hydropower production targets at the single hydropower plant level for both existing and planned infrastructures for the reference future scenario $\hat{\omega}$ are generated using the Osemosys energy model (Howells, 2011). The resulting targets are then increased following the overall energy demand trends described in Deliverable D2.2, up to the maximum installed capacity of each hydropower plant. Figure 6 shows the projected hydropower production targets [TWh/yr] at each of the existing/planned hydropower plants throughout the 2020-2060 evaluation horizon. All the power plants are characterized by an increasing production target, except for Itezhi-Tezhi, whose target was already matching its maximum installed capacity before applying the energy demand increasing trends. Moreover, Cahora Bassa is associated to the highest demand because it has the largest installed capacity among all the power plants in the ZRB.

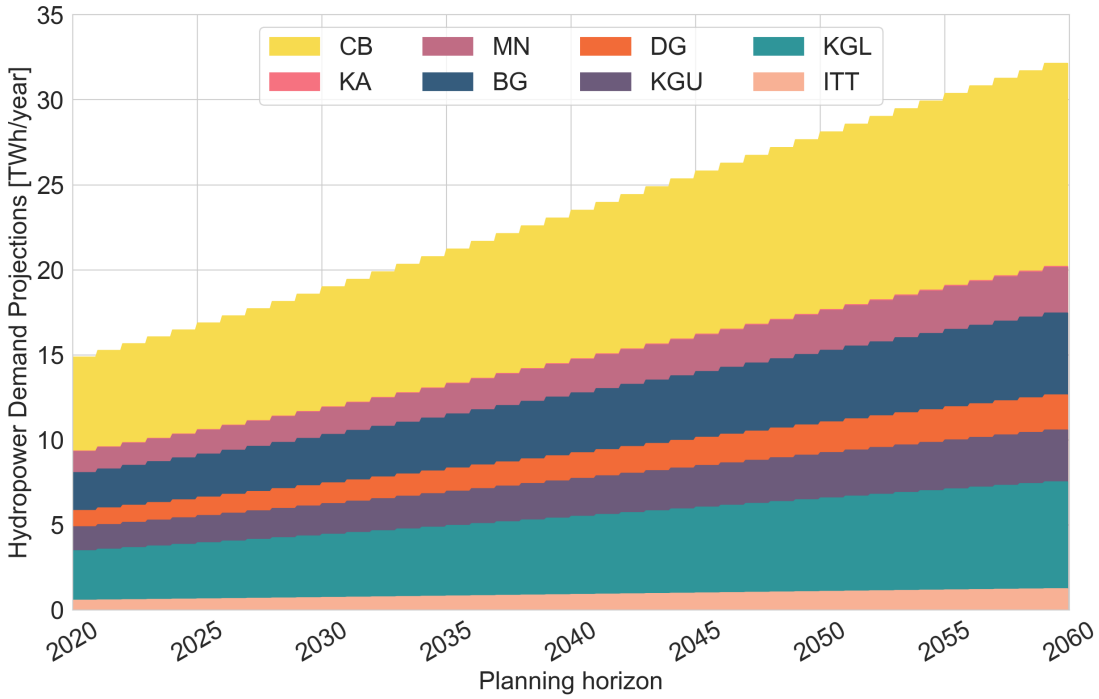

Figure 6 – Projected hydropower production targets [TWh/yr] at each existing/planned hydropower plant over the 2020-2060 horizon.

Irrigation demands projections

Irrigation demands projections for the reference future scenario $\hat{\omega}$ (Figure 7) have been generated by using the AquaCrop model (FAO, 2018). Specifically, these projections are the result of summing three components: currently existing irrigation schemes, irrigation schemes planned for the near future, and irrigated maize cultivation during the dry season to compensate projected food shortages. Water demands for these three components were calculated in AquaCrop by using the methodology described in Deliverable D2.2, and assuming a 45% irrigation efficiency. Further, the projected precipitation and temperature, the soil characteristics from ISRIC soil grids[1], and the default crop parameters available in AquaCrop were used as input for the crop model.

The simulations show that irrigated maize yield is expected to decrease under the RCP 4.5 scenario, while irrigated sugarcane yield is expected to increase. Irrigation demands are expected to increase, largely due to planned sugarcane developments on the one hand, and on the other hand increased irrigation of food crops for local consumption, aiming to achieve a local food calorie and protein balance in the sub-basins for which a calorie or protein deficit was predicted. In Figure 7, an increase in irrigation demand is illustrated for irrigation districts 3 and 4, located in sub-basin[2] 12261 (Kafue sub-basin), which contains large, already existing sugar estates.

[1] www.soilgrids.com

[2] HydroSHEDS Pfaffstetter level 5 subbasins (https://www.hydrosheds.org)

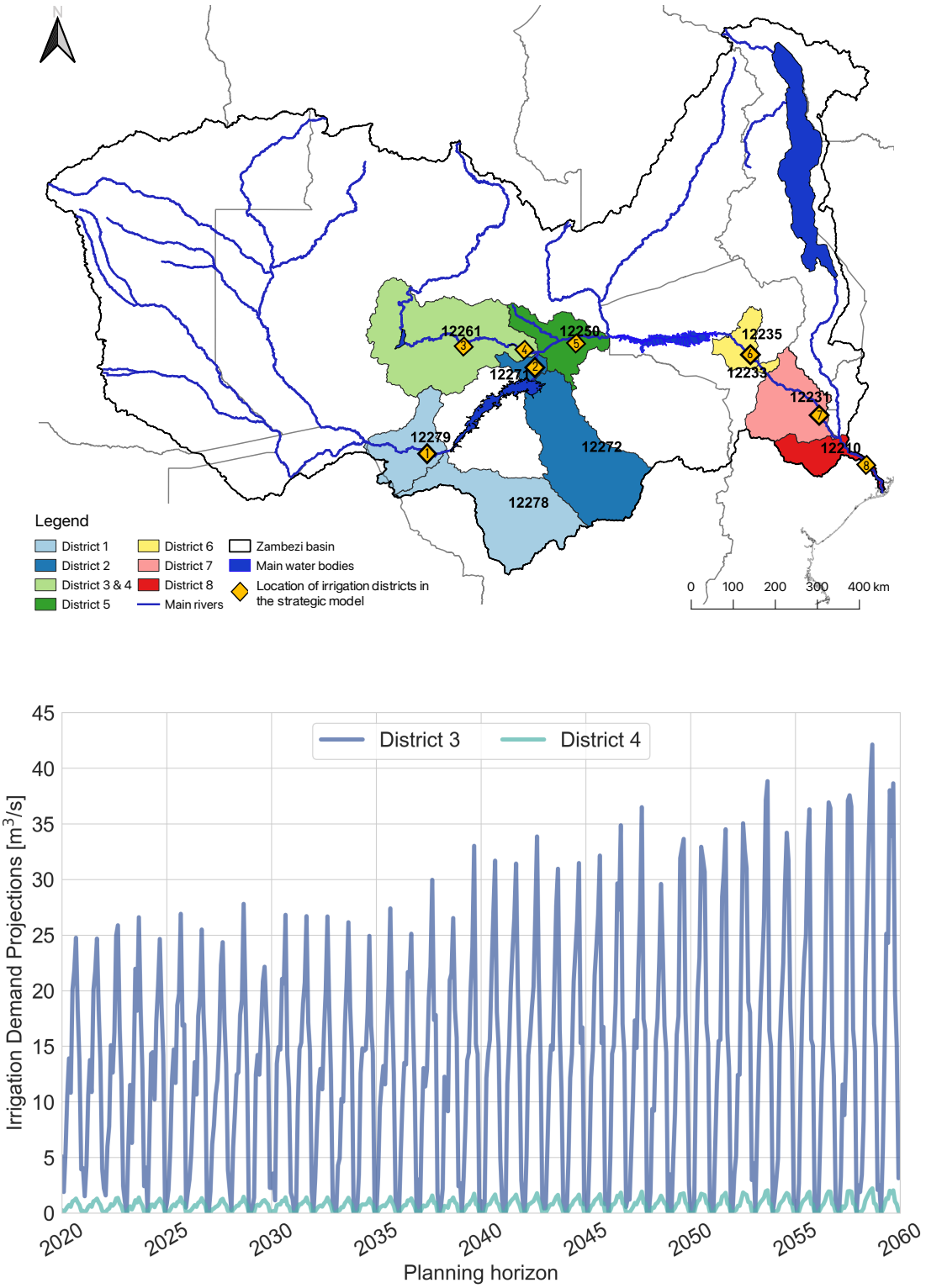

Figure 7 – Top panel - Assignment of the irrigation districts modelled in AquaCrop (see Deliverable D2.2) to the irrigation diversion channels in the strategic model. Bottom panel – projected irrigation demands over the time period (2020-2060) for two representative districts along the Kafue River.

4. PATHWAYS FOR THE ZAMBEZI RIVER BASIN

In this chapter, we present and discuss the pathways designed for the ZRB: we first analyse only the re-operation of the existing system; secondly, we report the results of the simulations of the five candidate pathways derived from the SHs suggestions and introduced in Deliverable D5.1; lastly, we investigate the performance of the efficient pathways designed using the DAF optimization.

4.1 OPTIMAL SYSTEM RE-OPERATION

The optimal ZRB system re-operation has been identified by optimizing only the management of the existing system (see Figure 3) with respect to the operating objectives and decision variables discussed in the previous chapter under the historical scenario $\bar{\omega}$, represented by observed hydrologic (e.g., streamflows) and socio-economic factors (e.g., energy and food demand).

The optimization results of the ZRB system re-operation are displayed in Figure 8 using a parallel axes plot (Inselberg, 1997) for understanding the key interactions and trade-offs among the three optimization objectives (i.e., minimization of hydropower, environmental and irrigation deficits formulated in section 3.2). Each of the solutions of the management optimization problem, namely the Pareto-optimal operating policies of the ZRB system (i.e., the operating policy of each dam and diversion dam in the system), is represented as a grey line crossing the three vertical axes, representing the three objectives, at the values of their associated performance. The values of the objectives are normalized between their minimum and maximum values and the ideal solution would be a horizontal line along the top of all the axes. The conflicts are displayed as diagonal lines between two adjacent axes. In Figure 8, four solutions are highlighted, namely three extreme operating policies minimizing each of the three objectives independently (purple, green, and blue lines for minimum hydropower, environmental, and irrigation deficits, respectively) and a compromise policy (pink line) achieving a satisfactory performance across all objectives. Figure 8 shows a clear trade-off between hydropower and environmental deficits, as the minimum hydropower deficit is attained when maximizing the environmental deficit and vice versa (purple and green lines). Since the environmental objective forces the reservoirs to release significant water volumes to meet the environmental flow requirement in the Delta, such water volumes cannot be stored in the reservoirs to produce enough hydropower and satisfy the production target. A smaller conflict also holds between hydropower/environmental and irrigation deficits, as irrigation is a consumptive water use that takes water away from the system.

To better understand the implications of the trade-offs illustrated in Figure 8, we analysed the simulated dynamics of the ZRB system under different operating policies. The cyclo-stationary inflow, storage and release monthly average trajectories for each of the five reservoirs (i.e., Itezhi-Tezhi, Kafue Gorge Upper, Kafue Gorge Lower, Kariba, and Cahora Bassa) are displayed from Figure 9 to Figure 13, respectively. Grey lines refer to the system dynamics simulated under all the Pareto-optimal policies, whereas the system trajectories attained under the three extreme and a compromise operating policies highlighted in Figure 8 are displayed as purple, green, blue, and pink lines, respectively.

Figure 9 and Figure 10 show the system dynamics for the Itezhi-Tezhi and Kariba reservoirs respectively. A single inflow trajectory is displayed in both **Figure 9**a and Figure 10a because both Itezhi-Tezhi and Kariba do not have any other reservoir upstream, thus their inflow corresponds to an observed streamflow record, which does not change according to the different operating policies that can be employed to manage the entire ZRB system. Both historical inflow records present a peak in February/March/April that corresponds to the high seasonal streamflow peak characterizing the ZRB hydrology. Multiple storage and release trajectories are instead plotted in Figure 9b/Figure 10b and Figure 9c/Figure 10c based on the trade-off operating policy selected to operate the system. Regardless of the operational trade-off considered, however, both Itezhi-Tezhi and Kariba reservoirs are mostly operated with the same annual strategy, following the inflow pattern (e.g., the Itezhi-Tezhi release trajectory presents a clear peak in March that corresponds to the maximum peak observed in its inflow records) and keeping the monthly average storages and releases within a restricted range of variability.

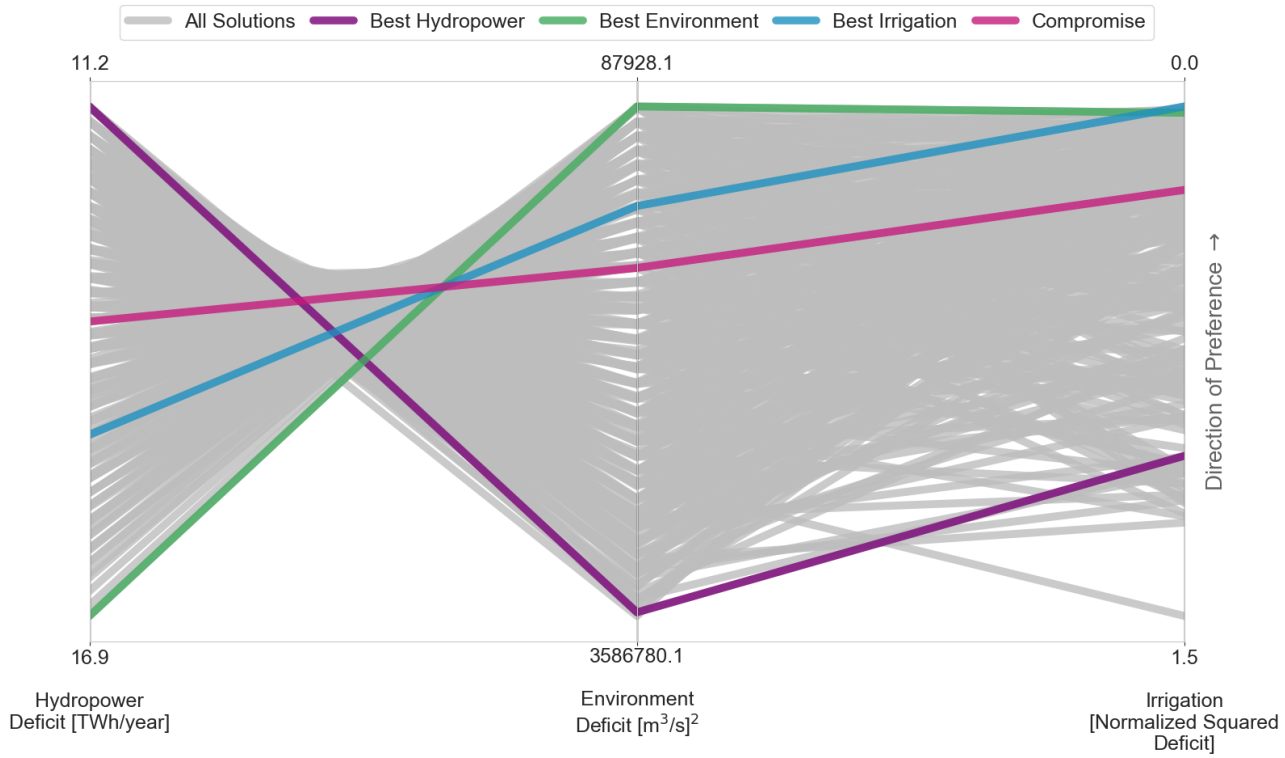

Figure 8 – Parallel axes plot representation of the ZRB trade-offs, where the three objective values are normalized between the minimum and maximum of each objective and the axes are oriented so that the direction of preference is always upward. All the Pareto-optimal policies are represented as grey lines, with four selected trade-off policies highlighted by different colours.

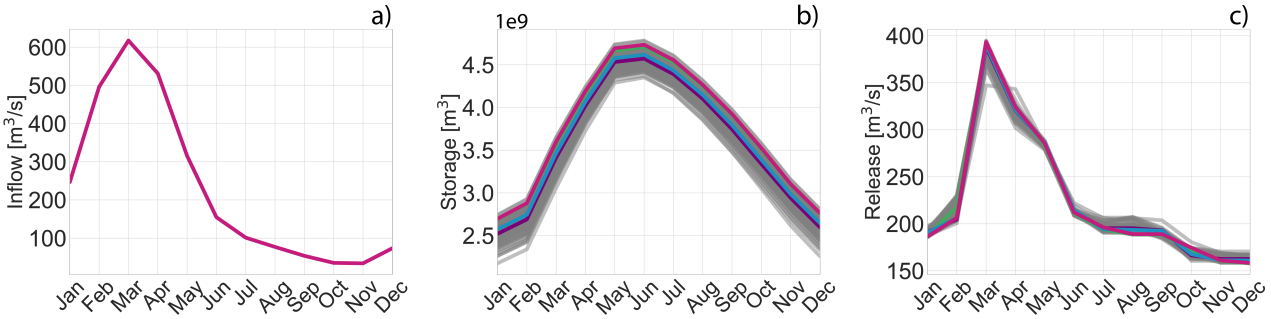

Figure 9 – Cyclo-stationary inflow (panel a), storage (panel b) and release (panel c) monthly average trajectories for the Itezhi-Tezhi reservoir. Grey lines identify the system dynamics attained under all the Pareto-optimal operating policies shown in Figure 8; coloured lines represent the best Hydropower (purple), best Environment (green), best Irrigation (blue), and compromise (pink) policies selected in Figure 8.

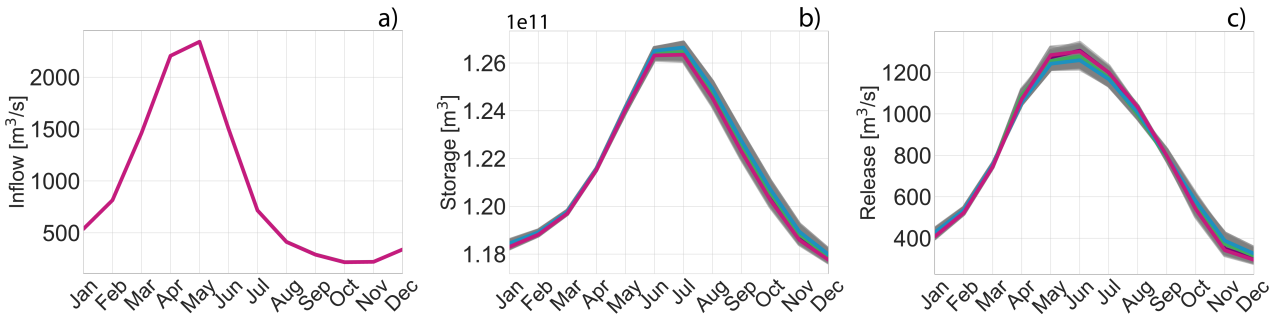

Figure 10 – Cyclo-stationary inflow (panel a), storage (panel b) and release (panel c) monthly average trajectories for the Kariba reservoir. Grey lines identify the system dynamics attained under all the Pareto-optimal operating policies shown in Figure 8; coloured lines represent the best Hydropower (purple), best Environment (green), best Irrigation (blue), and compromise (pink) policies selected in Figure 8.

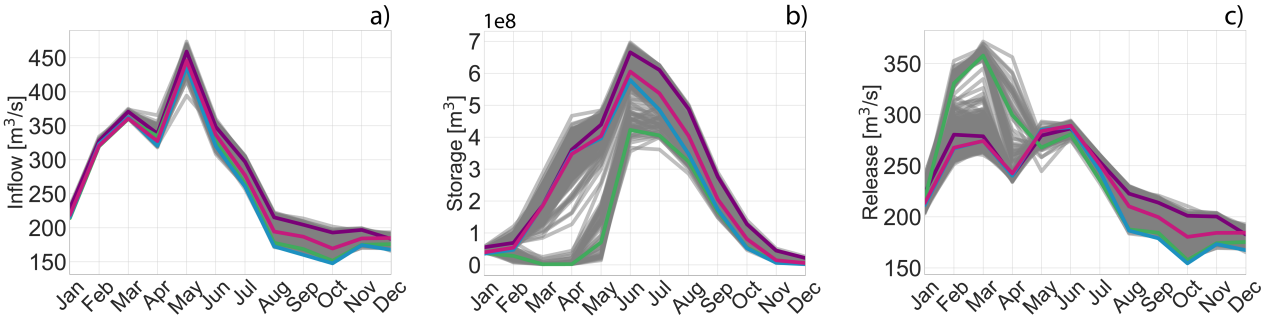

Figure 11 – Cyclo-stationary inflow (panel a), storage (panel b) and release (panel c) monthly average trajectories for the Kafue Gorge Upper reservoir. Grey lines identify the system dynamics attained under all the Pareto-optimal operating policies shown in Figure 8; coloured lines represent the best Hydropower (purple), best Environment (green), best Irrigation (blue), and compromise (pink) policies selected in Figure 8.

Figure 11 shows the system dynamics for the Kafue Gorge Upper reservoir. Since Kafue Gorge Upper is located downstream the Itezhi-Tezhi reservoir, its inflow trajectory shown in Figure 11a now changes according to the operating policy chosen to operate the entire ZRB system, including the upstream Itezhi-Tezhi reservoir. This inflow trajectory presents two peaks, namely a seasonal peak in February/March/April observed in the lateral streamflow contribution of the Kafue Flats, and a second peak in May that corresponds to the Itezhi-Tezhi release peak in March delayed by two months due to the two months travel time through the Kafue Flats (see Section 3.1). Multiple storage and release trajectories produced by different policies are plotted in Figure 11b and Figure 11c and correspond to alternative trade-offs. Regardless of the operational trade-off considered, however, the Kafue Gorge Upper reservoir is always operated following the double-peak inflow pattern and keeping the monthly average storages and releases within a restricted range of variability across all the months of the average cyclo-stationary year. However, an exception is made for the operating policy minimizing the environmental deficit in the Delta (green line), which aims at satisfying the environmental flow target of 7000 m^3/s in February and March in the Zambezi River delta. When the entire ZRB system is operated under this policy, Kafue Gorge Upper avoids storing water by releasing the total water volume entering the reservoir in February and March in order to help the downstream part of the system to meet the environmental flow requirement. This causes the reservoir storage to be almost empty during the first months of the year. Kafue Gorge Upper then exploits the second inflow peak in May to refill the reservoir and continue following the inflow pattern in its release trajectory until the end of the year.

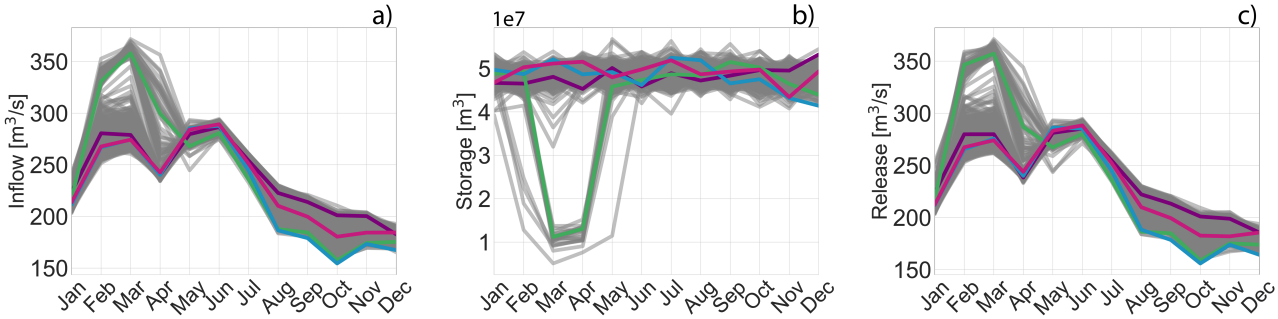

Figure 12 – Cyclo-stationary inflow (panel a), storage (panel b) and release (panel c) monthly average trajectories for the Kafue Gorge Lower reservoir. Grey lines identify the system dynamics attained under all the Pareto-optimal operating policies shown in Figure 8; coloured lines represent the best Hydropower (purple), best Environment (green), best Irrigation (blue), and compromise (pink) policies selected in Figure 8.

Figure 12 shows the system dynamics for the Kafue Gorge Lower reservoir, for which almost all the considerations made for the Kafue Gorge Upper reservoir still hold. Since Kafue Gorge Lower is located downstream the Kafue Gorge Upper reservoir, its inflow trajectory in Figure 11a corresponds to the Kafue Gorge Upper releases and changes according to the considered operating policy. This inflow trajectory presents two peaks, as discussed for the Kafue Gorge Upper release trajectory in Figure 11c. Again, multiple storage and release trajectories are plotted in Figure 12b and Figure 12c based on the selected operating policy. However, regardless of the considered trade-off, the Kafue Gorge Lower reservoir is always operated keeping the storage always at its full capacity in order to exploit the reservoir hydropower potential. Once again, the operating policy minimizing the environmental deficit in the Delta (green line) is the only solution that forces Kafue Gorge Lower to change its dynamics: as in the case of Kafue Gorge Upper, this solutions releases the total water volume entering the reservoir in February and March in order to help the downstream part of the system to meet the environmental flow requirement in the delta. Since the Kafue Gorge Lower reservoir can store very small water volumes, an apparently small difference of about 15 m^3/s (3.6 m^3/month) between inflow and release (with the release being higher than the inflow) in February causes the reservoir storage to significantly drop at the beginning of March. The opposite happens in April, when the inflow is about 15 m^3/s (3.6 m^3/month) higher than the release, driving the storage back up to its almost full capacity at the beginning of May.

Figure 13 shows the system dynamics for the Cahora Bassa reservoir. Since Cahora Bassa is the most downstream reservoir within the ZRB system, its inflow trajectory shown in Figure 13a is given by the observed streamflow record of the Luangwa tributary and both Kariba and Kafue Gorge Lower releases. However, since the Kariba releases are almost the same regardless of the operational trade-off considered (Figure 10c), and the difference in the Kafue Gorge Lower releases among different operating policies (Figure 12c) is negligible with respect to the magnitude of the Kariba releases and the Luangwa lateral contribution, the Cahora Bassa inflow trajectories do not differentiate substantially across all the different policies. These inflow trajectories present two peaks, namely a seasonal peak in February/March observed in the lateral streamflow contribution of the Luangwa tributary, and a second smaller peak in May/June that corresponds to the Kariba and Kafue Gorge Lower release peaks. Multiple storage and release trajectories of the Cahora Bassa reservoir are plotted in Figure 13b and Figure 13c based on the trade-off operating policy selected to operate the system. Differently from all the other reservoirs, the Cahora Bassa dynamics change significantly according to the selected trade-off. When operated under the policy minimizing the hydropower deficit (purple line), Cahora Bassa keeps the releases almost constant and equal to 1500 m^3/s to maximize its hydropower production and, consequently, meet its production target. As a consequence, it is able to partially store the 2500 m^3/s inflow peak occurring in March/April, allowing the associated storage trajectory to grow and reach its highest peak around May/June. On the other hand, when operated under the policy minimizing the environmental deficit (green line), Cahora Bassa releases almost 6000 m^3/s in February and March to satisfy the environmental flow requirement in the Delta, causing its storage to drop in March/April. From April on, Cahora Bassa reduces its releases to 500 m^3/s, allowing to store almost all the water flowing into the reservoir to reach its full capacity at the end of the year and then release again large volumes of water during February/March of the following year. When the reservoir is operated under either the compromise policy (pink line) or the one minimizing the irrigation deficit (blue line), its dynamics presents a storage-release pattern that looks similar to the one obtained under the policy minimizing the environmental deficit, yet less pronounced. This is due to the fact that both the best irrigation and the compromise policies attain a very low environmental deficit value, close to its minimum value (see the parallel-axes plot in Figure 8). These results suggest that the hydropower-environment conflict is almost fully concentrated in the operation of Cahora Bassa reservoir. In fact, being the most downstream reservoir in the ZRB system and having the largest storage capacity after Kariba, Cahora Bassa results to be the reservoir mostly responsible to release water for meeting the 7000 m^3/s flow requirement in the delta.

To sum up, the analysis of the reservoirs dynamics attained under the optimal system re-operation reveals that there is not much variability in the behaviour across most of the reservoirs/trade-offs. An exception is made for the Kafue Gorge Upper and Lower reservoirs when operated under an

environmental-prone operating policy, which draws down both reservoirs storages in March and April releasing large water volumes in order to help the downstream part of the basin to meet the environmental flow requirement in the delta. Another exception is made for the Cahora Bassa reservoir. When operated under an hydropower-prone operating policy, releases are kept almost constant in order to maximize hydropower production. In all the other cases, Cahora Bassa always aims at releasing more in February and March in order to at least partially satisfy the environmental flow requirement in the delta.

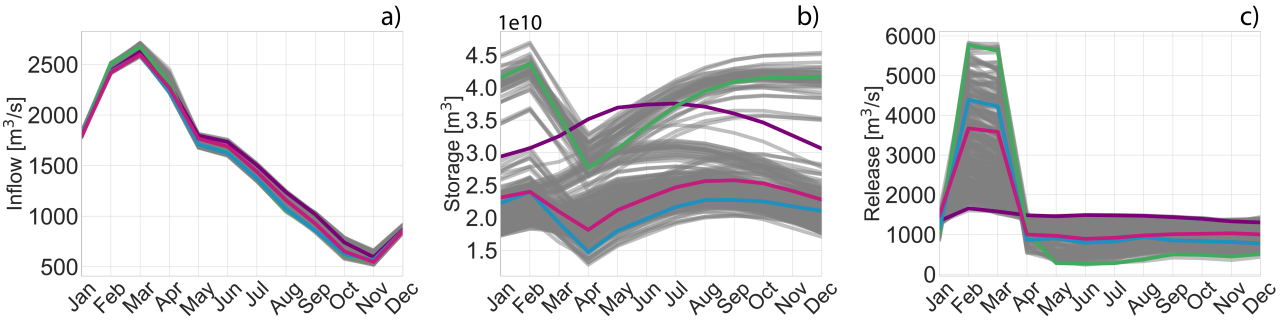

Figure 13 – Cyclo-stationary inflow (panel a), storage (panel b) and release (panel c) monthly average trajectories for the Cahora Bassa reservoir. Grey lines identify the system dynamics attained under all the Pareto-optimal operating policies shown in Figure 8; coloured lines represent the best Hydropower (purple), best Environment (green), best Irrigation (blue), and compromise (pink) policies selected in Figure 8.

4.2 SIMULATION OF CANDIDATE PATHWAYS

The candidate pathways proposed in Deliverable D5.1 are briefly summarised in Figure 14-Figure 18.

Business As Usual (BAU) pathway features five reservoirs and their associated hydropower plants, 1 run-of-the-river hydropower plant (black diamond), 8 major irrigation districts (white rectangles) and three environmentally vulnerable areas (i.e., Victoria Falls and Kafue Flats (grey rectangles - protected by Minimum Environmental Flow constraints), along with the Delta (white rectangle – modelled as objective function). This pathway corresponds to the topologic scheme displayed in Figure 3 and already includes Kafue Gorge Lower, which is already under construction, to reflect the system configuration for the planning horizon from 2020-2060. The current operation of the full system is driven by the hydropower interest.

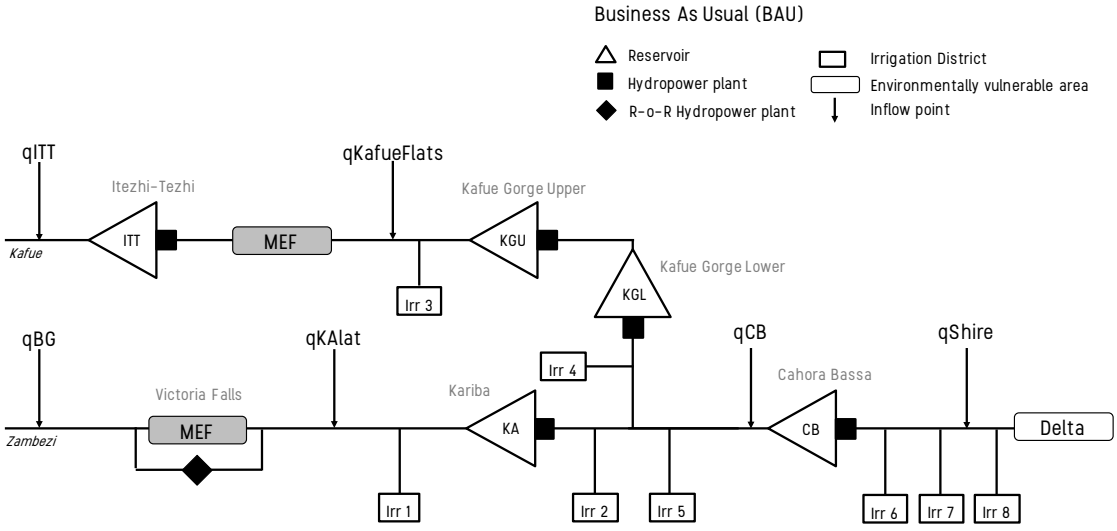

Figure 14 – Business as usual scenario with 5 reservoirs with a hydropower maximizing operating policy.

Food pathway focuses on the development of the food sector. In this pathway, the irrigation districts 1-7 are specified since the beginning of the planning period in 2020, and an 8th irrigation district on the border between Malawi and Mozambique is added in 2031. The operation of the system is driven by minimizing the water supply deficits across all the irrigation districts.

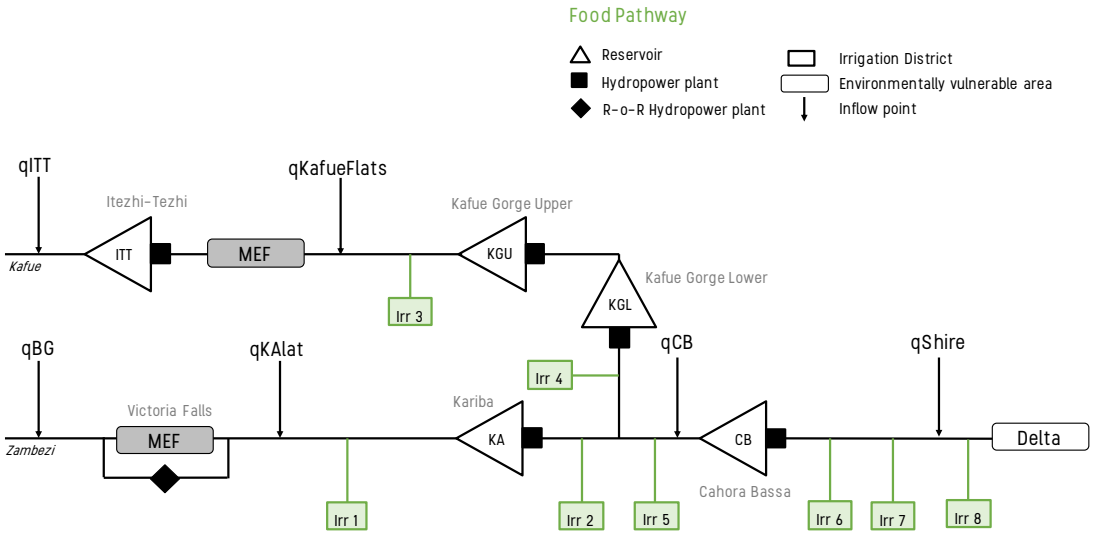

Figure 15 – Food pathway corresponding to the development of irrigated agriculture.

Energy pathway focuses on the development of the energy sector. This pathway includes the construction of three planned dam projects, Batoka Gorge, built at the beginning of the planning horizon in 2020, followed by the construction of Mphanda Nkuwa in 2026, and that of Devil's Gorge in 2029. The existing and planned dams are operated with a hydropower prone policy that minimizes energy deficit relative to the projections of the hydropower production targets shown in Figure 6.

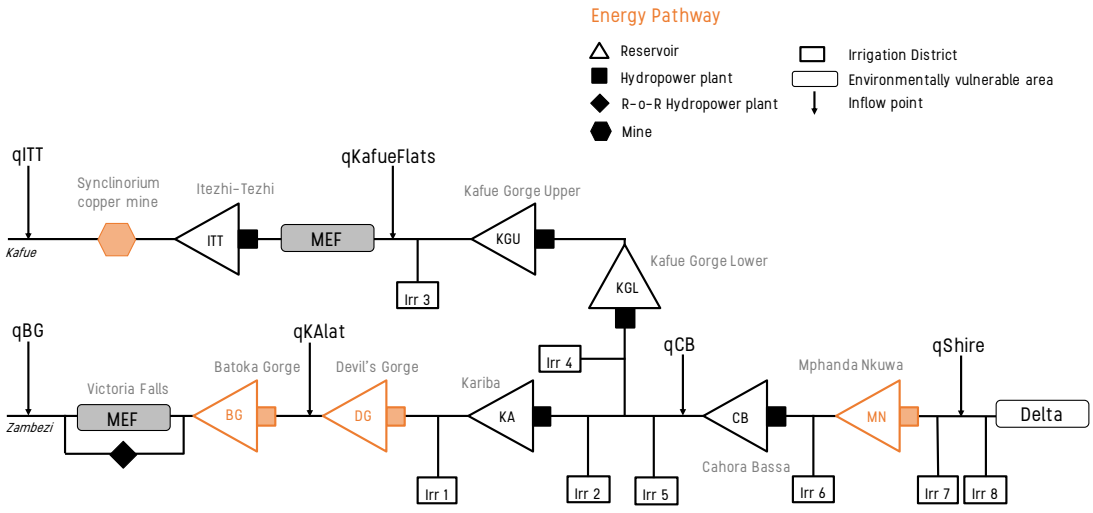

Figure 16 – Energy pathway corresponding to the full development of the energy sector.

Water pathway focuses on the preservation of natural ecosystems and hydrological regimes in the basin. This pathway favors a regulation of the existing hydropower reservoirs and irrigation diversions aimed to preserve natural flood regimes in the Zambezi Delta. The system is operated under

an environmental strategy aimed at minimizing the squared deficit relative to the required environmental flows in the Delta, constraining the environmental requirements to the Kafue flats and Victoria falls.

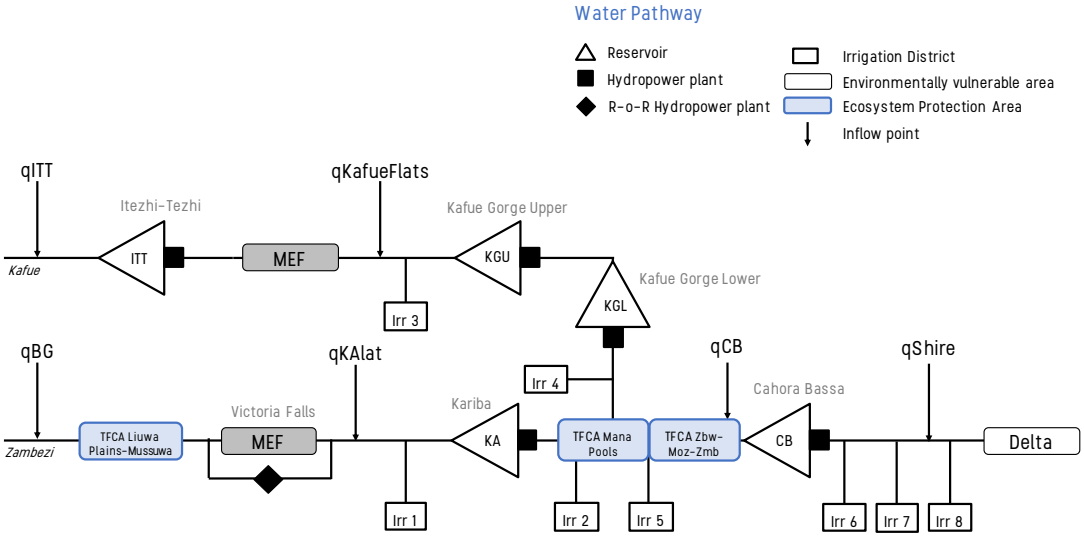

Figure 17 – Water pathway focused on the preservation of the natural ecosystem and hydrological regimes.

Full economic expansion pathway focuses on a balanced development of the energy and food sectors, while preserving the ecosystem requirements. This pathway includes the construction of Batoka Gorge in 2026, and the expansion of irrigated land in 2018 (Mozambique/Zimbabwe) and in 2031 (Mozambique/Malawi). Both the existing and planned reservoirs/irrigation water diversion schemes will be operated with respect to a balanced compromise between conflicting objectives for hydropower production, irrigation water supply deficit, and environmental deficit in the Delta.

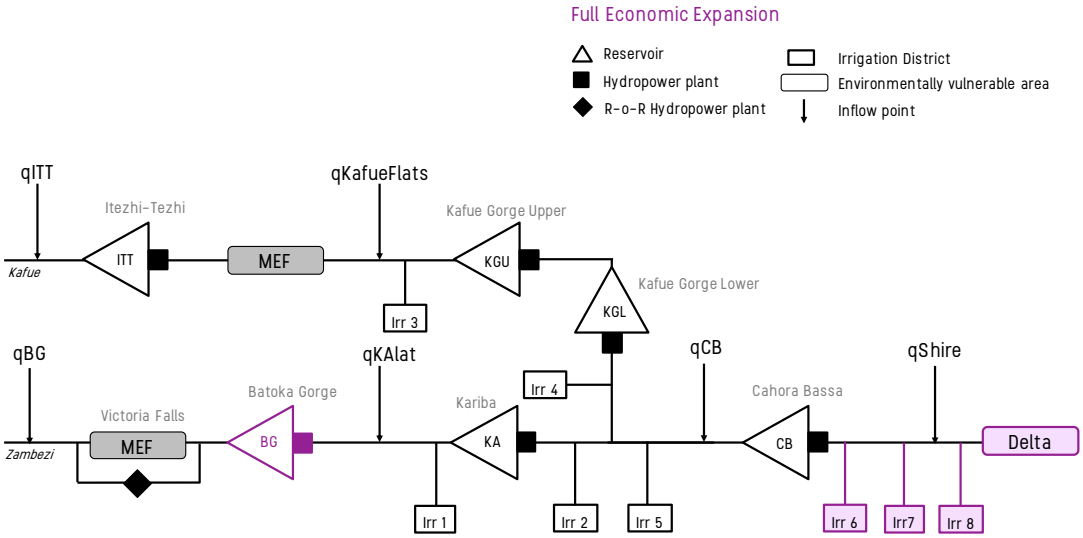

Figure 18 – Full economic expansion pathway focused on a balanced development of both energy and food sectors, while still preserving the ecosystem requirements.

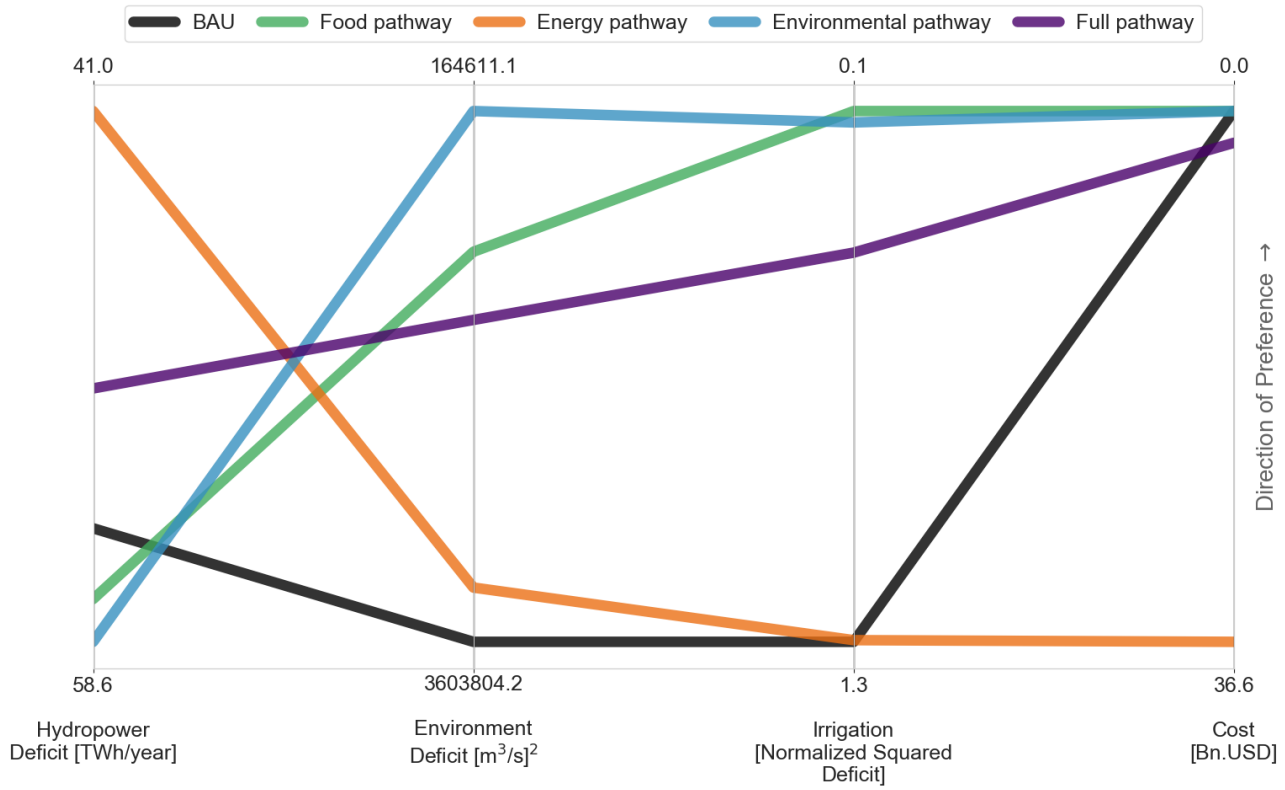

Figure 19 – Trade-offs of the candidate pathways across water, energy and food indicators, as well as construction costs of new dam projects.

Figure 19 depicts the system's trade-offs under the ZRB candidate pathways, where we evaluate each pathway based on its performance for hydropower, environment and irrigation, as well as the cost of infrastructure development. The parallel coordinates show the best attainable solution at the top of each axis; the preferred solution would therefore be a horizontal line on top of the coordinates. Each line shows the average performance across the planning horizon from 2020-2060. It is worth noting that the candidate pathways characterized by the construction of new dams, such as the full economic pathway and the energy pathway, do achieve an improvement in minimizing the hydropower deficit. However, they are not able to fully meet the energy targets shown in Figure 6 based on projections of population growth in the ZRB. The hydropower deficit gap is wider relative to the re-operation results in Figure 8, where constant hydropower targets are used to find Pareto approximate operating policies. In the best re-operation case, we observed a deficit of 11 TWh/year whereas here with increased production targets, we observe a deficit of 41 TWh/year in the energy pathway which is expressly designed to minimize this deviation. Even with the capacity expansion, the rapid population growth rates triggering energy demands cause a large average hydropower deficit for the entire planning horizon. Furthermore, there is a strong trade-off between the water pathway and the energy pathway, which is consistent with the observed re-operation trade-offs in Figure 8. The water pathway is operated to favour the environmental flow requirements in the Delta, potentially decreasing the head for hydropower production during the months of critical environmental flows generating the observed conflict. Another conflict is observed between the energy and the food pathway. In the latter case, the system is operated with a policy that prioritizes the minimization of irrigation deficit for each of the planned districts in Figure 15. As water is diverted to meet irrigation targets, this is expected to be in conflict with the storage available for hydropower production. As for the Business as usual pathway in black, it performs poorly for irrigation and the environment since it is operated to favour solely hydropower. However, the improvements to hydropower production under this scenario seem minor relative to the food and water pathways. On the other hand, the full economic pathway (in purple) strikes a balance across all the objectives. Since this pathway is operated under a compromise policy and foresees the construction of Batoka Gorge, it achieves the second smallest hydropower deficit relative to the energy pathway, with an infrastructure investment

of 2.18 Bn.USD proportional to the reservoir's size. This pathway also avoids further disruption of the natural flows downstream.

Figure 20 shows the average cyclo-stationary dynamics for each of the candidate pathways. Each row corresponds to a different reservoir and each column shows its average inflow, storage, and release trajectories. Following each panel by row, the inflow of a given reservoir is dictated by the operations of the immediate upstream reservoir, except for Itezhi-Tezhi and Batoka Gorge which are not preceded by an upstream reservoir. The inflow into a reservoir can also vary when a lateral flow or an irrigation diversion is encountered upstream. Starting with Itezhi-Tezhi in panels a)- c), all the candidate pathways show releases that closely follow the inflow patterns, especially the peak inflow in March. The releases from Itezhi-Tezhi flow into Kafue Gorge Upper with two months of delay. In addition, Kafue Gorge Upper receives additional flow from the lateral contribution of the Kafue Flats while water is diverted upstream to irrigation district 3 as shown in Figure 16. The storage to release patterns seem to be dictated by the inflows into Kafue Gorge Upper (panels d-f). In particular, the energy pathway shows an average release basically equal to the inflows, keeping the corresponding Kafue Gorge Upper reservoir storage almost empty. This is due to the fact that the system, when operated to minimize energy deficit/surplus, prefers to use Kafue Gorge Upper as a run-of-the-river power plant due to its rather small active storage capacity, avoiding to store water that could be instead used to fully exploit the higher hydropower potentials of downstream reservoirs. Moving to Kafue Gorge Lower, we can observe that the environmental objective is starting to drive the operations to cooperatively guarantee that the minimum environmental flows are met in the Delta with a decline in storage in the months of March and April for the water pathway (in panel h). Then, starting from the Zimbabwe/Zambia branch of the system downstream the Victoria Falls, we encounter Batoka Gorge (panels j-l), which is the first planned project analysed in the system. Only the full economic and the energy pathways foresee its construction. Therefore, we only show these two candidate pathways in the storage panel k. For all the other pathways the releases are set equal to the inflows to reproduce the natural flows in panels j) and l) respectively. We can observe that the average storage is kept constant for the full economic pathway and the releases very closely follow the inflow patterns. On the contrary, the energy pathway's average storage lies within the full operating range and the average releases are also very similar to the inflow.

Figure 21 can be seen as an extension of Figure 20 starting with Devil's Gorge (panels a-c), which is immediately downstream of Batoka Gorge. Devil's Gorge storage (panel b) shows only the energy pathway solution in orange since this is the only pathway that foresees its construction. The same logic used for Batoka Gorge is also applied here, where the releases are equal to the inflows for the remaining pathways to replicate natural flows. This logic is also extended to Mphanda Nkuwa, the last planned reservoir (panels j-l). Devil's Gorge shows that the rest of the pathways where natural flow is assumed, have high releases during March and April, whereas the energy pathway doesn't release more than 900 m^3/s during those critical months but keeps slightly higher releases at the end of the year. This behaviour allows to keep the releases rather constant throughout the years in order to maximize hydropower production and thus minimize the production deficit. Moving downstream to Kariba, we do not detect differences among the different candidate pathways except for the energy one. The inflow into Kariba coming from this pathway is entirely dictated by operations at Devil's Gorge and it looks very different from the natural flows approximated by the purple line. The releases from the energy pathway seem to be more evenly distributed throughout the year, whereas for the other candidate pathways have a peak release in May.

The next reservoir in line is Cahora Bassa (panels g-i). The inflow trajectory for this reservoir depends upon operations in Kafue Gorge Lower and Kariba, along with the natural streamflow contribution from the Luangwa tributary. The dynamics for this reservoir show that the water pathway achieves the highest releases in February and March (panel i), followed by the food and the full economic pathway, in order to meet the high environmental flow requirements in the Delta during those months. The releases under these pathways drop for the remainder of the year, especially for the water pathway which drop to nearly zero, in order to drive the reservoir storage back up to almost its full capacity and store water to be released the next year for meeting again the February and March environmental flow requirements. The business as usual and the energy pathways are not

able to release large volumes at the time of the critical environmental flows, instead they sustain constant releases throughout the year. A similar behaviour is observed in the most downstream reservoir in Mphanda Nkuwa (j-k). As previously mentioned, the construction of this reservoir is only considered in the energy pathway and the storage (orange line in panel k) remains constant at nearly full capacity in order to exploit its full hydropower potential. The rest of the pathways reflect the natural flow, again with the largest release in March and February able to better minimize the environmental flow deficit.

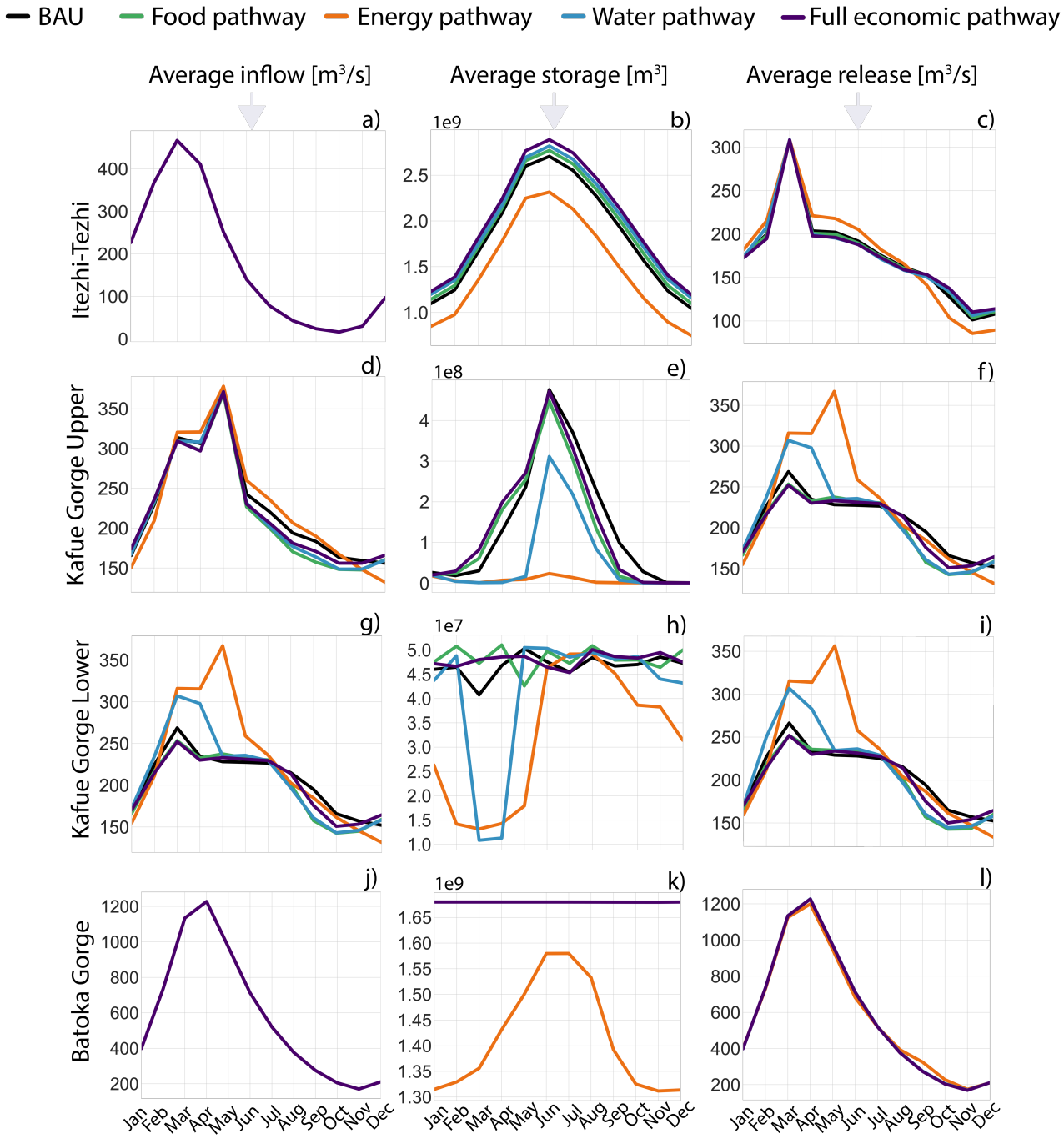

Figure 20 – Inflow, storage, and release dynamics for each of the candidate pathways for Itezhi-Tezhi, Kafue Gorge Upper and Lower, and Batoka Gorge reservoirs.

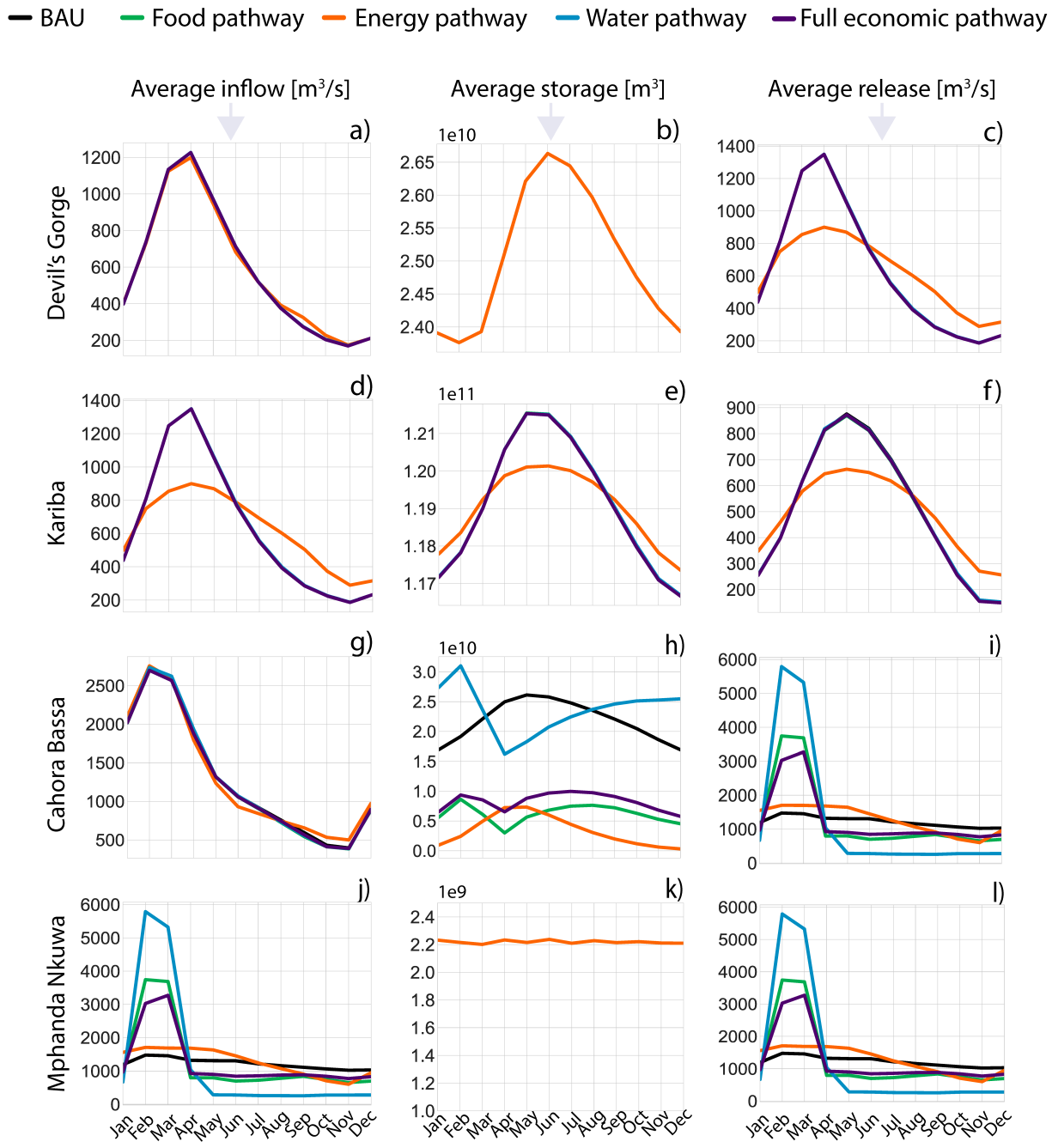

Figure 21 – Inflow, storage, and release dynamics for each of the candidate pathways for Devil's Gorge, Kariba, Cahora Bassa, and Mphanda Nkuwa reservoirs.

4.3 EFFICIENT PATHWAYS

In this section, we discuss the results of the efficient pathways design, i.e. the optimal time-sequencing of infrastructure expansion and their performance relative to water, energy and food indicators as well as the net present cost of the planned dam investments.

Figure 22 – ZRB Pareto approximate trade-offs of efficient pathways, showing the objectives of the system in the first four axis and the timing decisions in the last three axis.

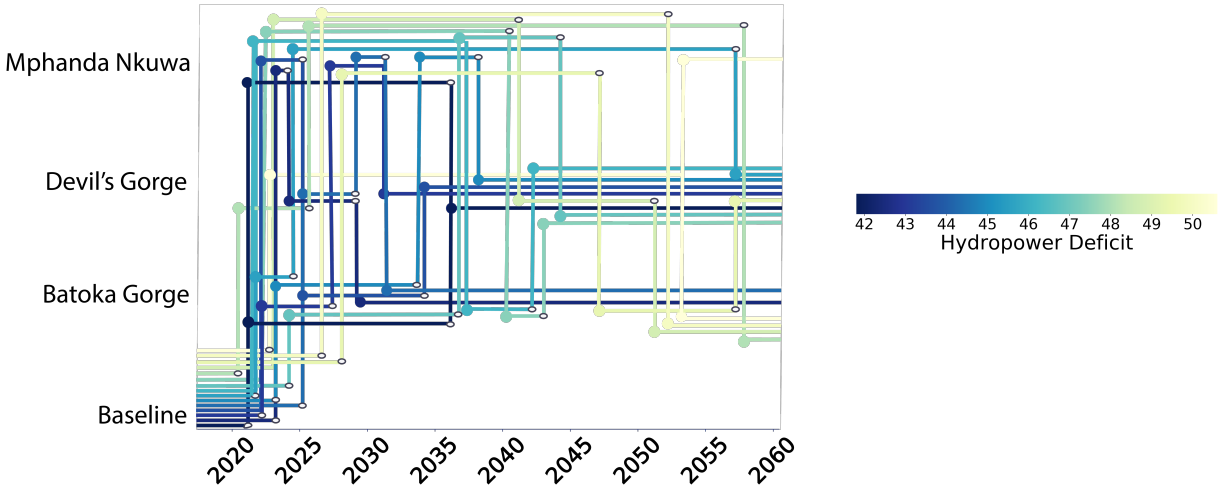

Figure 23 – Time sequencing of Batoka, Devil's Gorge, and Mphanda Nkuwa shaded by hydropower performance.

The parallel coordinates in Figure 22 show the Pareto approximate trade-offs of the optimal time sequencing for planned infrastructure projects in the ZRB. The first four axis of the parallel coordinates show the performance of the efficient pathways in terms of system's objectives, where the direction of preference is always upwards, whereas the last three axis show the decisions for the construction time of Batoka Gorge, Devil's Gorge, and Mphanda Nkuwa. The construction decision of each project lies between 2020 and 2060, showing an early construction in the bottom axis and a later construction in the upper axis. From the parallel coordinates we observe that Batoka and

Devil's Gorge are built in 2057 at the latest and Mphanda Nkuwa in 2053. The lines are shaded by hydropower performance where smaller deficit is depicted in dark blue and a larger deficit in light yellow. Hydropower is emphasized in this analysis since hydropower prone policies are used to operate the system. In particular, they are adapted as a new reservoir is added, starting from the baseline configuration with 5 reservoirs until the full 8 reservoir system is realized. A cooperative operating scheme is adopted so that all the reservoirs are operated to fulfil the systems' objectives simultaneously. Figure 23 is complementary to the trade-off analysis by showing the construction of each dam projects across time, where the pathways are shaded by hydropower performance from smaller deficit in dark blue to larger deficit in light yellow. Most of the solutions are built within the first 20 years of the optimization with only a few pathways delaying the construction of one or more projects until the last decade. The trade-offs show that, on average, a smaller deficit can be achieved for the entire planning horizon when the dam projects are built before 2040. This can also be observed in Figure 23 with a cluster of dark blue lines before 2040 depicting better hydropower performance. All the solutions eventually build all of the reservoirs within the time frame driven by the hydropower targets. The net present cost objective balances the need to meet hydropower production targets and pushes the construction of the largest reservoir towards the end. As mentioned in section 2.2, the cost is dependent upon the size of the reservoir and Devil's Gorge grants the largest storage capacity (i.e., 3.12 x 10^{10} m^3). There are, however, some intermediate pathways that balance the cost of opportunity of this dam despite the high net present cost. There is no clear trend between cost and the time for the construction of Mphanda Nkuwa. However, the solution that suggests the latest construction of Mphanda Nkuwa in 2053 generates the best environmental performance. Since Mphanda Nkuwa is the most downstream reservoir, its delayed construction also delays the alteration of the natural flows required in the Delta. Finally, moving to the irrigation objective, even if it shows a small range between its best and worst solution, a slight improvement is observed with the early construction of the reservoirs. This small range might be due to the fact that the system is always operated under a hydropower-prone operating policy. The reservoirs are therefore operated to minimize the hydropower production deficit, causing high irrigation deficits regardless of which infrastructures are built and when. The irrigation deficit objective seems to follow similar patterns as the hydropower objective, potentially benefitting from the increased storage capacity to fulfil the average irrigation targets. For detailed reservoir dynamics of this section, please refer to the Appendix.

5. DESIGN (STRATEGIC) MODEL FOR THE OMO-TURKANA BASIN

5.1 WATER SYSTEM MODEL

In this Chapter we report the building blocks constituting the strategic model for OTB illustrated in Figure 24. In this case, we present the model relative to the fully developed system, thus including both existing and planned infrastructures, which comprises all the elements necessary to formalize the objective functions.

The building blocks of the strategic model are 3 artificial reservoirs, Gibe I (GI), Gibe III (GIII), Koysha (K), with associated hydropower plants, one run-of-the-river hydropower plant, i.e., Gibe II (GII), one natural reservoir, lake Turkana (T), two irrigation districts, Kuraz (Ku) and a Private Agriculture (PA) district, and the river stretches connecting these elements. A daily modelling time-step is employed to capture the four reservoirs' dynamics through the following water mass balance equations:

$$s_{t+1}^{GI} = s_t^{GI} + q_{t+1}^{GI} - e_t^{GI} A_t^{GI} - r_{t+1}^{GI} \quad (15)$$

$$s_{t+1}^{GIII} = s_t^{GIII} + q_{t+1}^{GIII} - e_t^{GIII} A_t^{GIII} - r_{t+1}^{GIII} \quad (16)$$

$$s_{t+1}^{K} = s_t^{K} + q_{t+1}^{K} - e_t^{K} A_t^{K} - r_{t+1}^{K} \quad (17)$$

$$s_{t+1}^{T} = s_t^{T} + q_{t+1}^{Delta} + q_{t+1}^{Turkw} + q_{t+1}^{Ker} - e_t^{T} A_t^{T} \quad (18)$$

where s_t^r (r = GI, GIII, K, T) is the storage of the r-th reservoir at the beginning of day t, q_{t+1}^r is the inflow to the reservoir, r_{t+1}^r is the volume of water released, $e_t^r A_t^r$ is the water evaporated in the time

interval $[t; t+1)$. In particular, e_t^r is the mean daily evaporation rate, while A_t^r is the reservoir surface uniquely defined by a non-linear relation given s_t^r. In the adopted notation, the time subscript of a variable indicates the instant when its value is deterministically known. The release of the ar-th artificial reservoir (ar = GI, GIII, K) is defined as $r_{t+1}^{ar} = f(s_t^{ar}, u_t^{ar}, q_{t+1}^{ar}, e_t^{ar})$ where $f(\cdot)$ describes the nonlinear relation between the release decision determined by the operating policy, i.e. $u_t^{ar} = p(\cdot)$, and the actual release r_{t+1}^{ar} (Piccardi & Soncini-Sessa, 1991). The actual release at the end of the time interval is generally equal to the release decision unless physical constraints prohibit it (e.g., if the prescribed release lies outside the minimum and maximum allowable releases, if there is insufficient water to meet the prescribed release, or if the prescribed release would exceed the reservoir storage capacity). Lake Turkana, instead, is an endorheic lake, therefore the only water output is due to evaporation.

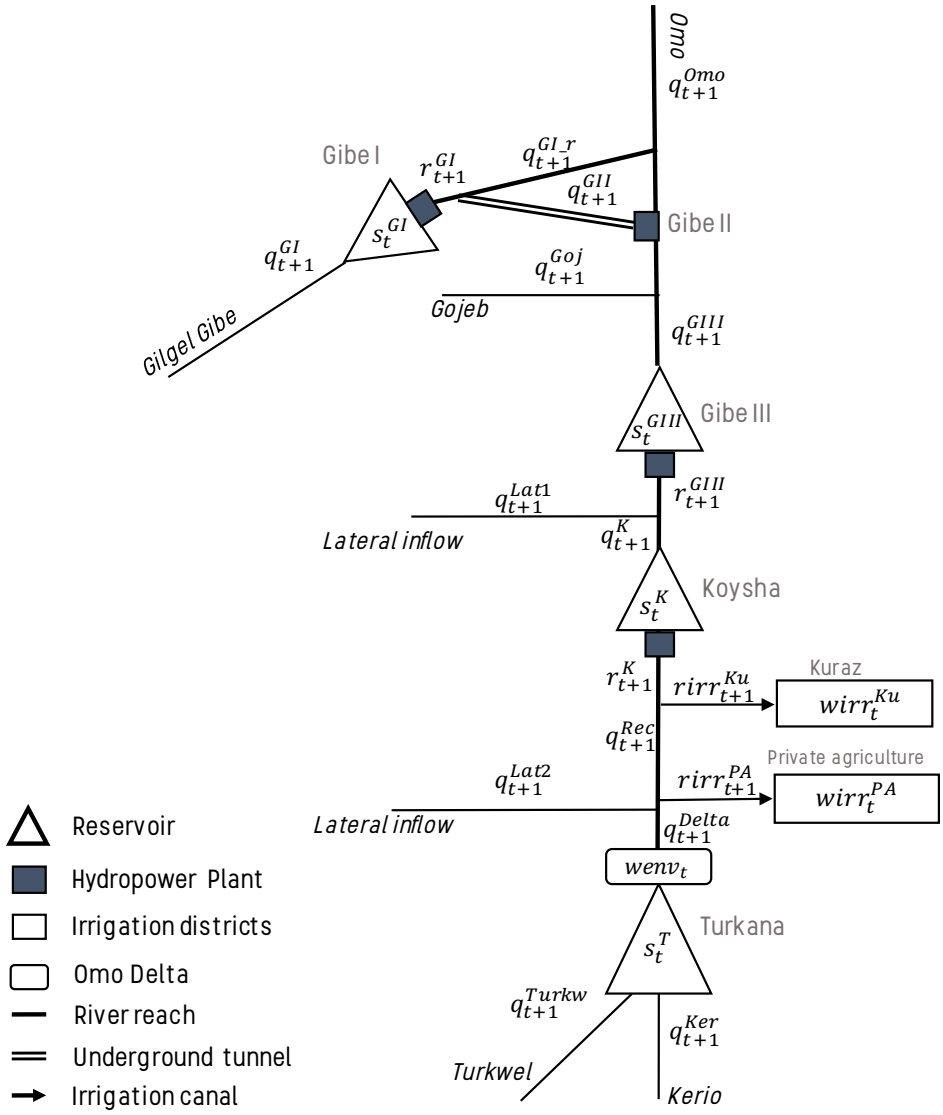

Figure 24 – Topologic scheme of the OTB including existing and planned infrastructures implemented in the strategic model.

According to the daily time-step adopted in the model, the river reaches are modelled as plug-flow canals in which the velocity and direction of flow are constant everywhere, without any lamination effect. Transit lag times reported below correspond to the average time employed by the water to transit between these two points.

$$q_{t+1}^{GII} = \min(\max(r_{t+1}^{GI} - MEF^{GI}, 0), \text{tunnCapacity}) \quad (19)$$

$$q_{t+1}^{GIII} = q_{t+1}^{Goj} + q_{t+1}^{GII} + q_{t+1-lagUp}^{Omo} + q_{t+1-lagUp}^{GI\_r} \quad (20)$$

$$q_{t+1}^{K} = q_{t+1}^{Lat1} + r_{t+1-lagGIII\_K}^{GIII} \quad (21)$$

$$q_{t+1}^{Rec} = r_{t+1}^{K} - rirr_{t+1}^{Ku} \quad (22)$$

$$q_{t+1}^{Delta} = r_{t+1-lagK\_T}^{Rec} - rirr_{t+1}^{PA} + q_{t+1}^{Lat2} \quad (23)$$

where $lagUp = 3$ days, $lagGIII\_K$ = 6 days, $lagK\_T$ = 12 days.

A regulated water diversion channel allows to abstract water from the main Omo river stretch to the two irrigation districts (id = Ku, PA). The volume of water abstracted $rirr_{t+1}^{id}$ is calculated according to a non-linear hedging rule (Celeste & Billib, 2009). For example, the id = Ku diversion channel for the Kuraz Sugar irrigation district is regulated as follows:

$$rirr_{t+1}^{Ku} = \begin{cases} \min\left(r_{t+1}^{K}, wirr_t^1 \cdot \left[\frac{q_{t+1}^{VF}+q_{t+1}^{KA}}{h^1}\right]^{m^1}\right) & if\ r_{t+1}^{K} \le h^{Ku} \\ \min\left(r_{t+1}^{K}, wirr_t^{Ku}\right) & else \end{cases} \quad (24)$$

where $q_{t+1}^{VF} + q_{t+1}^{KA}$ is the volume of water available in the river, $wirr_t^1$ is the daily water demand, and h^1 and m^1 are the parameters regulating the diversion channel.

5.2 OBJECTIVES AND DECISION VARIABLES

Similar to the case of ZRB illustrated in the previous chapter, the interests of the OTB stakeholders were modelled by a set of evaluation indicators which will be evaluated via simulation of the integrated WEF developed in Task 3.2. A subset of these indicators, namely the design indicators selected in Deliverable D5.1 for representing the main components of the WEF nexus, is used here to represent the vector of operating objectives $\boldsymbol{J} = |J^1, \dots, J^K|$ for the DAF optimization. Below, the mathematical formulation of the design indicators is presented and discussed in details.

- **Environment** in the Omo delta (water/ecosystem):

$$J^{Env} = \frac{1}{h}\left[\sum_{t=0}^{h-1}\left(wenv_t - q_{t+1}^{delta}\right)^2\right] \quad (25)$$

where $wenv_t$ is the cyclostationary trajectory of natural inflow regime in the Omo Delta, (Figure 25, left panel), and q_{t+1}^{delta} is the streamflow reaching the delta in the pathway under evaluation. The indicator is formulated as the average squared distance between these two values over the evaluation horizon [1, h]. This indicator is aimed at preserving natural flow conditions in the ecosystem of the Omo delta, penalizing both positive and negative deviations from the natural regime. According to the adopted squared formulation, smaller, and more frequent deviations are preferred to large concentrated deviations with respect to the target.

- **Hydropower Production** (energy):

$$q_{t+1}^{turb,r} = \min\left(r_{t+1}^{r}, TurbCapacity^{r}\right) \quad (26)$$

$$J^{HP} = \frac{1}{Nyears}\left[\sum_{t=0}^{h-1}\sum_{r=1}^{rmax} prod_{t+1}^{r}\right] \quad (27)$$

where $prod_{t+1}^{r}$ is the hydropower production of the power plant r, and $Nyears$ is the number of years within the evaluation horizon. This indicator aims at maximizing the annual hydropower production at the basin level.

- **Irrigation** (large scale food):

$$\mathrm{J^{Irr}} = \frac{1}{\mathrm{h}}\left[\sum_{\mathrm{t=0}}^{\mathrm{h-1}}\sum_{\mathrm{id=1}}^{\mathrm{idmax}}\left(\frac{\max\left(\mathrm{wirr_t^{id}} - \mathrm{rirr_{t+1}^{id}}, 0\right)}{\mathrm{wirr_t^{id}}}\right)^2\right] \quad (28)$$

where $wirr_t^{id}$ and $rirr_{t+1}^{id}$ are the irrigation water demand and abstraction of the irrigation district id. The normalized irrigation deficit is computed at the basin scale by summing the normalized deficit occurring in the irrigation districts each time step and averaged across the evaluation horizon. The normalization of deficit with respect to the water demand is motivated by the necessity of considering two districts characterized by very different water demands and owned by different entities.

- **Recession** flood (local scale food):

$$J^{Rec} = \frac{1}{h}\left[\sum_{t=0}^{h-1}(\max\left(wrec_t - q_{t+1}^{rec}, 0\right))^2\right] \quad (29)$$

where $wrec_t$ is a target flood requirement in the lower Omo valley needed for the recession agriculture practice (Figure 25, right panel) (Avery, 2012), and r_{t+1}^{rec}, is the streamflow transiting the same river reach in the pathway under evaluation. This indicator thus computes the average streamflow deficit over the evaluation horizon [1, h] with respect to recession requirements and it is aimed at guaranteeing the hydrological conditions required to perform recession agriculture.

- **Fish** in lake Turkana (water-local scale food):

$$J^{fish} = \max_{y=0,\dots,Ny-1}\left(\left|F^{nat} - F_{y+1}\right|\right) \quad (30)$$

$$F_y = \alpha\overline{h_{y-1}} + \beta ampl_y + \gamma$$

$$ampl_y = \max_{t\in[Sept-Dec]_y} h_{t,y} - \min_{t\in[Jan-Aug]_y} h_{t,y}$$

where F^{nat} is the average natural fish biomass present in lake Turkana, and F_{y+1} is the estimated fish biomass in year $t+1$ of the pathway under evaluation. J^{fish} assumes the value of the maximum distance between natural and simulated fish abundance: such *worst case* formulation guarantees a minimum acceptable performance in critical years. This choice is motivated by the fact the several tribes resort to fishing exclusively in exceptionally dry years, when other survival strategies fail to provide sustenance.

Fish biomass is estimated from hydrological variables: the average lake Turkana water level in the previous year $\overline{h_{y-1}}$, and the amplitude of lake level oscillation in the current year between dry season (January to August) and wet season (September to December). F^{nat} is estimated in an analogous way, from historical levels of Turkana from 1985 to 2001, when the system is considered in pristine conditions. The coefficients of this regression are $\alpha = 0.3252, \beta = 1.006$ and $\gamma = -110.91$. The relation between fish biomass and lake Turkana levels is retrieved from Gownaris et al., (2017).

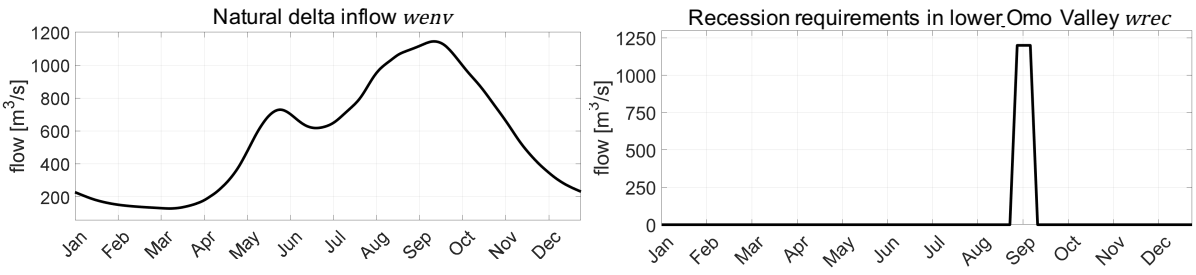

Figure 25 – Left panel – cyclostationary trajectory of natural inflow regime in the Omo Delta, computed averaging 15 years of inflow to the delta in a simulation of the pristine system (no dams). Right panel - target flood requirement in the lower Omo valley needed for the practice of recession agriculture.

5.3 NOMINAL SCENARIO

The optimization of the system management is performed for each portfolio over a historical scenario $\bar{\omega}$, represented by modelled historical hydrologic variables (i.e., streamflow) and socio-economic factors (i.e., irrigation demands), i.e. $\bar{\omega} = \{q_1^h; wenv_0^{h-1}; wrec_0^{h-1}; wirr_0^{h-1}\}$, presented in Deliverable D2.1. The exploration of optimal action sequencing is performed over a reference future scenario $\hat{\omega}$, which represent a plausible change in the historical scenario due to climate and societal change.

Streamflow projections

Streamflow projections for the reference future scenario $\hat{\omega}$ have been generated by using the precipitation and temperature projections generated by applying factors of change to the historical time-series, in order to bootstrap a high-resolution prediction model. To calculate the factors of change we analysed an ensemble of 22 Regional Climate Model and General Circulation Model pairs. Using the ensemble, we developed change factors by comparing the changes in meteorological variables (e.g. precipitation, temperature) between a historical control period (1976-2005) and for simulations of the future climate. The application of the change factor methodology is described in deliverable Deliverable D2.2. The resulting precipitation and temperature time-series were used to generate projected streamflow using the distributed hydrological model TOPKAPI-ETH (S Fatichi, 2015). The overall seasonal cycle of future streamflow in the Upper Omo and Omo Delta illustrated in Figure 26 shows a large variation in magnitude between the various 5-year averaging periods, with a more significant variability in the Omo Delta.

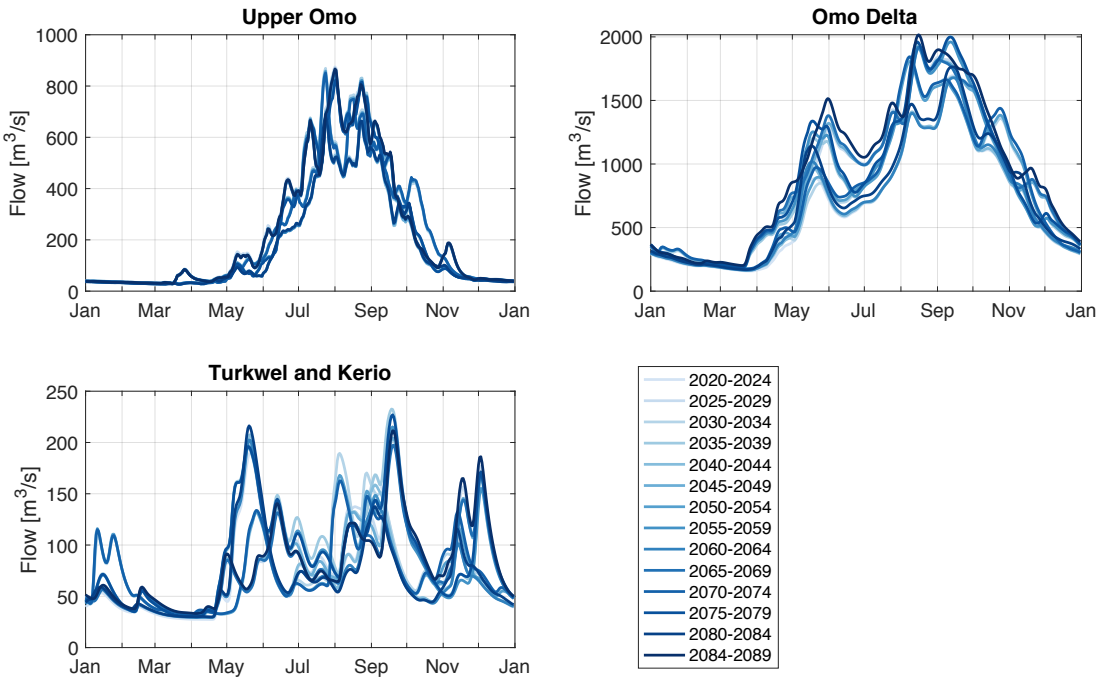

Figure 26 – Streamflow projections in three river reaches. Each line represents a 5 years mean, with lighter colours at the beginning of the evaluation horizon and darker colours towards the end.

Irrigation demands projections

Irrigation demands projections for the reference future scenario $\hat{\omega}$ (Figure 27) have been generated by using the AquaCrop model. These projections are the result of summing three components: currently existing irrigation schemes, irrigation schemes planned for the near future, and irrigated maize cultivation during the dry season to compensate projected food shortages. Water demands for these three components were calculated in AquaCrop by using the methodology described in Deliverable D2.2, and assuming a 60% irrigation efficiency. Further, the projected precipitation and temperature,

the soil characteristics from ISRIC[3] soil grids, and the default crop parameters available in AquaCrop were used as input for the crop model.

The simulations predict a stable trend in irrigation demands for abstraction point 1 (including sub-basins 11548 and 11549), where no calorie or protein deficit is predicted and no new irrigation schemes are planned for the near future. In abstraction point 2 (including sub-basins 11546 and 11547), the future demands are expected to be about two times the current demands, because of new irrigation schemes planned in the near future. An increasing trend is expected due to extra irrigated cropping for local consumption, aiming to meet the food requirements of the growing population. In abstraction point 3 (including sub-basins[4] 11542, 11543, 11544 and 11545), the extra irrigation demands resulting from irrigated cropping for local consumption are negligible compared to the large demands (roughly a 20-fold increase of the current demands) of the planned increases of the Kuraz sugar estate. The high irrigation demands of the sugarcane estates show a stable trend under the RCP 4.5 scenario and a clear seasonal pattern (Figure 17).

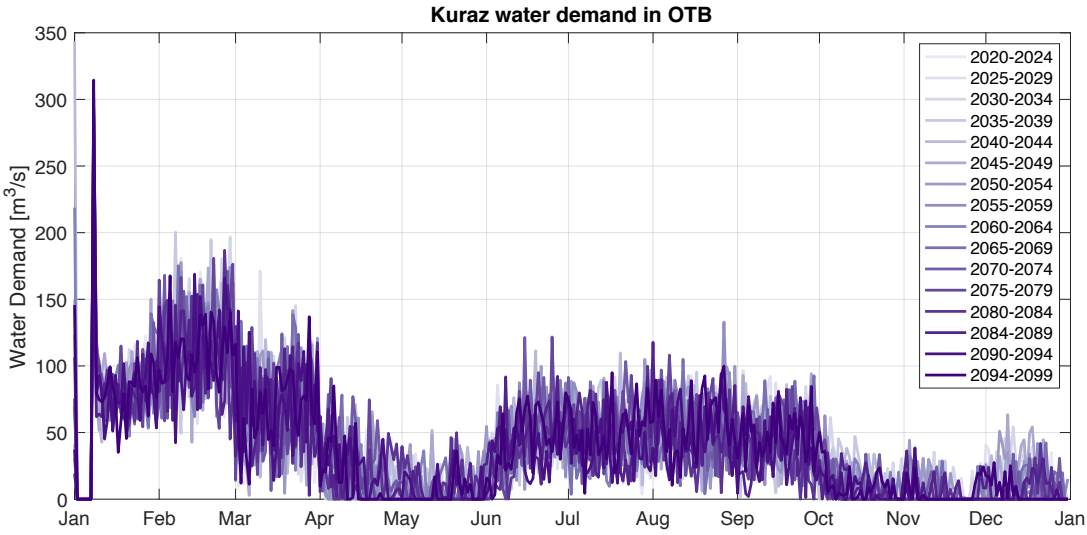

Figure 27 – Projected irrigation demand of the Kuraz district. Each line represents a 5 years mean, with lighter colours at the beginning of the evaluation horizon and darker colours towards the end.

6. PATHWAYS FOR THE OMO-TURKANA BASIN

In this chapter, we present and discuss the pathways designed for the OTB: we first analyse only the re-operation of the existing system under the historical scenario; secondly, we report the results of the simulations of the four candidate pathways derived from the SHs suggestions and introduced in Deliverable D5.1; lastly, we investigate the performance of the efficient pathways designed using the DAF optimization.

6.1 OPTIMAL SYSTEM RE-OPERATION

In this section, we will discuss the results of the Omo-Turkana Basin optimal re-operation. Since the construction of both Koysha and the irrigation districts in the Lower Omo valley has started, in this analysis we consider 4 different pathways (Table 2) and a 15-years historical horizon, from 2002 to 2016.

[3] www.soilgrids.com

[4] HydroSHEDS Pfaffstetter level 5 subbasins (https://www.hydrosheds.org)

Table 2 – A marker **x** indicates the infrastructures implemented (rows) in the four considered configurations (columns).

Infrastructure \ Pathway	Baseline	Koysha	Irrigation	Irrigation-Koysha
Koysha		x		x
Irrigation districts			x	x

Figure 28 reports the performance of the optimal system re-operation, where each panel in the figure corresponds to a different pathway, namely a *Baseline* representing the status quo with no infrastructural interventions, *Koysha* to simulate the construction of the new dam, *Irrigation* to simulate the construction of the irrigation districts, and *Irrigation-Koysha* which include both the new dam and the irrigation districts.

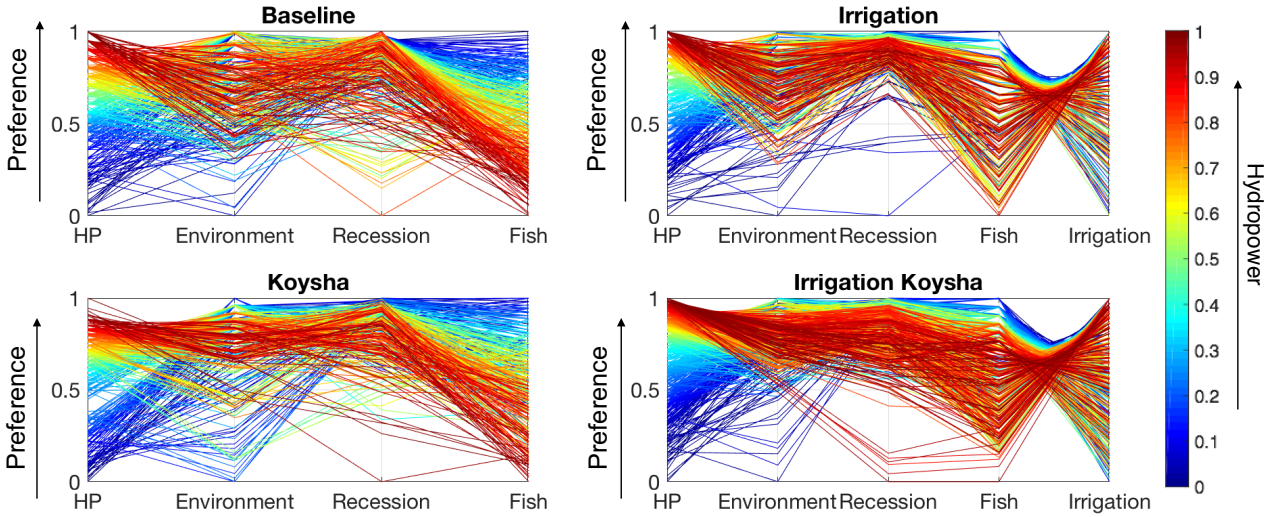

Figure 28 – Parallel axes plots reporting the performance of the optimal policies under 4 alternative pathways, namely, Baseline, Irrigation, Koysha, and Irrigation Koysha.

Each line in the plot represents the performance of one optimal policy with respect to the different objectives, corresponding to the 5 vertical axis: J^{hyd}, J^{env}, J^{rec}, J^{fish}, and J^{irr}. The objectives values are normalized between 0 and 1 with respect to the maximum and minimum value assumed in each pathway, where higher values correspond to better performance, as indicated by the preference arrow. Lines are coloured in accordance to the J^{hyd} objective, red for best alternatives, and blue for worst alternatives. A horizontal red line laying at the top of the graph would thus correspond to a policy that fully satisfies all sectors. However, such policy is unattainable for the system, given the presence of conflicts among objectives. Instead, the system optimal operation is composed of a set of Pareto-efficient policies exploring the trade-offs across the conflicting objectives.

In the represented Pareto fronts, blue lines (poor J^{hyd} performance) attain generally good results for J^{env}, J^{rec}, and J^{fish} indicating a conflict between these three objectives and the hydropower performance. Intuitively, a strong hydropower prone regulation can significantly alter the natural system hydrology, to which the environmental, recession, and fishing objectives are adapted. A sharper conflict is evident between J^{irr}, and J^{fish}, attributable to the fact that the water abstracted for the irrigation districts is consumed for agricultural production and does not contribute to the Lake Turkana inflows, impacting its ecosystem support to fish reproduction. Overall, little to no conflict is observed between J^{fish}, and J^{rec}, indicating that these two objectives have coadapted to the

same hydrologic conditions. Despite the conflicts, the numerosity of optimal solutions produced show that there is space for negotiation and numerous compromise alternatives exist.

In the following, we deepen the analysis for few representative policies for each pathway, looking at the trajectories of some key hydrological variables in the system under different operating policies in order to uncover the nature of the conflicts between objectives from an operational standpoint. For this analysis, we selected the best policies with respect to each objective, as highlighted in the parallel axes plots of Figure 29.

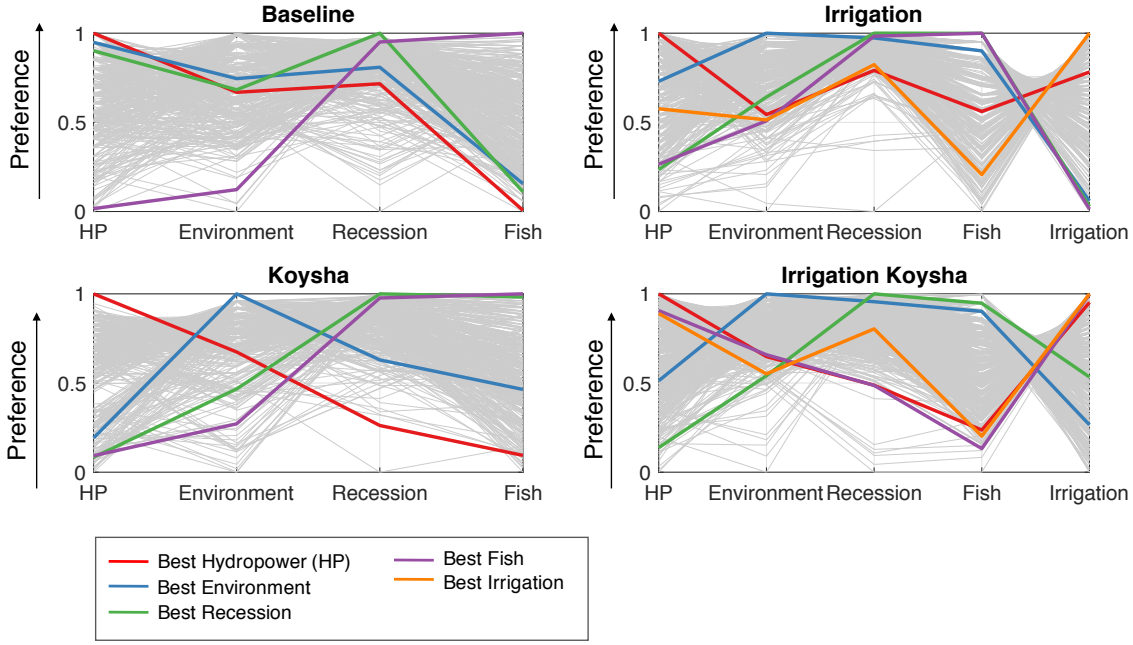

Figure 29 – Parallel axes plot highlighting the performance of the best policy for each objective in the 4 alternative pathways.

6.1.1 Analysis of extreme policies in the Baseline Pathway

Considering the Baseline pathway, a first variable of interest is Gibe III level (Figure 30), which plays a major role in determining the overall hydropower production, and the hydrologic conditions in the Lower Omo valley. The figure is composed of 4 panels, each representing the annual cyclostationary trend of a different policy. The shaded area represents the maximum and minimum values assumed by the variable over the evaluation horizon, and the bold line indicates the cyclostationary mean. Maximum and minimum operating levels of the reservoir are indicated by the dashed black lines. Proceeding clockwise, the first graph shows Gibe III level in the best policy for J^{hyd}: the dam is kept at near full capacity, in order to benefit from the higher water head and maximize hydroelectric production. The second graph shows the reservoir level under the best policy for environmental objective: here, a larger intra annual variability is observed, as to ensure a nearly natural streamflow pattern downstream. The Best Recession policy resembles that of the hydropower; however, the Recession objective exclusively concerns the system operation in late summer when recession agriculture is practiced, while the regulation in the most part of the year has virtually no effect on this objective. As a result, a good Recession performance can be obtained for a wide variety of policies, from hydropower oriented, as in this case, to more Fish and Environment oriented. Interestingly, the second best policy for the Recession objective almost coincides with the Best Environmental policy. Finally, Gibe III regulation under the best Fish policy maintains a very low reservoir during the January-July period to minimize loss of water due to evaporation, and recharges the reservoir in the July-September months, to create storage for sustaining the September-December level fluctuation in lake Turkana, vital for fish breeding.

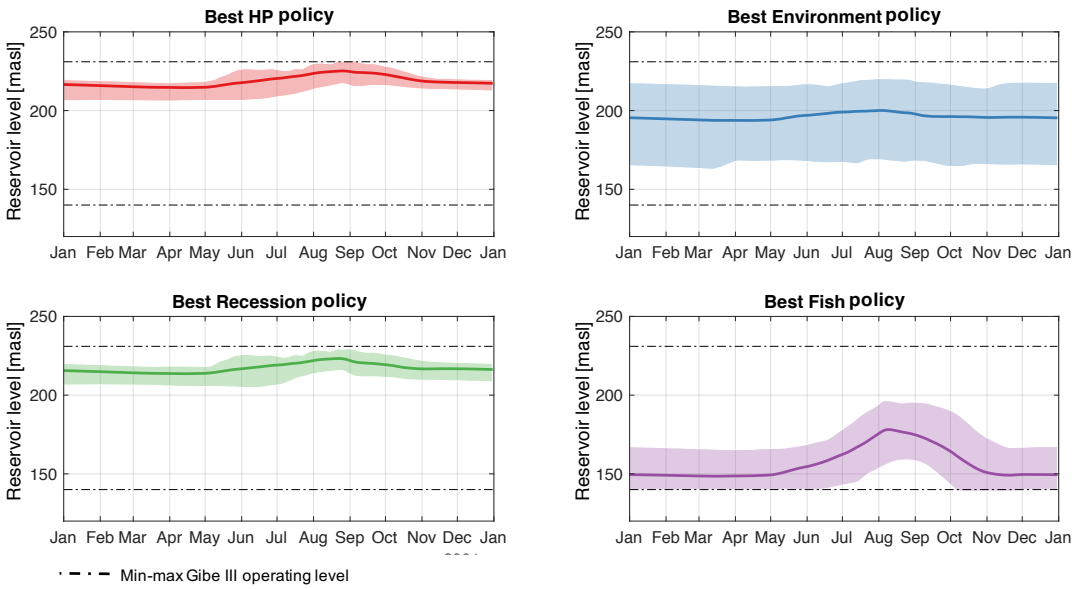

Figure 30 – Cyclostationary Gibe III levels simulated under the Baseline policies selected in Figure 29. The solid line represents the cyclostationary mean of the variable, and the shaded area represents its range over the historical horizon (2002-2016).

A second representative variable is the inflow at the Omo River's delta, illustrated in Figure 31, representative for J^{env}, whose target is reported as a black dashed line. As expected, the best Environmental policy allows to reproduce closely the environmental target with a small interannual variation. Recession and Hydropower solutions mostly follow the environmental target, but a deficit is frequently observed between June and September. The best Fish solution instead deviates from the natural pattern as to accentuate lake Turkana level fluctuations and ensure abundant fish production.

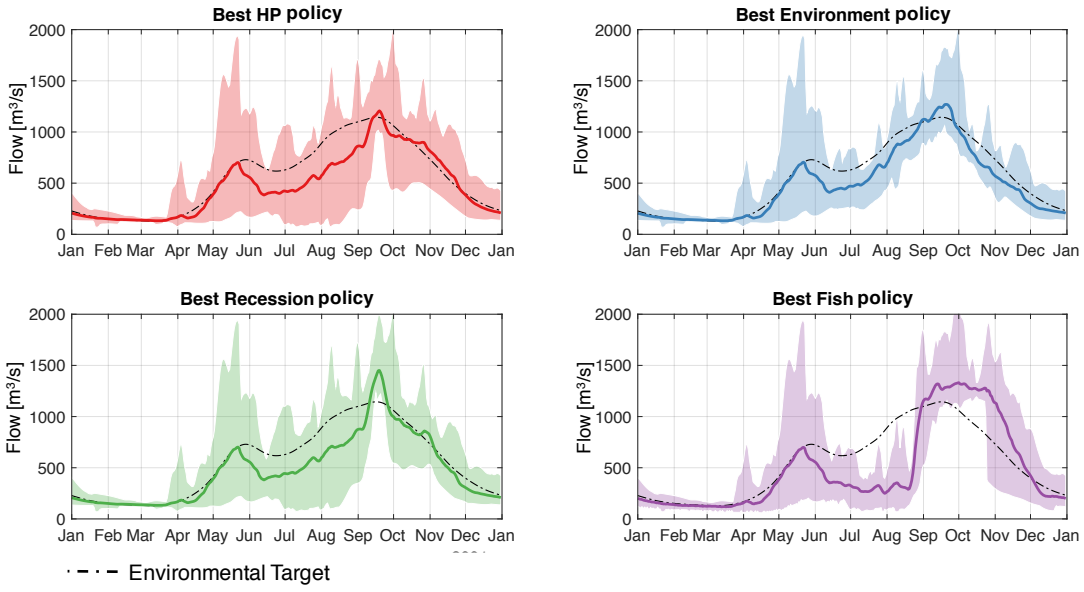

Figure 31 – Cyclostationary streamflow at the Omo river delta simulated under the Baseline policies selected in Figure 29. The solid line represents the cyclostationary mean of the variable, and the shaded area represents its range over the historical horizon (2002-2016).

The third analyzed variable is the streamflow in correspondence to the Omo river branch where Recession Agriculture activities mostly concentrate (Figure 32). In order to fully meet the Recession target (dashed black line), all the trajectories (entire shaded area) should lay above this target.

This is almost achieved in the Best Recession solution, while the simulated streamflow produced by the other policies often lays below the target. In particular, the best Hydropower policy does not meet the target in most years.

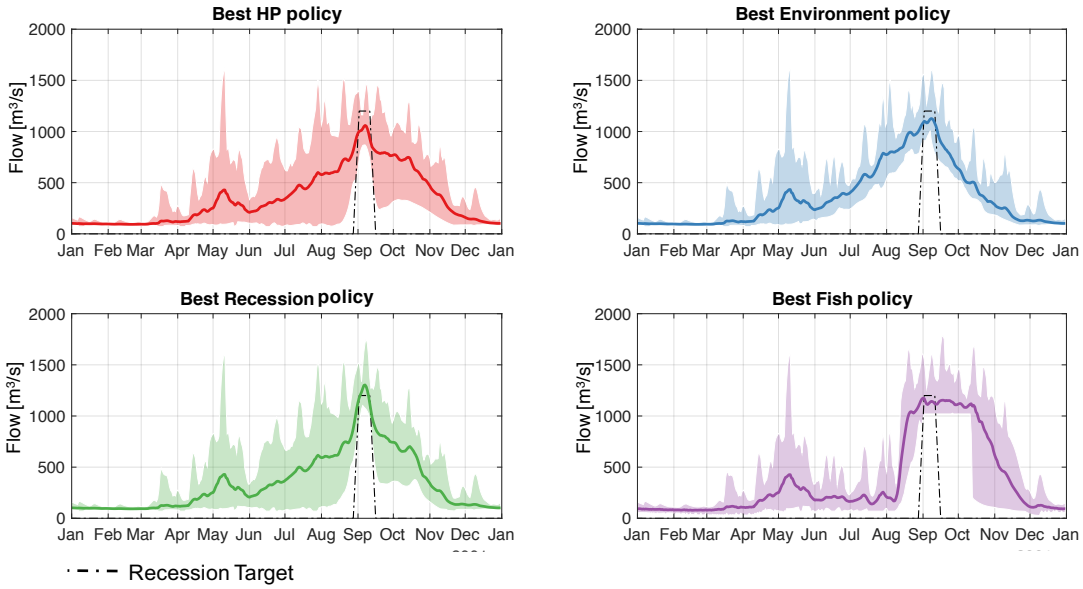

Figure 32 – Cyclostationary streamflow at the Recession agriculture hotspot simulated under the Baseline policies selected in Figure 29. The solid line represents the cyclostationary mean of the variable, and the shaded area represents its range over the historical horizon (2002-2016).

Finally, the fourth variable of interest is Turkana lake level (Figure 33), proxy of the fish yield. This variable is reported as a time series that comprises the full evaluation horizon, instead of a cyclostationary trajectory, to better capture both the intra- and the inter-annual lake dynamics impacting fish populations. As expected, the trajectory deriving from the application of the best Fish policy produces the highest levels for lake Turkana, as J^{fish} benefits from a higher average level of the lake. The Best Environment policy produces lake levels around 1 meter lower, and Recession and Hydropower policies place up to 2 meters below towards the end of the time horizon.

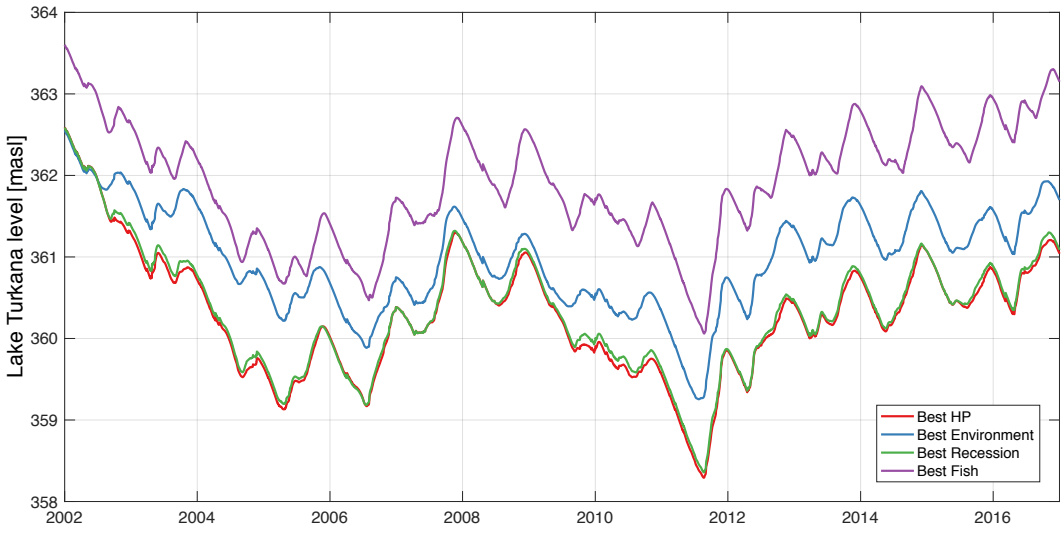

Figure 33 – Lake Turkana level simulated under the Baseline policies selected in Figure 29 over the historical horizon (2002-2016).

6.1.2 Analysis of extreme policies in the Irrigation-Koysha Pathway

Considering the fully developed Irrigation-Koysha pathway, we analyze the 5 extreme policies marked in Figure 29, namely Best Hydropower, Best Environment, Best Recession, Best Fish, and Best Irrigation. First of all, we notice that Hydropower and Irrigation best policies attain similar performance under all objectives thus suggesting that these two objectives are not conflicting, and the planned system expansion is well designed from an operational point of view. In other words, if the system is operated just considering hydropower and irrigation objectives, it is possible to find a policy that fully satisfies both objectives with no conflicts. Best Fish, best Recession and, to a lower extent, best Environment policies also display similar performance.

This pathway comprises two large reservoirs, Gibe III and Koysha, located at close distance from each other in the same river reach. The two reservoirs are operated conjunctively exploiting the benefits of their synchronized operation, which is evident by observing the cyclostationary trajectories of levels of Gibe III (Figure 34) and Koysha (Figure 35). The Best Hydropower policy (upper left panel), does not maintain Gibe III reservoir at full capacity as in the Baseline pathway, but, rather, its level shows a marked variability, as indicated by the large shaded area. On the other hand, Koysha reservoir level is maintained the highest and most constant possible. This is a conventional operational strategy for a reservoir cascade: the upstream reservoir acts as a buffer for the uncertain inflow of the Omo River, ready to accommodate an unexpected inflow peak without activating the spillways and release water that does not contribute to hydropower production. Because most of the inflow uncertainty is filtered by Gibe III, and lateral inflow between Gibe III and Koysha is negligible for the large part of the year, Koysha level can be maintained very close to the maximum operating level, maximizing its hydropower production, which can count on a larger installed turbine capacity. A similar dams' operation is observed for the Best Irrigation policy, supporting the absence of conflicts between the two objectives. However, dams' operations under the remaining three objectives is significantly different: Gibe III level is kept somewhat low and variable under Best Environment and Fish solutions, and completely empty in the Recession solution, likely with the aim of minimizing evaporation losses. Koysha level under these three objectives displays the summer recharge aimed at mimicking natural variability downstream the reservoir.

Figure 36 and Figure 37 report the simulated trajectories in correspondence to the Environment and Recession hotspots, respectively. These trajectories are similar to those reported for the Baseline pathway, but the presence of the two reservoir enlarges the space of operations allowing to exert a greater control on the natural system hydrology. In particular, the Best Environment solution follows more closely the natural pattern with a more contained inter-annual variability than in the Baseline pathway, and the Best Recession solution can satisfy the Recession target every year ensuring the full satisfaction of the sector. On the other hand, more regulation potential can also cause a larger damage these sectors, in particular the Best Irrigation and Hydropower solutions, which deviate from the targets significantly more than in the Baseline pathway.

Figure 38 reports the water cumulatively diverted for the irrigation districts, compared with the sum of irrigation demands, represented as a black dashed line. While hydropower and irrigation solutions display again similar behavior in attempting to satisfy the irrigation demand, Environment, Recession, and Fish solutions obtain very poor performance under the irrigation objective, and abstract a very low amount of water for irrigation purposes. This result, in combination to the previously discussed Figure 36 and Figure 37, offers a physical explanation of the large conflict between and J^{env}, J^{rec}, J^{fish}, and J^{irr}: in order to satisfy J^{env}, J^{rec}, or J^{fish} the flow to agricultural districts has to be significantly lower than the demand, even nearly null, as to preserve natural streamflow conditions in the lower Omo valley; on the other hand, when water is abstracted for agricultural purposes, significant damages are observed downstream. Notably, no policy is capable of satisfying the entire water demand, especially during the dry season, even adopting a completely irrigation-oriented policy. Given these results, the irrigation district seems to be oversized for the system, and such conclusion seems to be in accordance to the recent decision of the Ethiopian Sugar Company to modify the Kuraz Sugar Development project, which was recently officially downsized from the 175'000 ha originally envisioned in the Master Plan, to 100'000 ha (Ethiopian Sugar Corp., 2018).

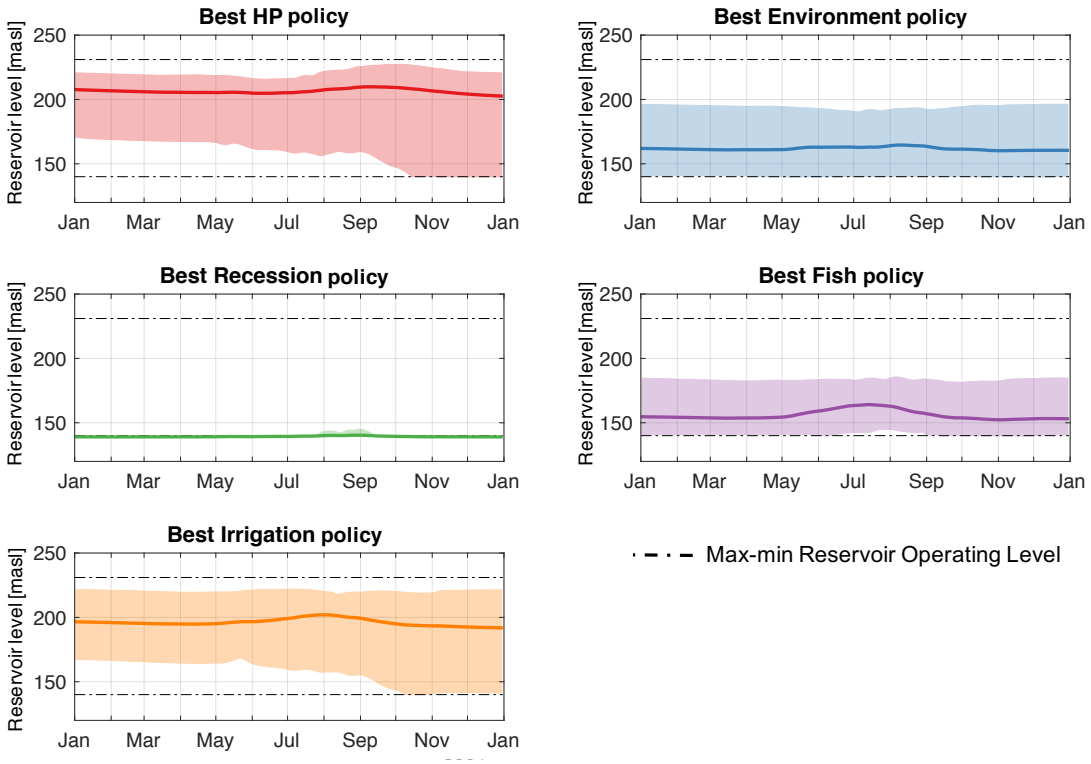

Figure 34 – Cyclostationary level of Gibe III simulated under the Irrigation-Koysha policies selected in Figure 29. The solid line represents the cyclostationary mean of the variable, and the shaded area represents its range over the historical horizon (2002-2016).

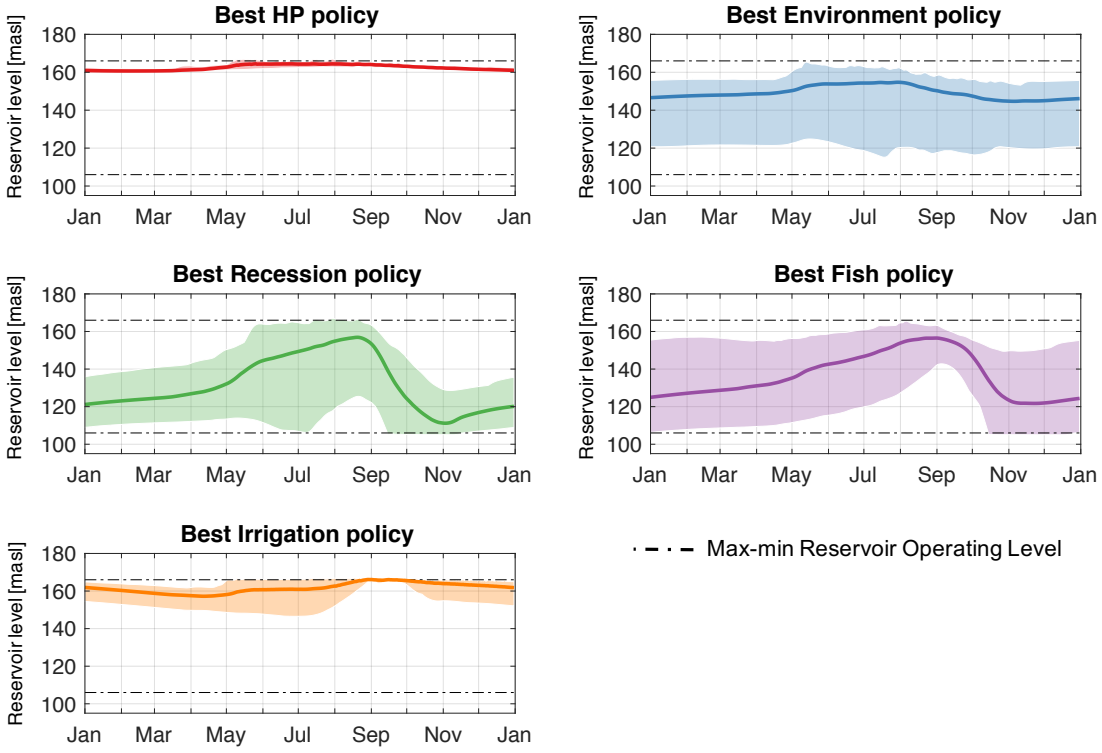

Figure 35 – Cyclostationary level of Koysha simulated under the Irrigation-Koysha policies selected in Figure 29. The solid line represents the cyclostationary mean of the variable, and the shaded area represents its range over the historical horizon (2002-2016).

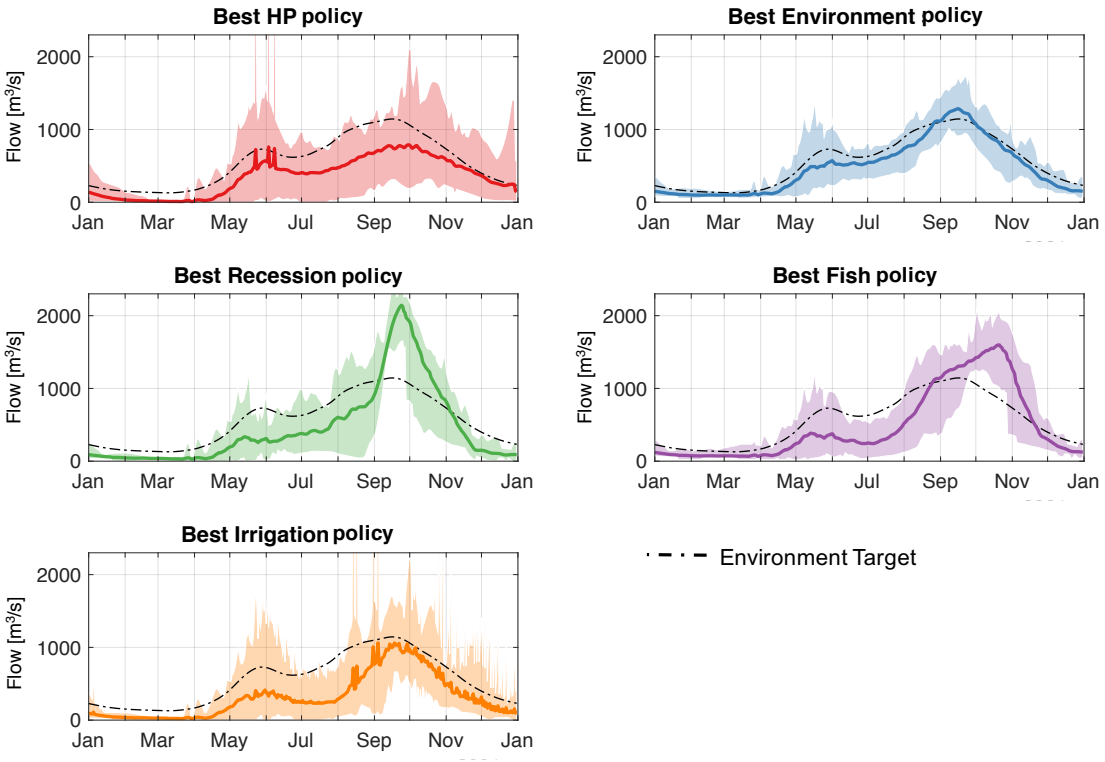

Figure 36 – Cyclostationary streamflow at the Omo river delta simulated under the Irrigation-Koysha policies selected in Figure 29. The solid line represents the cyclostationary mean of the variable, and the shaded area represents its range over the historical horizon (2002-2016).

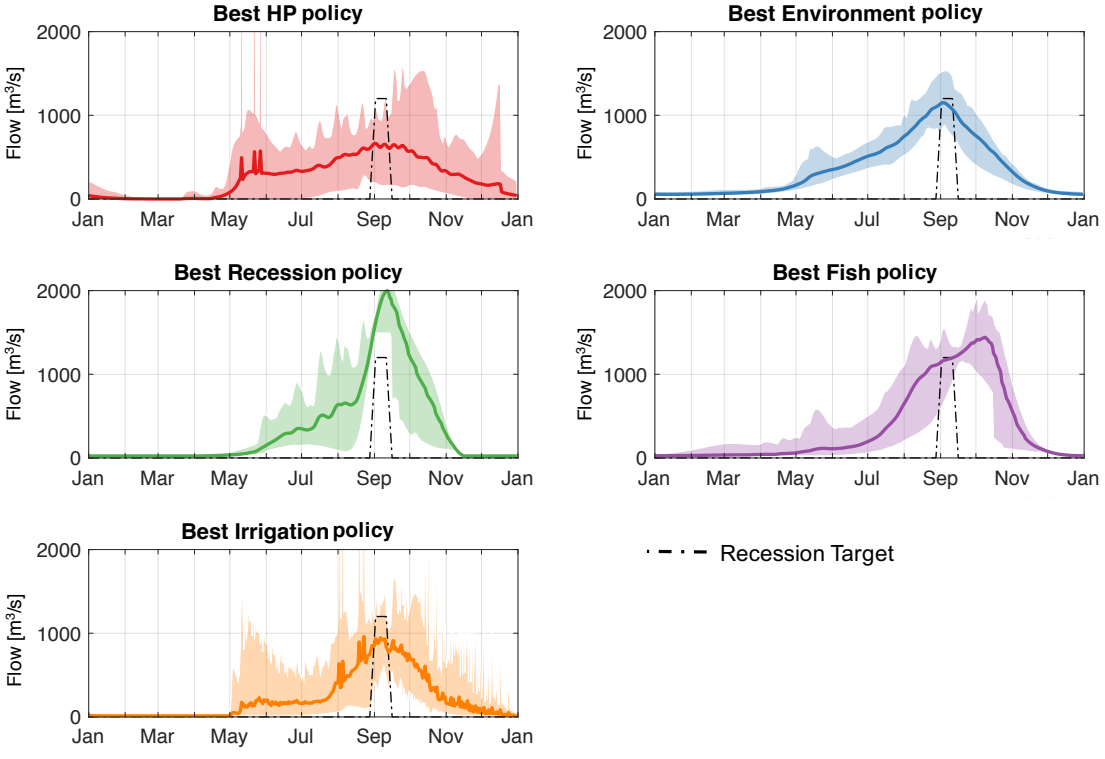

Figure 37 – Cyclostationary streamflow at the Recession agriculture hotspot simulated under the Irrigation-Koysha policies selected in Figure 29. The solid line represents the cyclostationary mean of the variable, and the shaded area represents its range over the historical horizon (2002-2016).

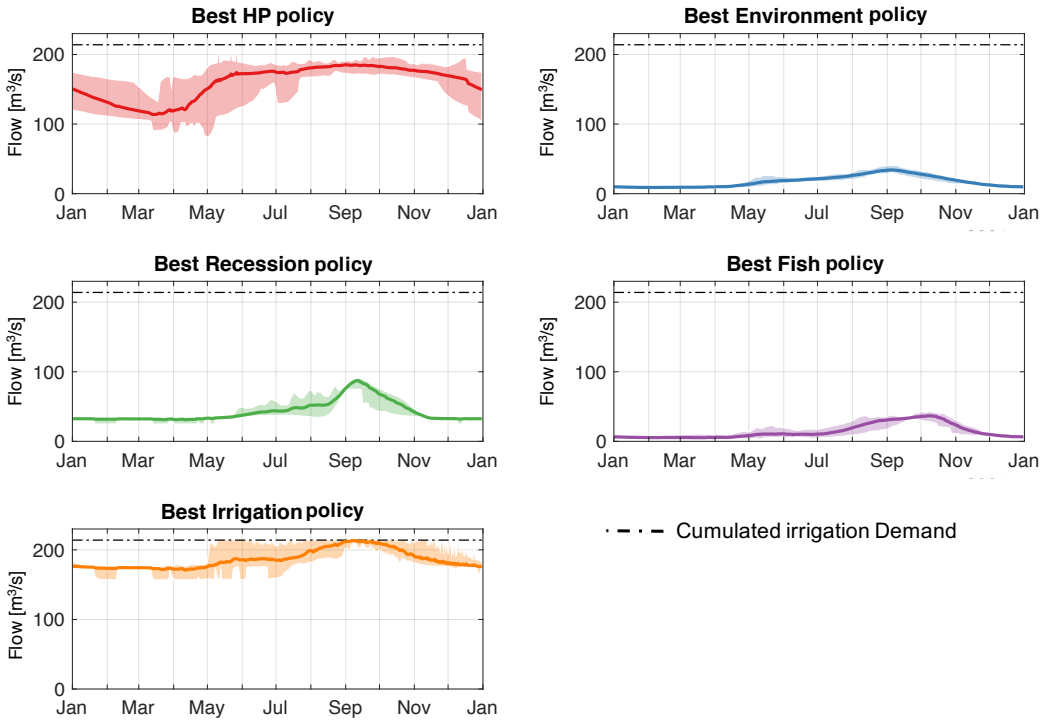

Figure 38 – Cyclostationary water diversion for agriculture cumulated for the two irrigation districts (Kuraz and Private Agriculture) simulated under the Irrigation-Koysha policies selected in Figure 29. The solid line represents the cyclostationary mean of the variable, and the shaded area represents its range over the historical horizon (2002-2016).

Lastly, the simulated Lake Turkana levels produced by alternative operations (Figure 39) show a dramatic decrease in level under the best policies for J^{hyd} , and especially J^{irr}, the latter producing a 15 meters drop in the 15 years time horizon considered. Best Environment, Recession, and Fish solutions, instead, show a variability of less than 2 meters, comparable to the results observed for the Baseline pathway. In order to investigate the cause of the Turkana level drop, in Figure 40 we report the lake level trajectories produced under the best policies for the Koysha and Irrigation pathways. In the Koysha pathway, the difference among policies is again contained in a 2 meters range, while, on the contrary, the Irrigation pathway is again responsible for the severe level decline. Evidently, Lake Turkana is much more sensible to the installation of the irrigation districts, which constitute a substantial consumptive use of water, rather than to the construction of Koysha, which can certainly modify the river hydrology, but ultimately does not subtract water to the system.

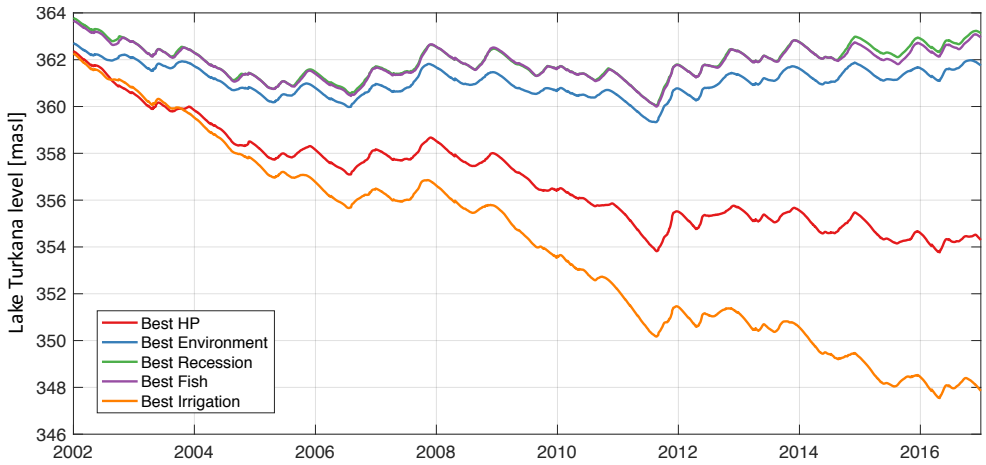

Figure 39 – Lake Turkana level simulated under the Irrigation-Koysha policies selected in Figure 29. The solid line represents the cyclostationary mean of the variable, and the shaded area represents its range over the historical horizon (2002-2016).

6.1.3 Comparison among Pathways

Figure 41 allows a comparison of the policies obtained under the 4 different pathways. The two pathways that do not consider the construction of the irrigation districts, namely Baseline and Koysha, are assigned the worst value under the J^{irr}, objective, as they do not support any large-scale food production. What is mostly evident from this parallel axes plot is that the pathways considering the construction of the irrigation districts tend to produce large negative consequences on J^{env}, J^{rec}, and especially J^{fish}, which are not envisaged for Baseline and Koysha pathways.

On the other hand, the presence of Koysha dam seems to enlarge the system flexibility and the space for operations, not only greatly improving the J^{hyd} objective, but also attaining the best performance with respect to J^{irr}, J^{env}, J^{rec}, and J^{fish} given that the corresponding policies occupy the uppermost part of the objectives axis. Under an optimal management of the system, the presence of Koysha reservoir could reduce the conflict between stakeholders, facilitating the negotiation and selection of compromise solutions.

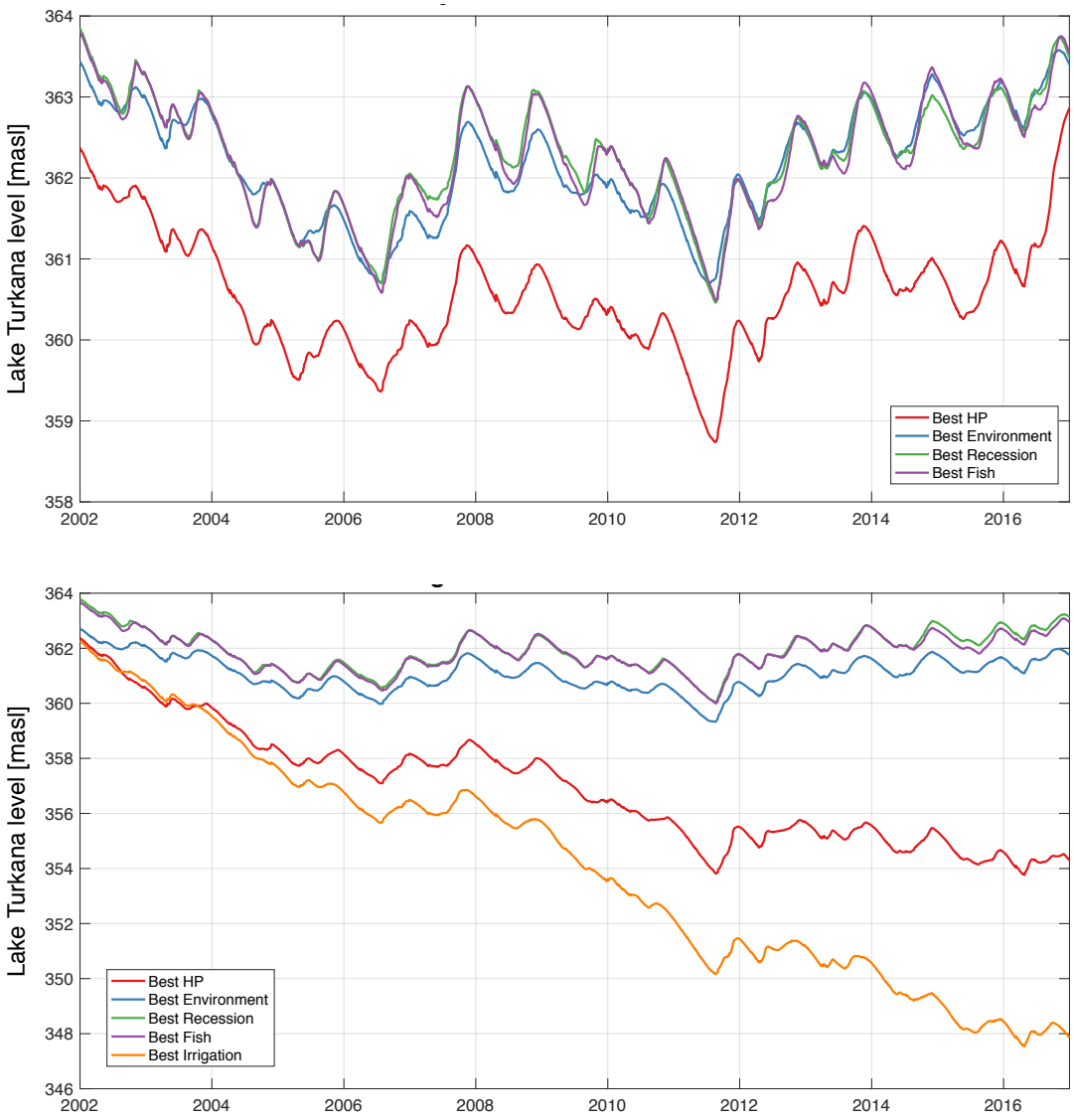

Figure 40 – Lake Turkana level simulated under the Koysha (top panel) and Irrigation (bottom panel) policies selected in Figure 29. The solid line represents the cyclostationary mean of the variable, and the shaded area represents its range over the historical horizon (2002-2016).

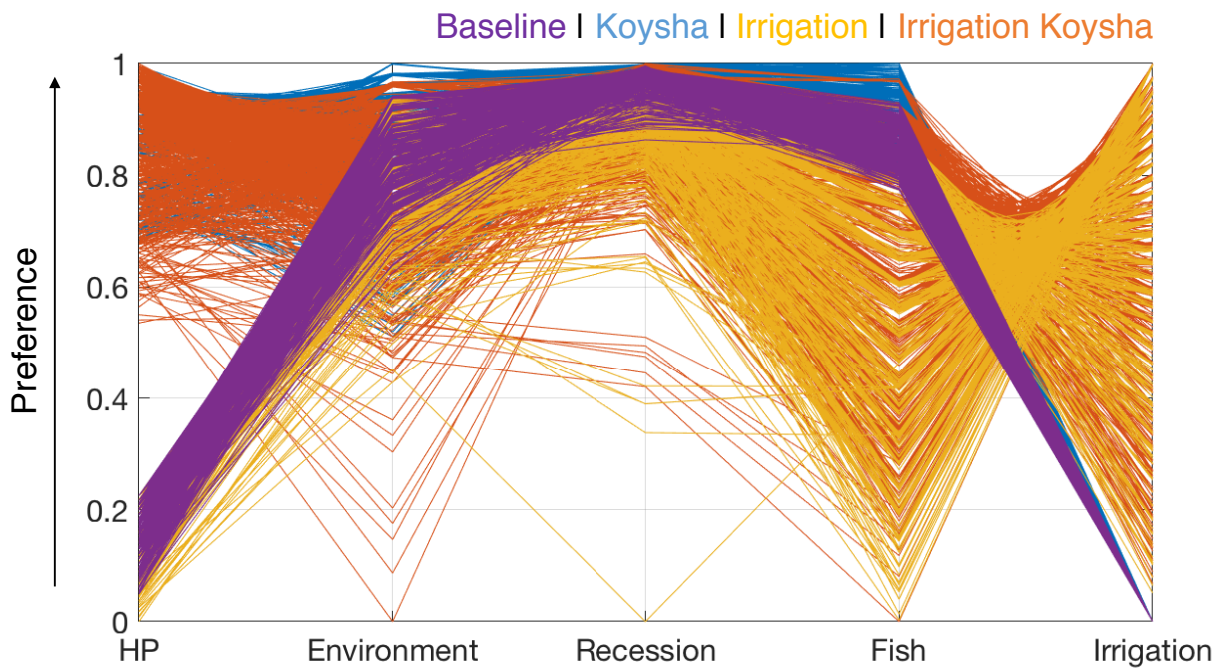

Figure 41 – Comprehensive parallel plot overlapping the 4 pathways represented with different colours.

6.2 SIMULATION OF CANDIDATE PATHWAYS

In this section, we present the candidate pathways identified from SHs suggestions and described in Deliverable D5.1, namely the Energy pathway, the Food Pathway, the Environment pathway, and the Full Development pathway. Their performance will be evaluated over the nominal future scenario introduced in the previous chapter, with respect to the design objectives and key hydrological variables.

Figure 42 presents the simulated annual energy production for different pathways under the considered future scenario, to be maximized. Each pathway is indicated with a differently coloured area, while the solid line of corresponding colour represents the long-term trend. The two pathways considering the construction of Koysha dam, namely Full Development and Energy, achieve an energy production that more than doubles the other two pathways, with the Energy pathway slightly higher than the Full Development, especially towards the end of the century. However, their energy production results fairly unstable in the future, oscillating between 3000 and 8000 GWh/year in different years. This is probably a consequence of the delicate synchronized management of Gibe III and Koysha dam, which is fine-tuned for historical conditions, but may fail when exposed to unprecedented hydrological years. The hydropower production of Food and Environment pathways is significantly lower, but more stable, especially in the Food pathway.

The simulated annual environmental damage (to be minimized) is reported in Figure 43, which shows that the Food pathway is the most damaging for the Omo delta ecosystem, recording large deviations in several years, and an increasing trend towards the end of the century. The increasing trend is visible for the Full Development pathways as well, although the damage magnitude is around one third of what is caused by the Food pathway. The least damaging pathway for this objective is, as expected, the Environment pathway.

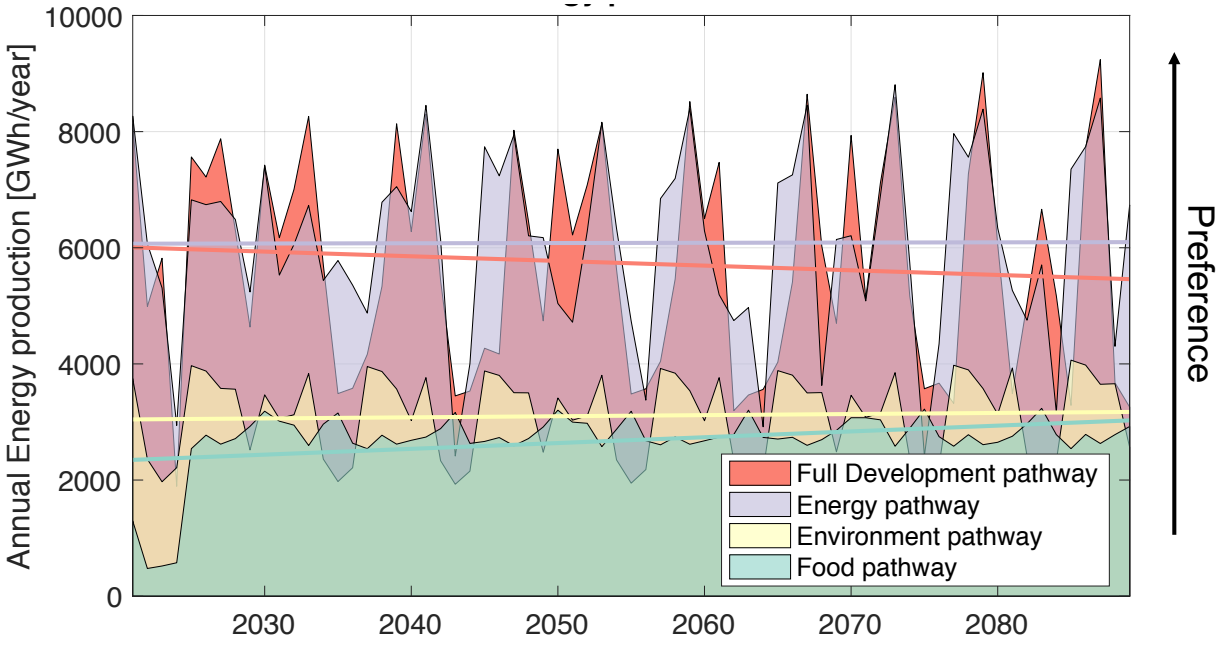

Figure 42 – Simulated annual future energy production cumulated for all the installed power plants under the 4 candidate pathways.

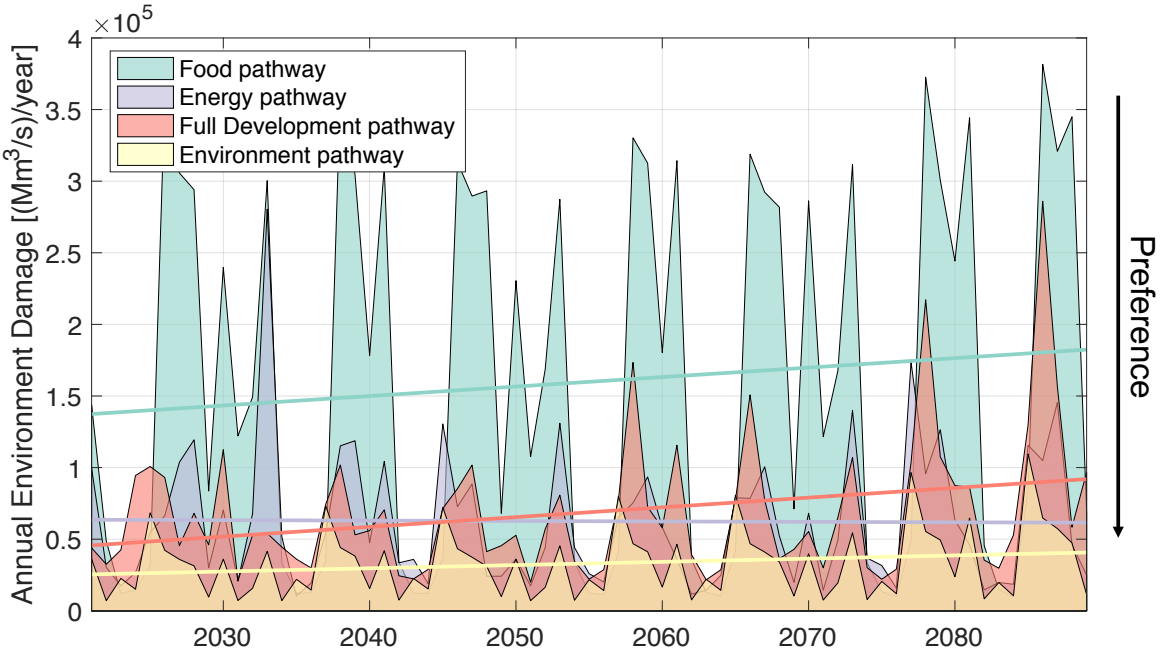

Figure 43 – Simulated annual future environmental damage evaluated at the Omo river delta under the 4 candidate pathways.

Figure 44 reports the simulated annual Recession damage (to be minimized). In this case, the Full Development Pathway records the largest damage, doubling the damage associated to the Food pathway. Analogously to the previous plot, the Environment pathway produced the least damage to the Recession sector both in terms of magnitude and interannual variations.

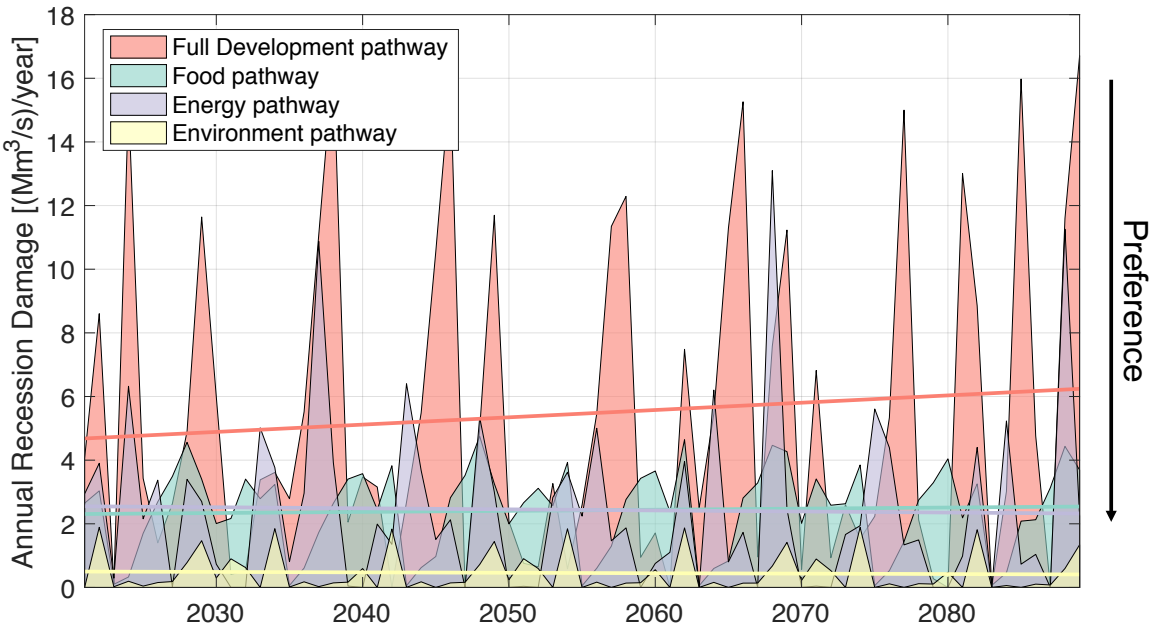

Figure 44 – Simulated annual future Recession damage under the 4 candidate pathways.

The mean daily irrigation deficit for each year, to be minimized, is reported in Figure 45 for the two pathways considering the construction of the irrigation districts, namely the Food, and the Full Development pathways. The irrigation deficit is a proxy of the large scale food production achievable under the considered pathway, where low deficit is associated to high food production. Hence, the Environment and Energy pathways, not reported in the graph, should be considered as if they assume the worst possible value for the entire time horizon, as they are not associated with any large scale food production. In the other two candidate pathways, instead, irrigation districts will be operative starting from 2025 (for the first 5 years of the simulations are also associated with the worst value of the objective). Both represented pathways maintain an irrigation deficit lower than 5% for the entire horizon, and among the two, the Food pathway records a lower and less variable deficit.

As already discussed for the historical re-operation, the abstraction of water for agricultural purposes exerts a significant stress on lake Turkana level and ecosystem, visible in Figure 46 (annual fish yield) and Figure 47 (lake level). The two pathways considering irrigation display a steep downward trend in fish yield and in Turkana level, and by the end of the time horizon Food pathway records a 20 meter drop in Turkana level, and one fourth of the Fish Yield produced by the Environment pathway. Environment and Energy pathways show an increasing trend in both lake Turkana level and fish yield, resulting from the overall increasing streamflow availability displayed by the hydrologic scenarios.

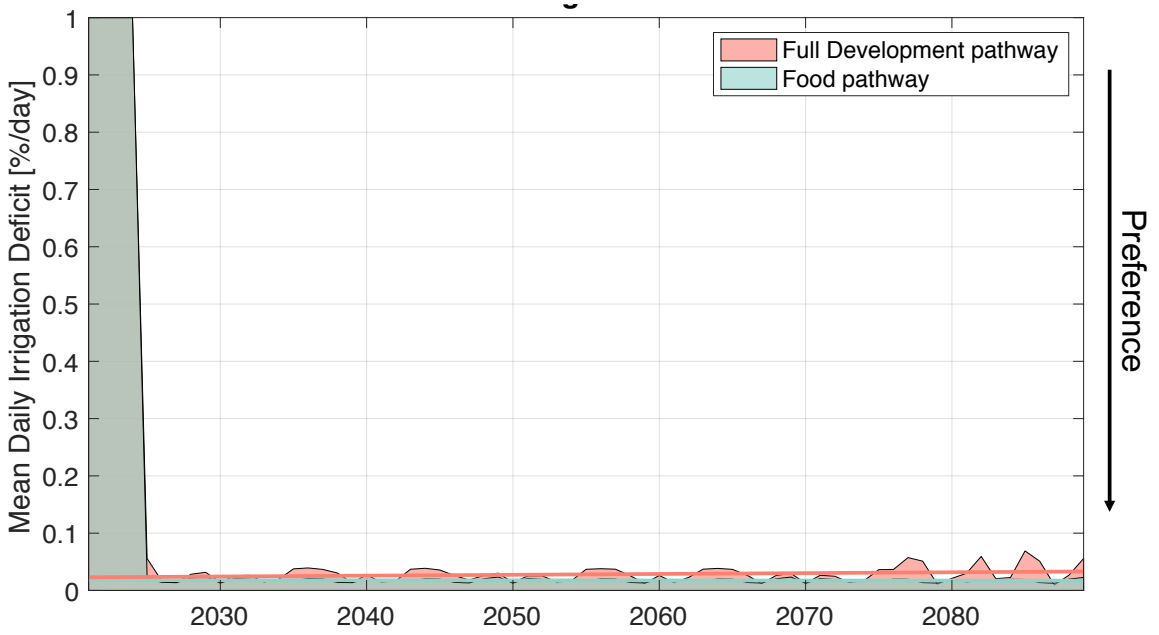

Figure 45 – Simulated annual mean daily normalized irrigation deficit for the two irrigation districts (Kuraz and Private Agriculture) under the 4 candidate pathways.

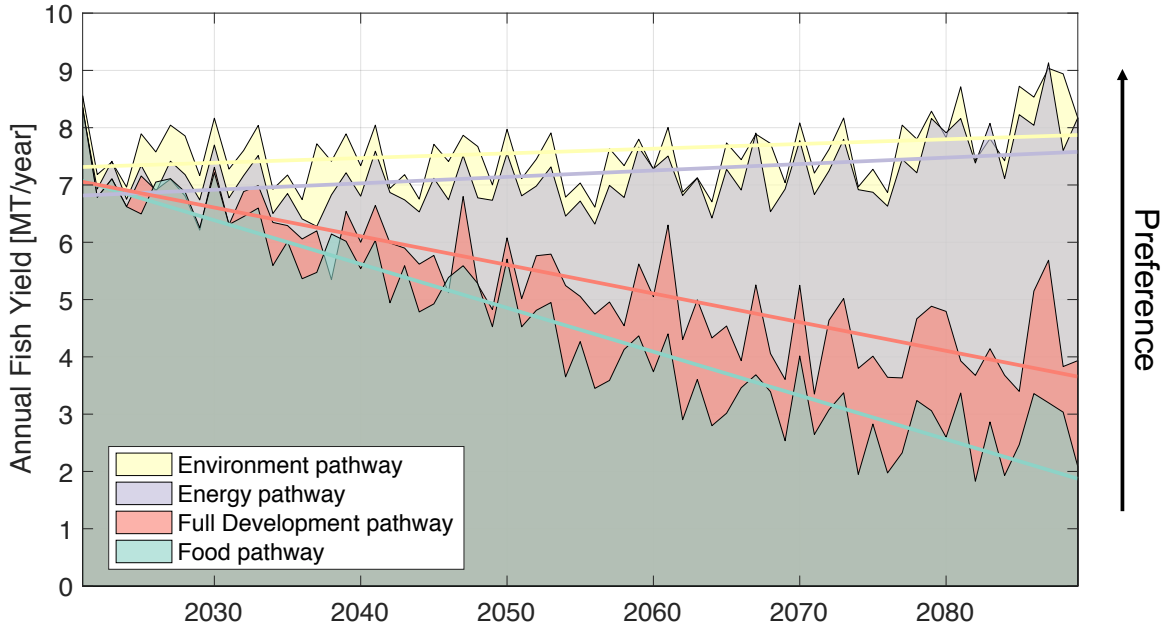

Figure 46 – Simulated annual future fish yield under the 4 candidate pathways.

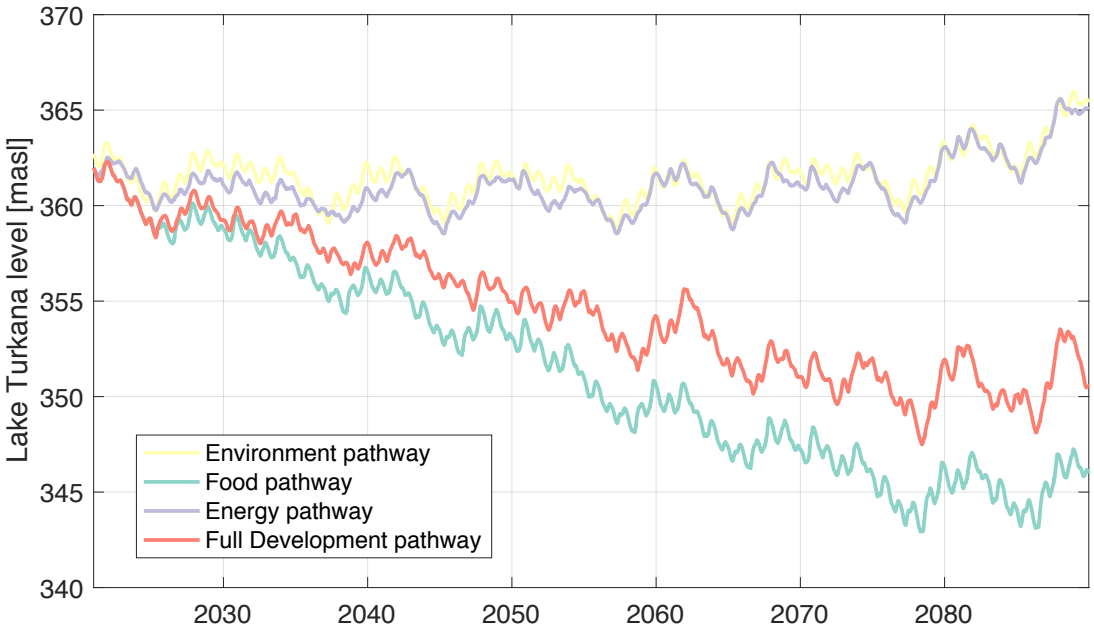

Figure 47 – Simulated future Lake Turkana level under the 4 candidate pathways.

6.3 EFFICIENT PATHWAYS

In this last section, we discuss the efficient pathways optimized for the OTB. Differently from the ZRB, in this case we did not explore different timing of infrastructural development as both Koysha and Kuraz are already under construction and expected to be operated in a couple of years. As a consequence, the focus of this analysis is the exploration of the trade-offs in the full set of Pareto optimal policies associated to the Irrigation-Koysha pathways when simulated over the future horizon with projected streamflow and irrigation demands.

The parallel axes plot representing the normalized performance of efficient pathways in the future is reported in Figure 48, where colours are assigned to solutions in accordance to the Hydropower objective (red lines correspond to the best HP values, and blue lines to the worst). From this paral lelaxes plot we can recognize the persistence of a conflict between Irrigation and Fish objectives as observed under historical conditions, and, by inspecting the line colours, between Hydropower and Fish. This latter conflict is however less sharp, and it is possible to identify highly performing solutions for the Fish objective within the top 10% HP solutions as denoted by the presence of red lines in the lowest section of the Fish objective axis.

To better understand the impacts generated by climate and irrigation demands trend, in Figure 49 we compare the system performance in the near future (2021-2036) with the far future (2074-2089). Generally, the conflict between objectives is preserved, but some modifications are expected in the absolute performance. For instance, we can observe that the hydropower performance is expected to slightly increase in the far future for some alternatives as a result of the increasing streamflow. Conversely, the Fish objective will largely deteriorate by the end of the century as a result of the significant stress exerted on lake Turkana mainly attributable to irrigation practices. Environment and Recession objectives show a slight degradation of performance in the future, evidenced by the fact that near future solutions occupy the uppermost part of the relative axis. On the contrary, Irrigation seem to slightly improve in the future given the higher density of far future solutions with respect to near future solutions in the upper part of the irrigation axis.

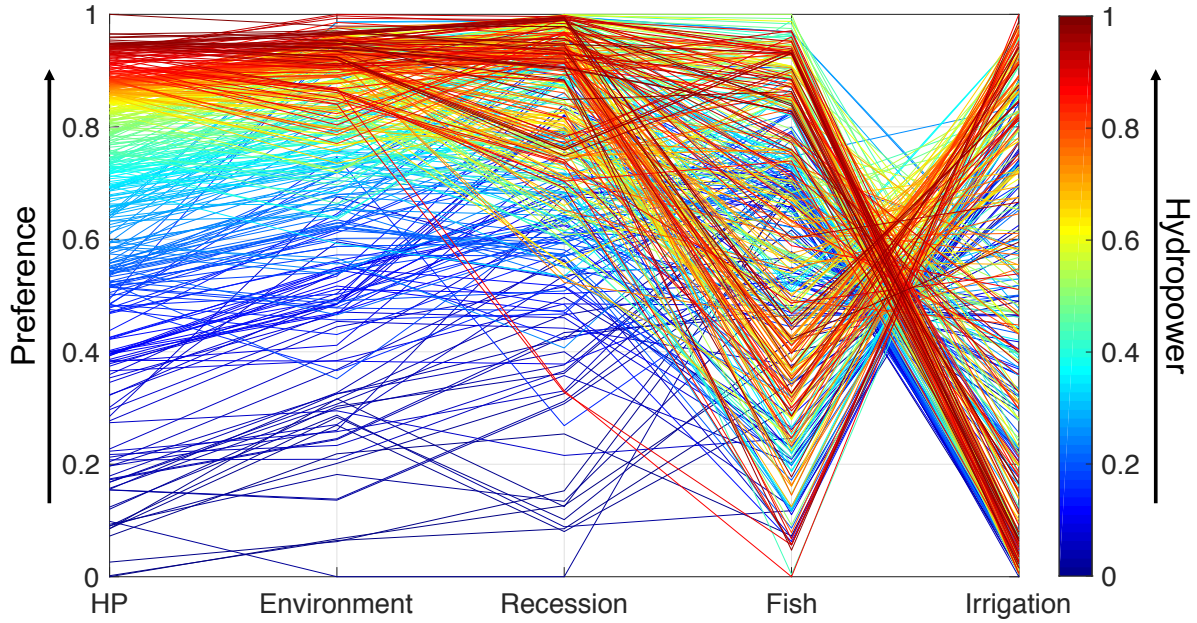

Figure 48 – Parallel axes plot representing the performance of efficient pathways evaluated over the future scenario.

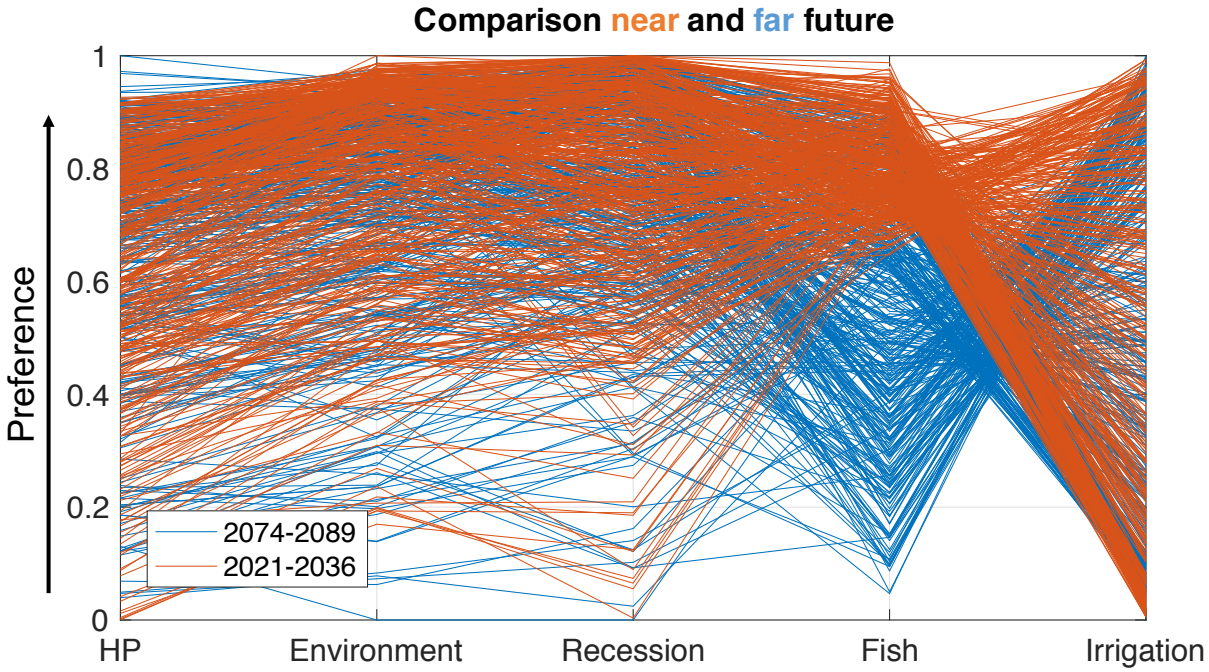

Figure 49 – Parallel axes plot comparing the system performance in the near and far future under the efficient pathways.

In the following, we analyze the system trajectories for a selected subset of pathways, corresponding to the best solutions identified for each objective in the Irrigation-Koysha pathway under the historical evaluation horizons (see Figure 29). Their performance re-evaluated on the future scenario is reported in Figure 50 and these solutions will be referred to as Hydropower, Environment, Recession, Fish, and Irrigation pathways.

We can notice that despite each solution maintains a good performance with respect to its name objective, they do not necessarily rank as best performing in future hydrology as well. This is particularly evident in the HP objective, for which the previously best policy place, in the future, within the top 20%, but it is outperformed by several solutions in terms of energy production. The reason is again related to the fact that a very precise coordination of a reservoir cascade can bring significant benefits under observed hydrological conditions. Under unknown future conditions, however, the synchronization may fail, for instance when the upstream reservoir does not appropriately filter hydrological variability thus forcing inefficient spillway releases in the downstream reservoir. In this case, a more conservative policy may achieve a higher energy production under unknown future hydrology.

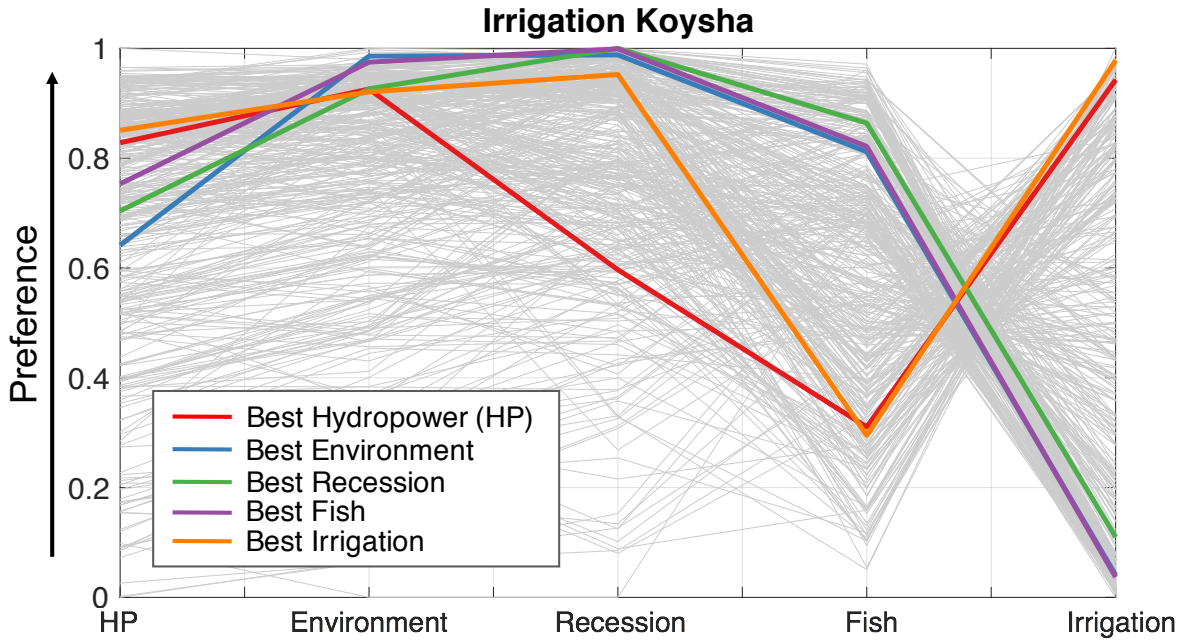

Figure 50 – Parallel axes plot highlighting the selected efficient pathways.

Mirroring the previous section, the analysis of the highlighted pathways will focus on the yearly values of the design objectives and on key hydrological variables. Figure 51 reports the simulated annual total energy production of the system, computed by cumulating the energy productions of the different power plants. Hydropower and Irrigation pathways attaining the highest energy production, followed somewhat closely by Fish, Recession, and Environment pathways. The Environment pathway, despite attaining the lowest production overall, is associated with the lowest fluctuations in energy production, guaranteeing a more stable firm energy (i.e., guaranteed minimum energy production). It's interesting to notice how the gap among hydropower productions under different operating policies tends to diminish towards the end of the time horizon.

The analyzed Hydropower pathway seems also to be highly damaging for the practice of Recession agriculture, as reported in Figure 53. However, the inspection of the parallel axes plot in Figure 48 suggests these two objectives are not necessarily highly conflicting, as we can find several policies located in the lower section of both Hydropower and Recession axis. Other pathways show more contained damages, in particular Fish and Recession pathways, that produce close to zero costs most of the years.

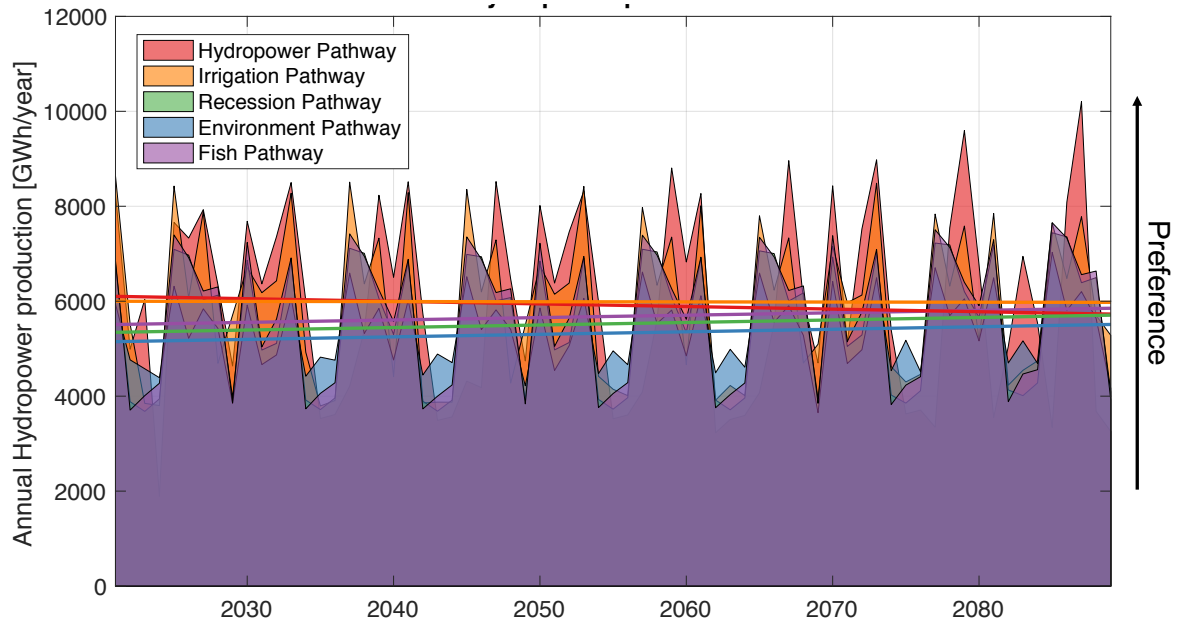

Figure 51 – Simulated annual future hydropower production under the 5 analyzed efficient pathways.

The annual Environmental damage is reported in Figure 52, which shows that Environment and Fish pathways are associated with the lowest environmental cost, while the Hydropower pathway tends to cause big spikes of damages especially towards the end of the time horizon. Across all the pathways, especially Hydropower, damage to the environment shows an increasing trend.

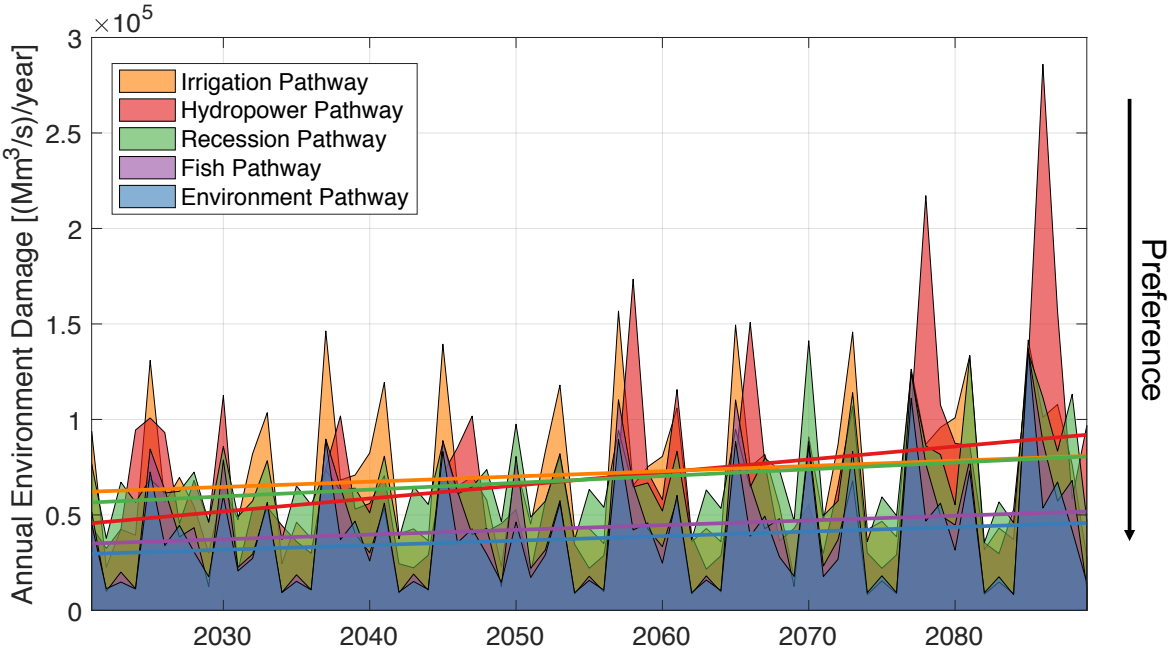

Figure 52 – Simulated annual future environmental damage under the 5 analyzed efficient pathways.

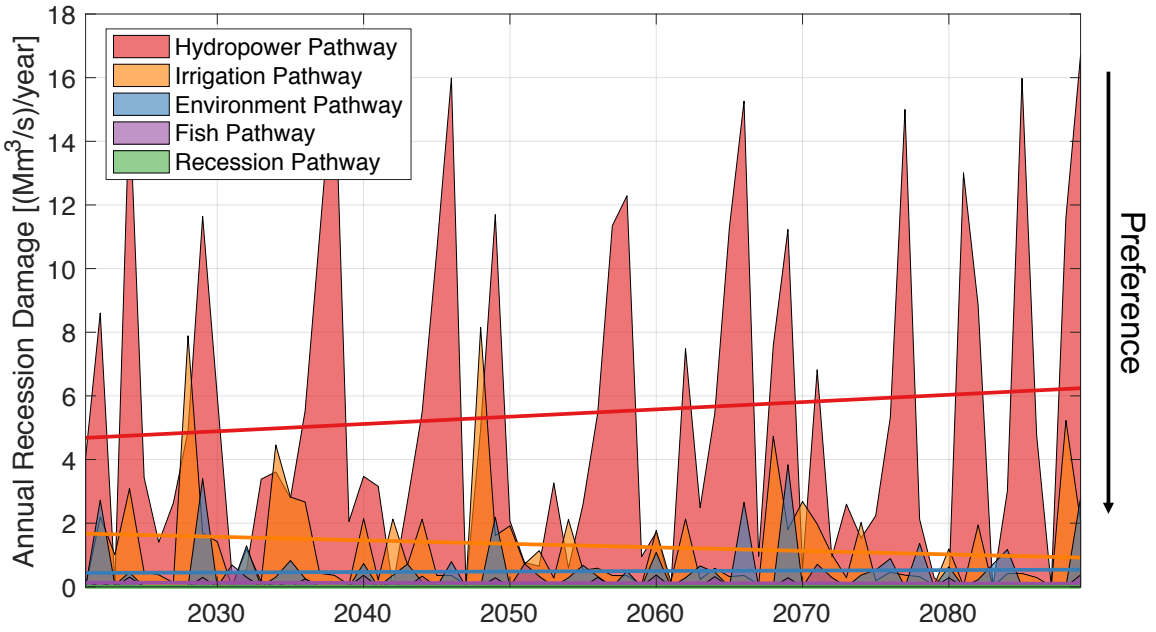

Figure 53 – Simulated annual future recession damage under the 5 analyzed efficient pathways.

The synergies between Hydropower and Irrigation interests are confirmed also in Figure 54, which shows that the two corresponding pathways generate very small irrigation deficit also in the future. As already observed in previous sections, the best solutions for Environment, Recession, and Fish curtail the diversion and generate large deficits in the attempt of restoring the natural conditions in the lower Omo valley.

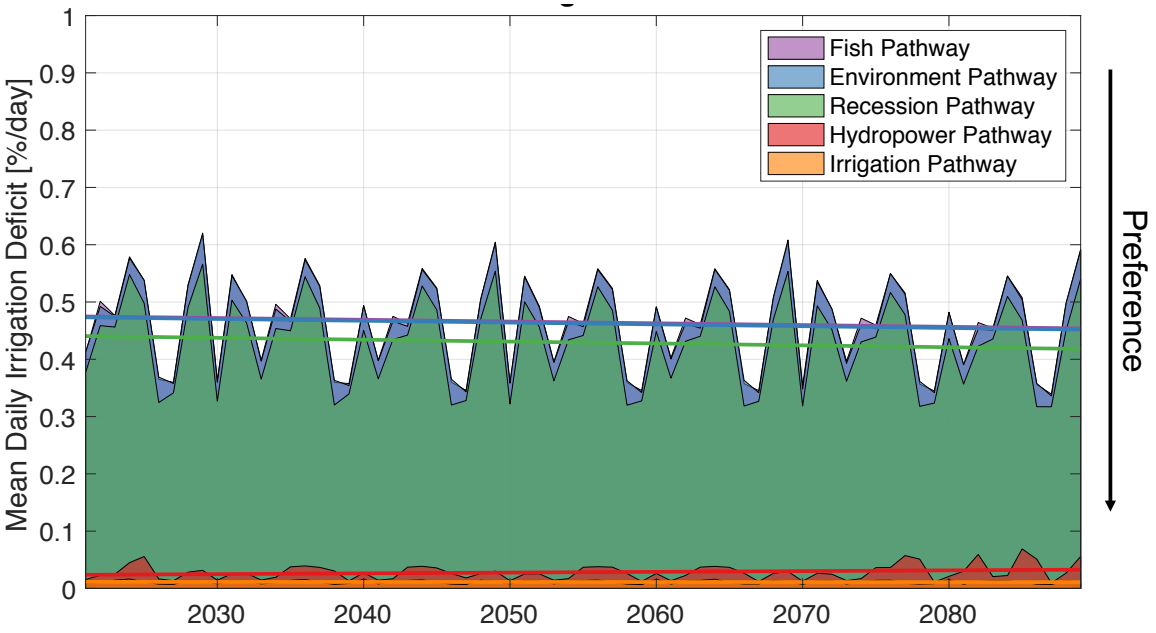

Figure 54 – Simulated annual future irrigation deficit under the 5 analyzed efficient pathways.

Finally, Fish Yield (Figure 55) and Lake Turkana level (Figure 56) are again declining fast under Hydropower and Irrigation pathways, as a response to the Irrigation abstractions which are expected to halve the Fish Yield, and cause a lake level Turkana reduction of around 15 meters by

the end of the evaluation horizon compared to Recession and Fish pathways. The Environment pathway displays a stable trend in Fish Yield and lake level, while Recession and Fish pathways show an increasing trend likely due to more abundant future inflows.

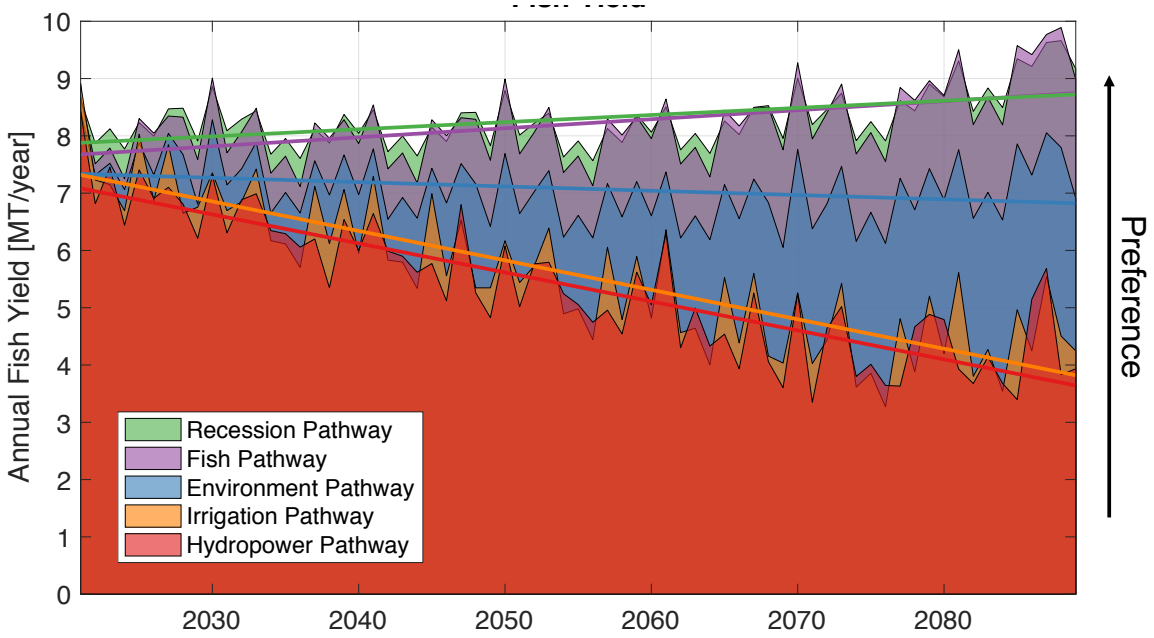

Figure 55 – Simulated annual future fish yield under the 5 analyzed efficient pathways.

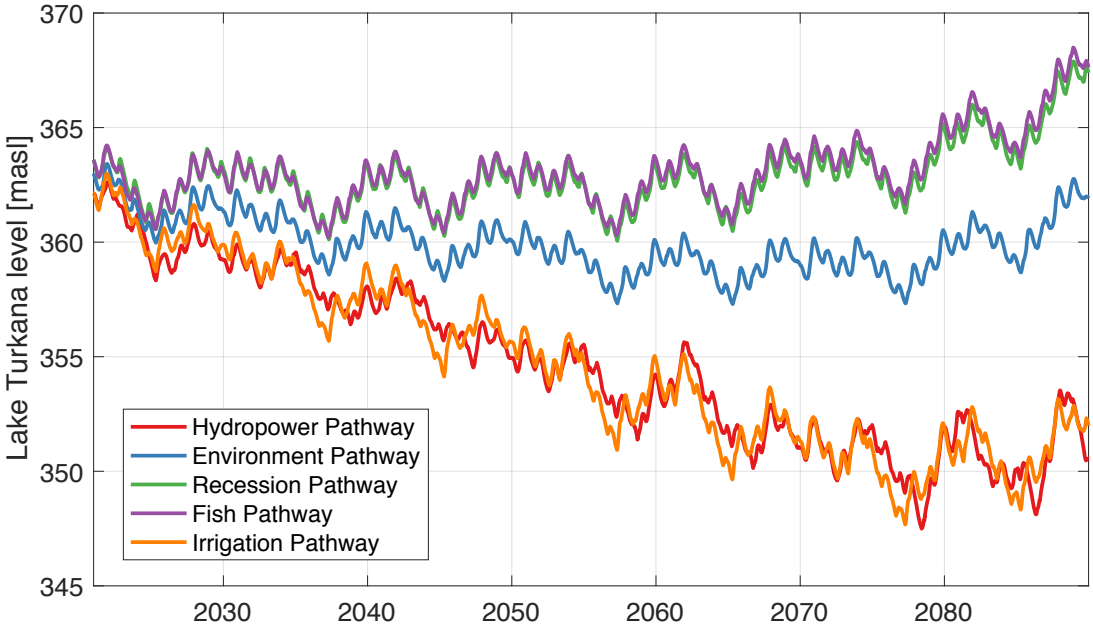

Figure 56 – Simulated annual future lake Turkana levels under the 5 analyzed efficient pathways.

7. CONCLUSIONS

This deliverable presents and analyzes the efficient pathways generated by the developed Decision Analytic Framework for both the Zambezi River Basin and the Omo River Basin. These solutions meet or exceed the performance of the candidate pathways identified in Deliverable D5.1, while also providing a rich context for supporting the identification of compromise solutions, which better address the trade-offs across the conflicting components of the Water-Energy-Food Nexus involved in the two case studies. Moreover, the extensive trade-off analysis investigating alternative operations of the existing system suggests there is also space for enhancing the flexibility and the adaptive capacity of the two systems without the need of infrastructural upgrades and their associated financial outlays.

A few key findings about the ZRB indicate that cooperative operations across existing and new planned infrastructure will be key in meeting environmental requirements in the Zambezi delta as well as balancing irrigation and hydropower demands. Our re-operation analysis indicates that operating preferences can yield widely different tradeoffs, namely a hydropower prone policy will create high environmental deficit, as an environmental prone policy will create a stark draw in reservoir storages during March and April, impacting hydropower generation for the downstream reservoirs which play a crucial role meeting the environmental requirements. This finding was also supported by the candidate pathways evaluation, where extreme operation preferences of the system create large deficit across the remaining sectors, for instance the BAU and energy pathways operated to maximize hydropower, fail to consider the other water needs in the ZRB, here a compromise policy is more suitable striking a balance across all sectors. The tradeoff between environment and hydropower production also drives the decision of the time in which a new dam is added, even when the system is operated to favor hydropower. Policies that perform moderately well for the environment suggest a later construction, whereas the policy that achieves the smallest hydropower deficit advocates for an earlier construction. The analysis also shows that if energy targets increase alongside with projections of population growth, the construction of all the dams will be inevitable within the planning horizon regardless of the net present cost objective.

As for the OTB, the analysis shows that fisheries in lake Turkana may be subject to significant stress in the future, mainly attributable to irrigation practices. Environment and Recession sectors are expected to slightly degrade under the nominal scenario, in response to changes in the hydrological cycle. On the contrary, Irrigation and Hydropower sectors are expected to benefit from future hydroclimatic conditions, given a general increment of water availability. Finally, despite the existence of conflicts between SHs, and the expected future trends, the numerosity of optimal solutions produced show that there is space for negotiation among the numerous compromise alternatives.

Most of the results included in this report will be presented to the Stakeholders participating to the Negotiation Simulation Labs in Addis Ababa and Lusaka in early July 2019. During those NSLs, SHs will run a preliminary negotiation and identify a sub-set of pathways that look more interesting according to their point of views, which will be then further analysed in the following months through the simulation of the integrated WEF model (WP3) and by testing their robustness against an ensemble of alternative future scenarios (WP5). Moreover, the interactions with the SHs is expected to potentially generate some potential modifications to be implemented in the DAF. Lastly, it is worth mentioning that the overall DAF experiments for the design of efficient pathways are based on a reference future scenario assumed as representative for plausible future climatic and socio-economic conditions (for details, see *Deliverable D2.2 Future drivers and scenarios*). Being the fully integrated WEF model still under development in WP3, the scenario used here should be therefore considered as preliminary because the climate and socio-economic components are not integrated yet. However, this temporary lack of integration is not expected to undermine the design of the pathways as this latter was already foresee to be run with a strategic design model, with the resulting performance to be validated via simulation of the integrated WEF model, which will eventually include also a revised version of the future scenario explicitly integrating climate and socio-economic conditions.

8. REFERENCES

A. Castelletti, F. P. R. S. S., 2008. Water reservoir control under economic, social and environmental constraints. *Automatica,* 44(6), p. 1595–1607.

Balon, E. K. & Coche, A. G., 2012. *Lake Kariba: A man-made tropical ecosystem in Central Africa (Vol. 24).* Berlin: Springer Science & Business Media.

Baxter, J. & Bartlett, P. L., 2001. Infinite-Horizon Policy-Gradient Estimation. *Journal of Artificial Intelligence Research,* Volume 15, pp. 319-50.

Bellman, R., 1957. *Dynamic Programming.* s.l.:s.n.

Benigni, B. et al., 2018. *Robust planning of agricultural expansion in Zambezi river basin under climate and socio-economic changes.* MSc thesis, Politecnico di Milano.

Bertsekas, D. P., 2005. Dynamic Programming and Suboptimal Control: A Survey from ADP to MPC. *European Journal of Control,* 11(4-5), pp. 310-34.

Bertsekas, D. P. & Tsitsiklis, J. N., 1995. Neuro-Dynamic Programming: An Overview. *In Proceedings of 1995 34th IEEE Conference On Decision and Control,* Volume 1, pp. 560-64.

Busa-Fekete, R. et al., 2014. Preference-Based Reinforcement Learning: Evolutionary Direct Policy Search Using a Preference-Based Racing Algorithm. *Machine Learning,* 97(3), p. 327–51.

Celeste, A. B. & Billib, M., 2009. Evaluation of stochatic reservoir operation optimization models. *Water Resources,* 32(9), pp. 1429-1443.

Chankong, V. & Haimes, Y. Y., 1983. Optimization-Based Methods for Multiobjective Decision-Making - An Overview. *Large Scale Systems In Information And Decision Technologies ,* 5(1), pp. 1-33.

Chen, T. & Chen, H., 1995. Universal Approximation to Nonlinear Operators by Neural Networks with Arbitrary Activation Functions and Its Application to Dynamical Systems. *IEEE Transactions on Neural Networks ,* 6(4), pp. 911-17.

Coello, C. A. C., Lamont, G. B. & Van Veldhuizen, D. A., 2007. *Evolutionary algorithms for solving multi-objective problems (Vol. 5, pp. 79-104).* New York: Springer.

Cybenko, G., 1989. Approximation by Superpositions of a Sigmoidal Function. *Mathematics of Control, Signals, and Systems (MCSS),* 2(4), pp. 303-14.

Denaro, S., Anghileri, D., Giuliani, M. & Castelletti, A., 2017. Informing the Operations of Water Reservoirs over Multiple Temporal Scales by Direct Use of Hydro-Meteorological Data. *Advances in Water Resources,* Volume 103, pp. 51-63.

Ethiopian Sugar Corp., 2018. *Kuraz Sugar Development Project.* [Online]
Available at: http://www.ethiopiansugar.com/projects/omo-kuraz-sugar-development-project-2/
[Accessed 9 7 2019].

FAO, 2018. *AquaCrop.* [Online]
Available at: http://www.fao.org/aquacrop/en/

Funahashi, K., 1989. On the Approximate Realization of Continuous Mappings by Neural Networks. *Neural Networks,* 2(3), pp. 183-92.

Gandolfi, C., Guariso, G. & Togni, D., 1997. Optimal flow allocation in the Zambezi river system. *Water Resources Management,* Volume 11, pp. 377-393.

Giuliani, M. et al., 2016. Curses, Tradeoffs, and Scalable Management: Advancing Evolutionary Multiobjective Direct Policy Search to Improve Water Reservoir Operations. *Journal of Water Resources Planning and Management,* 42(2), p. 4015050.

Giuliani, M. H. J. D., Castelletti, A. & Reed, P. M., 2014. Many-Objective Reservoir Policy Identification and Refinement to Reduce Policy Inertia and Myopia in Water Management. *Water Resources Research,* 50(4), p. 3355–77.

Hadka, D. & Reed, P. M., 2013. Borg: An Auto-Adaptive Many-Objective Evolutionary Computing Framework. *Evolutionary Computation ,* 21 (2), p. 231–59.

Hashimoto, T., Stedinger, J. & Loucks, D., 1982. Reliability, resilience, and vulnerability criteria for water resource system performance evaluation. *Water Resources Research,* 18(1), pp. 14-20.

Howells, M. R. H. S. N. H. C. H. H. K. S. H. A. S. S. D. J. a. B. M., 2011. OSeMOSYS: the open source energy modeling system: an introduction to its ethos, structure and development. *Energy Policy,* 39(10), pp. 5850-5870.

Inselberg, A., 1997. *Multidimensional detective.* Phoenix, AZ, Proceedings of the IEEE Symposium on Information Visualization and Parallel Rendering.

Lindström, G. et al., 1997. Development and test of the distributed HBV-96 hydrological model. *Journal of Hydrology,* 201(1-4), pp. 272-288.

Loucks, D. P. & Van Beek, E., 2017. *Water resource systems planning and management: An introduction to methods, models, and applications.* New York: Springer.

Maier, H. R. et al., 2014. Evolutionary algorithms and other metaheuristics in water resources: Current status, research challenges and future directions. *Enviornmental Modelling & Software,* Volume 62, pp. 271-299.

Marbach, P. & Tsitsiklis, J. N., 2001. Simulation-Based Optimization of Markov Reward Pro-cesses. *IEEE Transactions on Automatic Control ,* 46(2), pp. 191-209.

Park, J. & Sandberg, I. W., 1991. Universal Approximation Using Radial-Basis-Function. *Neural Computation,* 3(2), pp. 246-57.

Piccardi, C. & Soncini-Sessa, R., 1991. Stochastic dynamic programming for reservoir optimal control: Dense discretization and inflow correlation assumption made possible by parallel computing. *Water Resources Research,* 27(5), pp. 729-741.

Powell, W. B., 2007. *Approximate Dynamic Programming: Solving the curses of dimensionality (Vol. 703).* Hoboken: John Wiley & Sons.

Reed, P. M. et al., 2013. Evolutionary multiobjective optimization in water resources: The past, present, and future. *Advances in Water Resources,* Volume 51, pp. 438-456.

Revelle, C. & McGarity, A. E., 1997. *Design and Operation of Civil and Environmental Engi-neering Systems.* Hoboken: John Wiley & Sons.

Rosenstein, M. T. & Barto, A. G., 2001. *Robot Weightlifting by Direct Policy Search.* s.l., International Joint Conference on Artificial Intelligence, pp. 839-46.

S Fatichi, S. R. P. B. R. B. P. M., 2015. High-resolution distributed analysis of climate and anthropogenic changes on the hydrology of an Alpine catchment. *Journal of Hydrology,* Issue 525, pp. 362-382.

Soncini-Sessa, R., Weber, E. & Castelletti, A., 2007. *Integrated and Participatory Wa-ter Resources Management-Theory.* Amsterdam: Elsevier.

Tikk, D., Kóczy, L. T. & Gedeon, T. D., 2003. A Survey on Universal Approximation and Its Limits in Soft Computing Techniques.. *International Journal of Approximate Reasoning,* 33(2), p. 185–202.

Tilmant, A., Beevers, L. & Muyunda, B., 2010. Restoring a flow regime through the coordinated operation of a multireservoir system: The case of the Zambezi River basin. *Water Resources Research,* Volume 46, p. W07533.

Tsitsiklis, J. N. & Van Roy, B., 1996. Feature-Based Methods for Large Scale Dynamic Programming. *Machine Learning,* 22(1-3), pp. 59-94.

Woodruff, M. J., Reed, P. M. & Simpson, T. W., 2013. Many Objective Visual Analytics: Rethinking the Design of Complex Engineered Systems. *Structural and Multidisciplinary Optimization,* 48(1), pp. 201-19.

World Bank, 2019. *Real interest rate, inflation, lending and deposit interest rate.* [Online] Available at: https://data.worldbank.org/indicator?tab=all

Yeh, W. W. G., 1985. Reservoir Management and Operations Models. *Water Resources Research ,* 21(12), p. 1797–1818.

ZAMCOM, 2016. *Intregrated water resources management strategy and implementation plan for the Zambezi River Basin,* Harare: ZAMCOM.

Zatarain Salazar, J. et al., 2016. A diagnostic assessment of evolutionary algorithms for multi-objective surface water reservoir control. *Advances in Water Resources,* Volume 92, pp. 172-185.

Zoppoli, R., Sanguineti, M. & Parisini, T., 2002. Approximating Networks and Extended Ritz Method for the Solution of Functional Optimization Problems. *Journal of Optimization Theory and Applications,* 112(3), pp. 403-40.

9. APPENDIX

9.1 RESERVOIR DYNAMICS FOR THE EFFICIENT PATHWAYS

The average reservoir dynamics of the efficient pathways are shown in

Figure 57 and Figure 58, following an upstream to downstream reservoir sequence with each column representing its inflow, storage, and release. The lines are shaded by hydropower performance following the same solutions of the trade-off analysis, where dark blue and yellow mean low and high hydropower deficits respectively. The patterns are very similar to what we previously observed in the reservoir dynamics for the candidate pathways. Itezhi Tezhi (panels a-c), for instance, follows the peak release in March which corresponds to its peak inflow. All the pathways, from large to small hydropower deficit have similar storage patterns. Then, Kafue Gorge Upper (panels d-f) has a peak release in May, consistent with the delayed inflow from Itezhi-Tezhi. The releases for the best hydropower solution look smoother throughout the year, since the reservoir must be actively operated to meet the production target and thus minimize the overall hydropower deficit. As for the other pathways, they have a more pronounced spike in March and April following the corresponding inflow. Subsequently, the releases from Kafue Gorge Upper are the inflow to Kafue Gorge Lower (panel d). For this latter reservoir, most of the policies show a draw in storage in March and April, except for the best hydropower solution which keeps storage constant and closer to the maximum operating level (panel e), similar to Kafue Gorge Upper. This pathway shows flatter releases throughout the year as opposed to the sharp ones observed for the rest of the solutions, for the same reasons given for Kafue Gorge Upper. The releases for Batoka Gorge shown in panel (l) are averaged by the releases once the construction decision was made and also by the releases equivalent to the inflows when the reservoir was not yet built. The storage panel for Batoka Gorge (panel k) shows that the storage is kept constant on average and that the best hydro pathway operates almost at its maximum storage capacity and the releases are equivalent to the inflows, again to exploit the full hydropower potential of the reservoir and thus minimize the basin-scale hydropower deficit. Moving downstream to Devil's Gorge in Figure 58 panels (a-c), the releases are higher in March through April for the best environmental policy depicted in light yellow, whereas for the hydropower prone pathways, the releases are less pronounced for those months and are slightly higher throughout the year. The storage for this reservoir is kept relatively constant and only one policy keeps the storage very close to the maximum level.

All the efficient pathways lie within a similar operating storage range for Kariba (panels d-f), which is the reservoir with the largest storage capacity in the system and is mainly operated with the same annual policy following the inflow pattern. Next, continuing downstream, we encounter Cahora Bassa (panels g-i), whose inflow depends upon operations at Kariba and Kafue Gorge Lower, as well as the lateral Luangwa flows upstream the reservoir. The peak releases from Cahora Bassa are experienced from February to March, when the environmental flow requirement in the Delta is high. This behaviour is replicated for the most downstream reservoir in the system, Mphanda Nkuwa (panels j-l). For this last reservoir, most of the solutions show a draw in March and April which corresponds to the minimum environmental flows released to the Delta in February and March. Only the hydropower prone pathway in dark blue keeps a constant level in Mphanda Nkuwa and it releases half of the requirements during the critical months for environmental flows while keeping a constant release for the rest of the year. This allows to maximize its hydropower production in order to minimize the deficit with respect to the corresponding target. These last dynamics highlight the conflict between hydropower and the environment, where there is tension in keeping both the reservoir levels high and almost constant releases to guarantee hydropower production but failing to meet the environmental requirements. It is also worth noting that this analysis was carried with a hydropower prone policy, which emphasizes current preferences in the system. With this underlying operating policy, the best environmental pathway would be left with a deficit of around 2000 m^3/sec.

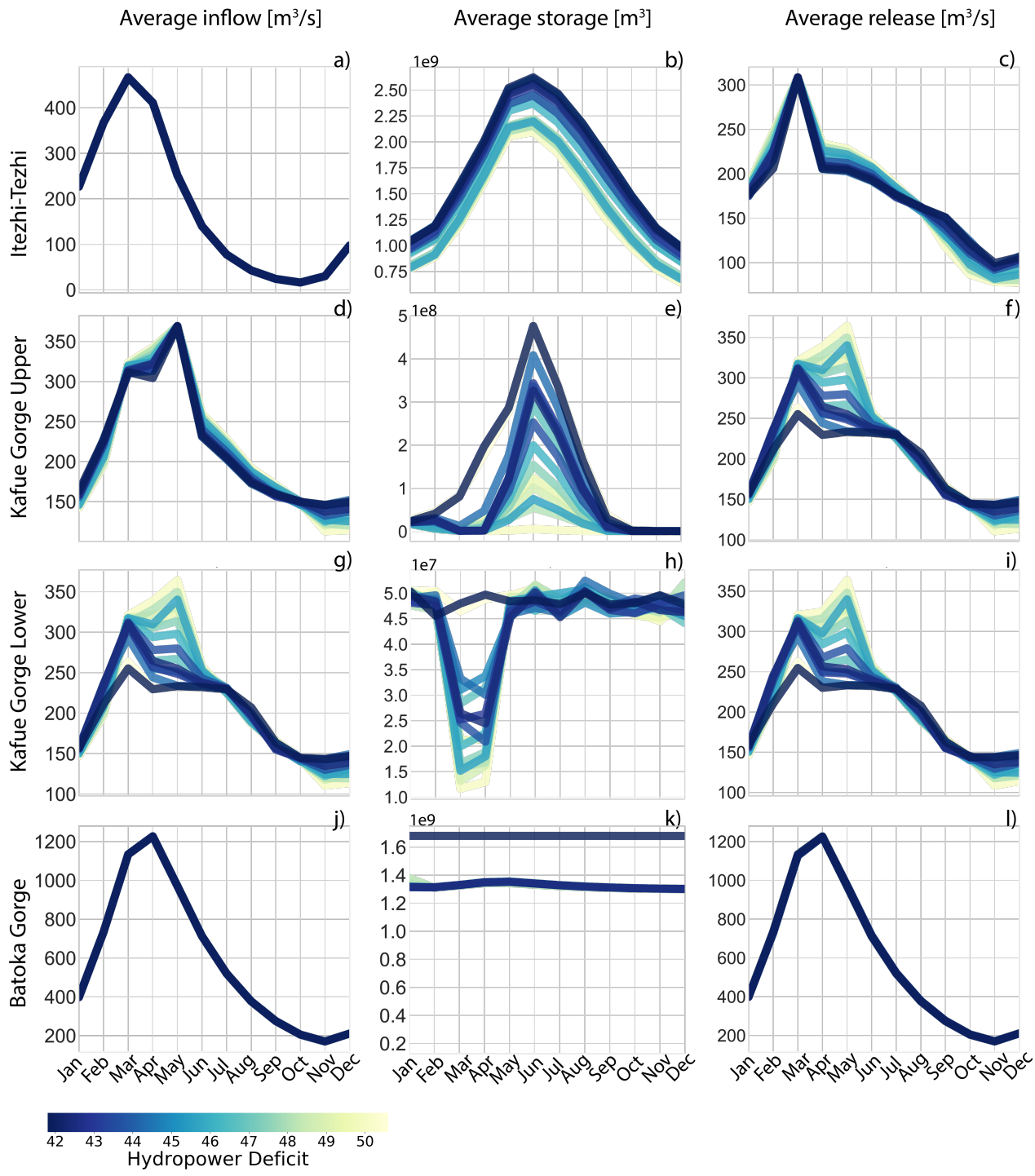

Figure 57 – Inflow, storage, and release dynamics for Itezhi-Thezi, Kafue Gorge Upper, Kafue Gorge Lower, and Batoka Gorge reservoirs under different solutions shaded by their performance for hydropower deficit.

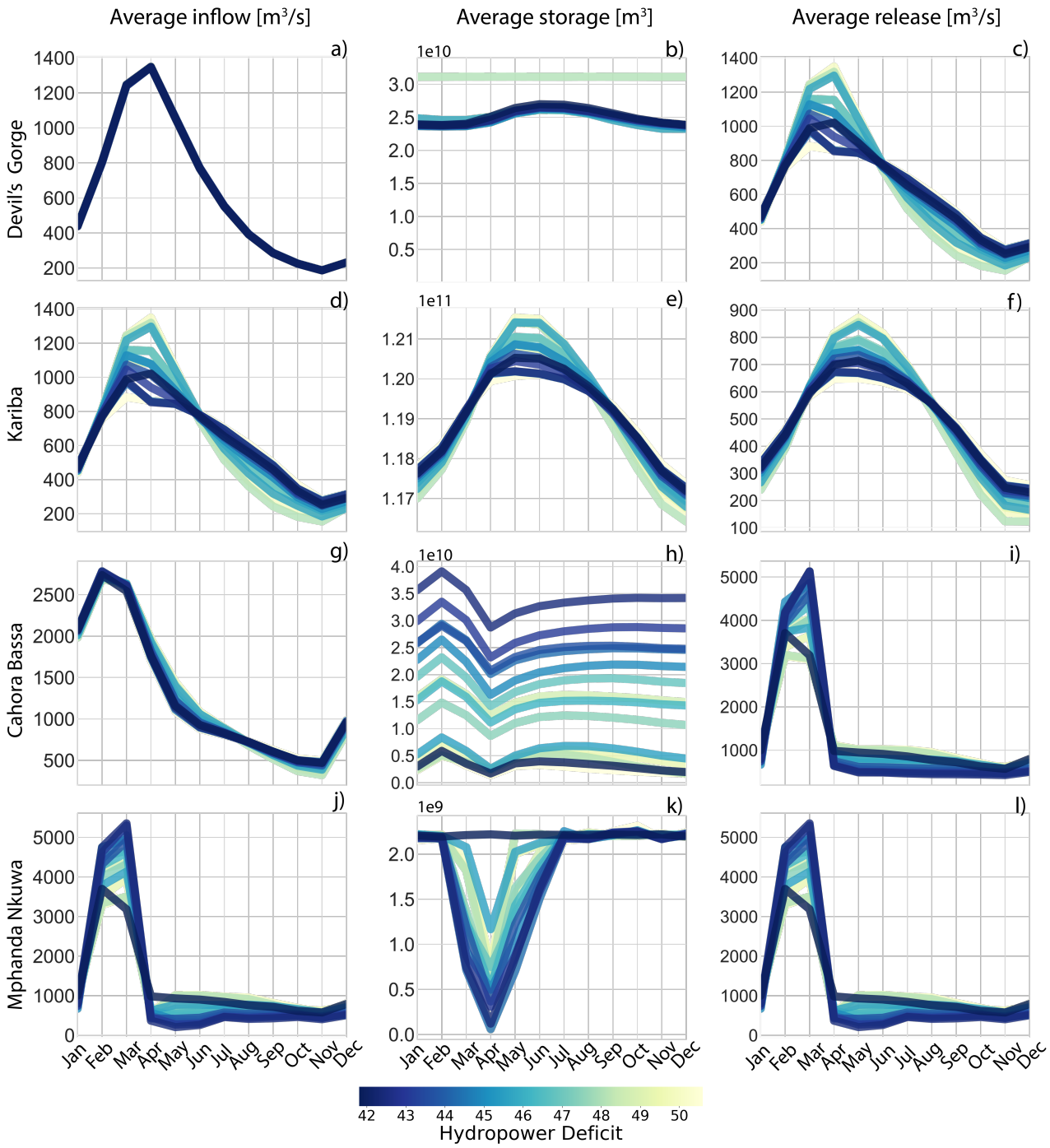

Figure 58 – Inflow, storage, and release dynamics for Devil's Gorge, Kariba, Cahora Bassa, and Mphanda Nkuwa reservoirs under different solutions shaded by their performance for hydropower deficit.